

2004

## Binding studies on molecularly imprinted polymers

Lucy Yue Hu

*College of William & Mary - Arts & Sciences*

Follow this and additional works at: <https://scholarworks.wm.edu/etd>



Part of the [Polymer Chemistry Commons](#)

---

### Recommended Citation

Hu, Lucy Yue, "Binding studies on molecularly imprinted polymers" (2004). *Dissertations, Theses, and Masters Projects*. William & Mary. Paper 1539623453.

<https://dx.doi.org/doi:10.21220/s2-5d2c-5973>

This Dissertation is brought to you for free and open access by the Theses, Dissertations, & Master Projects at W&M ScholarWorks. It has been accepted for inclusion in Dissertations, Theses, and Masters Projects by an authorized administrator of W&M ScholarWorks. For more information, please contact [scholarworks@wm.edu](mailto:scholarworks@wm.edu).

**BINDING STUDIES ON  
MOLECULARLY IMPRINTED POLYMERS**

---

A Dissertation

Presented to

The Faculty of the Department of Applied Science

The College of William and Mary in Virginia

In Partial Fulfillment

Of the Requirements for the Degree of

Doctor of Philosophy

---

by

Lucy Yue Hu

2004

**APPROVAL SHEET**

This dissertation is submitted in partial fulfillment of

The requirements for the degree of

Doctor of Philosophy

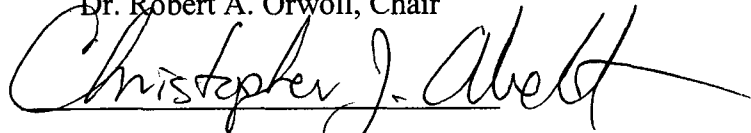


Lucy Yue Hu

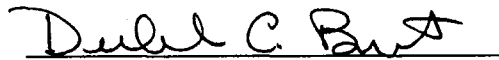
Approved by the Committee, July 2004



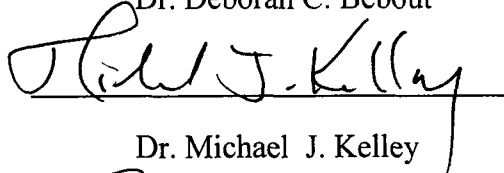
Dr. Robert A. Orwoll, Chair



Dr. Christopher J. Abelt



Dr. Deborah C. Bebout



Dr. Michael J. Kelley



Dr. Richard L. Kiefer

## TABLE OF CONTENTS

	<b>Page</b>
<b>Acknowledgements</b>	viii
<b>List of Figures</b>	ix
<b>List of Tables</b>	xiv
<b>Abstract</b>	xv
<b>CHAPTER 1. INTRODUCTION</b>	<b>2</b>
1.1. Molecular recognition and molecular imprinting	2
1.2. Scheme to make molecularly imprinted polymers (MIPs)	3
1.2.1. Principle of making MIPs	5
1.2.2. Non-covalent imprinting preparation of MIPs	6
1.2.3. Characteristics and applications of MIPs	10
1.3. Properties of binding sites in MIPs	11
1.3.1. Experimental methods for the characterization of MIPs	11
1.3.2. Models used for binding evaluation on MIPs	13
1.3.2.1. Scatchard analysis	13
1.3.2.2. Model of multiple independent classes of binding sites	18
1.3.2.3. Affinity spectrum (AS) method	19
1.4. Motivation for this work from previous studies	22
1.5. Proposal for this study	24
<b>REFERENCES</b>	<b>26</b>
<b>CHAPTER 2. BINDING STUDIES ON RESINS IMPRINTED WITH HYDROXYBENZOIC ACID ISOMERS</b>	<b>30</b>

	<b>Page</b>
2.1. Hydroxybenzoic acid isomers	30
2.2. Experimental	33
2.2.1. Materials	33
2.2.2. Preparation of molecularly imprinted polymer with 4HBA (MIP4HBA) and non-imprinted polymer (NIP)	33
2.2.2.1. Interaction study between 4HBA and AA by titration experiment via <sup>1</sup> H-NMR	33
2.2.2.2. Preparation of MIP4HBA and NIP	34
2.2.2.3. Template extraction by Soxhlet extraction	35
2.2.2.4. 4HBA, 3HBA and BA binding experiments	36
2.2.2.5. Kinetic study of 4HBA binding experiment	36
2.2.3. Preparation of molecularly imprinted polymer with 3HBA (MIP3HBA) and non-imprinted polymer (NIP')	37
2.2.3.1. Preparation of MIP3HBA and NIP'	37
2.2.3.2. 4HBA, 3HBA and BA binding experiments	38
2.3. Results and discussion	38
2.3.1. Binding studies on 4HBA imprinted polymer system	38
2.3.1.1. Interaction between 4HBA and AA before polymerization	38
2.3.1.2. Preparation of MIP4HBA	46
2.3.1.3. Binding analyses of MIP4HBA and NIP resins	47
2.3.1.3.1. Comparison of different polymerizations' binding analyses	47
2.3.1.3.2. Reproducibility of rebinding experiment on MIP4HBA and NIP resins	51

	<b>Page</b>
2.3.1.3.3. Binding analyses of MIP4HBA and NIP resins	52
2.3.1.4. Kinetic study of 4HBA binding procedure	59
2.3.1.5. Substrate selectivity of MIP4HBA and NIP	60
2.3.1.6. Comparison of batch analyses and chromatographic evaluation	61
2.3.2. 3HBA imprinted polymer system	63
2.3.2.1. Interaction study of 3HBA and AA	63
2.3.2.2. Preparation of MIP3HBA	66
2.3.2.3. Binding analyses of MIP3HBA and NIP'	66
2.3.2.4. Substrate selectivity of MIP3HBA and NIP'	71
2.4. Summary	72
REFERENCES	73
<b>CHAPTER 3. EXTRACTION AND BINDING STUDIES ON (S)- NAPROXEN IMPRINTED POLYMERS</b>	<b>75</b>
3.1. Literature review	75
3.2. Experimental	78
3.2.1. Materials	78
3.2.2. 4VP used in the preparation of non-imprinted polymer (NIP1) and molecularly imprinted polymer with (S)-naproxen (4VPMIP )	79
3.2.2.1. UV study of the interaction between 4VP and (S)-naproxen	79
3.2.2.2. Preparation of NIP1 and 4VPMIP	79
3.2.2.3. Extraction analyses of NIP1 and 4VPMIP	80
3.2.2.4. Fourier transformation infrared spectra (FT-IR) of 4VPMIP and NIP1	80

	<b>Page</b>
3.2.3. AA used in the preparation of non-imprinted polymer (NIP2) and molecularly imprinted polymer with ( <i>S</i> )-naproxen (AAMIP)	81
3.2.3.1. Preparation of NIP2 and AAMIP	81
3.2.3.2. ( <i>S</i> )-naproxen binding experiment	82
3.3. Results and discussion	82
3.3.1. 4VPMIP system	82
3.3.1.1. Interaction between monomer and template	82
3.3.1.2. Extraction analyses of 4VPMIP resins	86
3.3.2. AAMIP system	90
3.3.2.1. Preparation of AAMIP	90
3.3.2.2. Binding analyses of AAMIP and NIP2 resins	92
3.4. Summary	97
REFERENCES	98
<b>CHAPTER 4. DISCUSSION</b>	<b>99</b>
4.1. Anatomy of binding sites in MIPs	99
4.2. Analyses of the binding sites parameters in MIPs	102
4.3. MIPs in the bulk format	109
REFERENCES	111
<b>CHAPTER 5. SUMMARY AND CONCLUSIONS</b>	<b>112</b>
<b>APPENDICES</b>	<b>114</b>
Appendix A. GC-MS spectra of EGDMA.	114
Appendix B. UV spectra of 4HBA, 3HBA and BA in acetonitrile.	115

	<b>Page</b>
Appendix C. $^1\text{H-NMR}$ spectra of AA in acetonitrile- $d_3$ .	116
Appendix D. $^1\text{H-NMR}$ spectra of 4HBA and AA in acetonitrile- $d_3$ .	119
Appendix E. $^1\text{H-NMR}$ spectra of 3HBA and AA in acetonitrile- $d_3$ .	123
Appendix F. Uncertainty analysis by least-squares fitting procedure.	126
REFERENCES	137
<b>VITA</b>	138

## ACKNOWLEDGEMENTS

The author would like to express her sincere appreciation to her advisor Dr. Robert A. Orwoll for his invaluable guidance and understanding during this research. He invested so much time discussing and providing his wise insight into both research and life as a mentor and a friend. The author is also indebted to Dr. Christopher J. Abelt, Dr. Deborah C. Bebout, Dr. Michael J. Kelley and Dr. Richard L. Kiefer for their contributions to this manuscript and careful instructions during this endeavor.

The author wishes to acknowledge the exceptional support of the departments of applied science and chemistry and the entire Orwoll group without which her research experience would not have been completed.

In addition, the author is very grateful to all her friends from all over the world for their friendship, care and pray.

Finally, the author wishes to thank her husband and parents for their very generous unending support, encouragement and love.

## LIST OF FIGURES

	<b>Page</b>
Figure 1.1. “Lock and key” analogy for making MIPs.	4
Figure 1.2. Scheme of making MIPs.	5
Figure 1.3. Two experimental methods to evaluate the binding sites of MIPs.	12
Figure 1.4. Two kinds of Scatchard plots shown in literature.	15
Figure 1.5. The experimental scheme used in this study to make MIPs and NIPs.	25
Figure 2.1. Chemical structures of the structural related molecules.	31
Figure 2.2. Intramolecular hydrogen bonding in SA.	32
Figure 2.3. <sup>1</sup> H-NMR spectrum of AA in acetonitrile- <i>d</i> <sub>3</sub> .	41
Figure 2.4. <sup>1</sup> H-NMR spectrum of 4HBA in acetonitrile- <i>d</i> <sub>3</sub> .	41
Figure 2.5. <sup>1</sup> H-NMR spectrum of 4HBA and AA in acetonitrile- <i>d</i> <sub>3</sub> in which the concentration ratio of 4HBA : AA = 1:6.	41
Figure 2.6. NMR signals from AA’s two amide protons at varying concentrations in <i>d</i> <sub>3</sub> -acetonitrile.	43
Figure 2.7. NMR signals from AA’s two amide protons at varying concentrations in the presence of 4HBA in <i>d</i> <sub>3</sub> -acetonitrile.	44
Figure 2.8. Chemical shifts for the two amide protons in AA as a function of the concentration of AA.	45
Figure 2.9. Probable hydrogen bonding between 4HBA and AA.	45
Figure 2.10. Scanning electron micrographs of MIP4HBA particles at (a) 380× and (b) 10,000× magnification.	46
Figure 2.11. Binding isotherms for 4HBA on different batches of MIP4HBA and NIP.	48
Figure 2.12. Reproducibility of 4HBA rebinding on MIP091302 and NIP091302.	52

	<b>Page</b>
Figure 2.13. Binding isotherms for 4HBA on MIP4HBA and NIP.	53
Figure 2.14. Percentage uptake from MIP4HBA and NIP binding solutions.	54
Figure 2.15. Scatchard plots of MIP4HBA and NIP for 4HBA.	55
Figure 2.16. Scatchard plot for the special binding sites with $[MT]_s$ determined using Equation (2-5).	57
Figure 2.17. Representation of the observed binding data using Equation (2-6).	58
Figure 2.18. Kinetic study of 4HBA binding on MIP4HBA and NIP resins.	59
Figure 2.19. Structures of the substrates used in this study: (a) 4HBA; (b) 3HBA and (c) BA.	60
Figure 2.20. Binding isotherms of 4HBA, 3HBA and BA on (a) NIP and (b) MIP4HBA.	61
Figure 2.21. NMR signals from AA's two amide protons at varying concentrations in the presence of 3HBA in $d_3$ -acetonitrile.	64
Figure 2.22. Chemical shifts for the two amide protons in AA as a function of the concentration of AA.	65
Figure 2.23. Probable hydrogen bonding between 3HBA and AA.	65
Figure 2.24. Binding isotherms for 3HBA on MIP3HBA and NIP'.	67
Figure 2.25. Scatchard plot of MIP3HBA and NIP' for 3HBA.	68
Figure 2.26. Scatchard plot for the special binding sites with $[MT]$ determined using Equation (2-5).	69
Figure 2.27. Representation of the observed binding data using Equation (2-6).	70
Figure 2.28. Binding isotherms of 4HBA, 3HBA and BA on (a) NIP' and (b) MIP.	71
Figure 3.1. Scheme of making MIP for (S)-naproxen.	77

	<b>Page</b>
Figure 3.2. Structures of the compounds used in the experiment.	78
Figure 3.3. UV absorption spectra of ( <i>S</i> )-naproxen and 4VP in THF.	83
Figure 3.4. Delocalization of $\pi$ electrons in ( <i>S</i> )-naproxen with the addition of 4VP.	84
Figure 3.5. FT-IR Spectra for (A) NIP1; (B) 4VPMIP before ( <i>S</i> )-naproxen extraction; (C) 4VPMIP after ( <i>S</i> )-naproxen extraction.	85
Figure 3.6. HPLC chromatograph of four consecutive washings of MIP and its control experiment.	87
Figure 3.7. The reversible model reaction for washing analyses.	88
Figure 3.8. Two-site Scatchard plot showing the quantity of ( <i>S</i> )-naproxen absorbed at the weak (dashed line) and strong (dotted line) binding sites.	89
Figure 3.9. Scheme of making MIP for ( <i>S</i> )-naproxen while AA was the monomer.	91
Figure 3.10. Binding isotherms for ( <i>S</i> )-naproxen on AAMIP and NIP2.	93
Figure 3.11. Scatchard plot of AAMIP and NIP2 for ( <i>S</i> )-naproxen.	94
Figure 3.12. Scatchard plot for the special binding sites with [MT] determined using Equation (2-5).	95
Figure 3.13. Representation of the observed binding data using Equation (2-6).	96
Figure 4.1. Mechanisms for the formation of the binding sites in MIPs: (a) “frozen”-in ; (b) step-by-step.	101
Figure 4.2. Structures of templates and functional monomers used in Zhang’s research.	102
Figure 4.3. Binding isotherm (a) for MIP4HBA and the corresponding affinity distribution (b) according to Shimizu.	109
Figure A.1. GC-MS spectra of EGDMA which was purified under vacuum distillation.	114

	Page
Figure B.1. UV spectrum of 4HBA acetonitrile solution.	115
Figure B.2. UV spectrum of 3HBA acetonitrile solution.	115
Figure B.3. UV spectrum of BA acetonitrile solution.	116
Figure C.1. $^1\text{H-NMR}$ spectrum of AA in acetonitrile- $d_3$ and the concentration of AA is same as the one in which the concentration ratio of 4HBA : AA = 1:2.	116
Figure C.2. $^1\text{H-NMR}$ spectrum of AA in acetonitrile- $d_3$ and the concentration of AA is same as the one in which the concentration ratio of 4HBA : AA = 1:4.	117
Figure C.3. $^1\text{H-NMR}$ spectrum of AA in acetonitrile- $d_3$ and the concentration of AA is same as the one in which the concentration ratio of 4HBA : AA = 1:6.	117
Figure C.4. $^1\text{H-NMR}$ spectrum of AA in acetonitrile- $d_3$ and the concentration of AA is same as the one in which the concentration ratio of 4HBA : AA = 1:8.	118
Figure C.5. $^1\text{H-NMR}$ spectrum of AA in acetonitrile- $d_3$ and the concentration of AA is same as the one in which the concentration ratio of 4HBA : AA = 1:12.	118
Figure C.6. $^1\text{H-NMR}$ spectrum of AA in acetonitrile- $d_3$ and the concentration of AA is same as the one in which the concentration ratio of 4HBA : AA = 1:16.	119
Figure D.1. $^1\text{H-NMR}$ spectrum of 4HBA in acetonitrile- $d_3$ .	119
Figure D.2. $^1\text{H-NMR}$ spectrum of AA in acetonitrile- $d_3$ .	120
Figure D.3. $^1\text{H-NMR}$ spectrum of 4HBA and AA in acetonitrile- $d_3$ in which the concentration ratio of 4HBA : AA = 1:2.	120
Figure D.4. $^1\text{H-NMR}$ spectrum of 4HBA and AA in acetonitrile- $d_3$ in which the concentration ratio of 4HBA : AA = 1:4.	121
Figure D.5. $^1\text{H-NMR}$ spectrum of 4HBA and AA in acetonitrile- $d_3$ in which the concentration ratio of 4HBA : AA = 1:6.	121

	<b>Page</b>
Figure D.6. $^1\text{H-NMR}$ spectrum of 4HBA and AA in acetonitrile- $d_3$ in which the concentration ratio of 4HBA : AA = 1:8.	122
Figure D.7. $^1\text{H-NMR}$ spectrum of 4HBA and AA in acetonitrile- $d_3$ in which the concentration ratio of 4HBA : AA = 1:12.	122
Figure D.8. $^1\text{H-NMR}$ spectrum of 4HBA and AA in acetonitrile- $d_3$ in which the concentration ratio of 4HBA : AA = 1:16.	123
Figure E.1. $^1\text{H-NMR}$ spectrum of 3HBA in acetonitrile- $d_3$ .	123
Figure E.2. $^1\text{H-NMR}$ spectrum of 3HBA and AA in acetonitrile- $d_3$ in which the concentration ratio of 3HBA : AA = 1:2.	124
Figure E.3. $^1\text{H-NMR}$ spectrum of 3HBA and AA in acetonitrile- $d_3$ in which the concentration ratio of 3HBA : AA = 1:4.	124
Figure E.4. $^1\text{H-NMR}$ spectrum of 3HBA and AA in acetonitrile- $d_3$ in which the concentration ratio of 3HBA : AA = 1:8.	125
Figure E.5. $^1\text{H-NMR}$ spectrum of 3HBA and AA in acetonitrile- $d_3$ in which the concentration ratio of 3HBA : AA = 1:12.	125
Figure F.1. Calibration graph for the standard solutions.	127

## LIST OF TABLES

	Page
Table 1.1. Summary of Scatchard analyses from the literature.	16
Table 2.1. Physical constants of acetamide and acetic acid.	39
Table 2.2. Composition in each NMR tube.	40
Table 2.3. The selectivity factors from MIP4HBA binding experiment and its chromatographic evaluation.	62
Table 2.4. Composition of each polymerization imprinted with 3HBA and 4HBA.	66
Table 3.1. Composition of each polymerization imprinted with ( <i>S</i> )-naproxen.	92
Table 4.1. Binding parameters derived from the Scatchard analysis.	103
Table 4.2. Comparison of binding parameters in three MIP systems.	105
Table 4.3. The thermophysical properties of water, acetic acid and benzoic acid at the equilibrium of solid and liquid	107
Table F.1. Binding analysis of NIP.	134
Table F.2. Calculations of $\hat{c}$ , $\hat{d}$ and their standard deviations $\sigma(\hat{c})$ and $\sigma(\hat{d})$ based on Table F.1.	136

## ABSTRACT

Molecular imprinting is a rapidly developing technique for the preparation of polymeric materials that are capable of molecular recognition for selective separation and chemical identification. To prepare molecularly imprinted polymers (MIPs), a functional monomer and a crosslinker are polymerized in the presence of a template molecule. Then the template is extracted leaving sites which are complementary in both shape and chemical functionality to those of the template. This resin then becomes capable of selectively absorbing the template species. Because of MIPs' stability, predesigned selectivity, and easy preparation, they have been used for separation, sensor, drug development and directed synthesis.

In this study, we focused on characterizing and understanding the mechanism underlying formation and recognition of MIPs. Three resins imprinted with 4-hydroxybenzoic acid, 3-hydroxybenzoic acid and 6-methoxy- $\alpha$ -methyl-2-naphthaleneacetic acid ((*S*)-naproxen) were prepared in a free radical polymerization. Hydrogen bonding between the template and functional monomer is the main interaction: it not only controls the template molecules in and out of the binding sites, but also contributes a high concentration of specific binding sites in the resulting polymer resin. After polymerization, the amount of template that can be effectively removed during each extraction was quantified in the naproxen imprinted system. For comparison, another resin was prepared under the same condition without the presence of the template, which was designated as NIP.

The binding experiments were performed for the affinity and selectivity tests. The MIP showed a special affinity for the template, but not for other analytes, which is consistent with the principle that an imprinted resin's recognition ability is dependent on the analyte's size, shape, and functionality. The NIP had similar affinities for the analytes and thus it could not differentiate among them. The binding behavior of the MIP is characterized by an association constant and the density of each kind of site using a simple two-binding-site model with one kind of sites special for the template and the others being more general with similar affinities as the NIP. The binding sites common to both the imprinted resin and the non-imprinted resin were found to have higher affinity but are less numerous than the sites unique to the imprinted resin.

**BINDING STUDIES ON  
MOLECULARLY IMPRINTED POLYMERS**

## CHAPTER 1. INTRODUCTION

### 1.1. Molecular recognition and molecular imprinting

Molecular recognition is essential for the existence of life. For example, the receptors in the cell membranes bind only a specific hormone; each enzyme exclusively chooses a specific substrate; some amino acid residues of antibodies are oriented complementarily to the functional groups of the target antigens, etc. It has been found<sup>1</sup> that in the substrate-binding sites of enzymes, several functional groups like OH, NH<sub>2</sub>, COOH, main-chain amide groups, etc., precisely interact with the complimentary functional groups of a specific substrate.

Although such biological recognition involves simple interactions, they are always in short supply and also unstable when they are not in their native environment. So, the challenge of synthesizing “artificial receptors” that are capable of molecular recognition has drawn special attention. Artificial receptors can be designed freely according to any molecule of interest; they generally possess excellent stability, flexibility and other properties according to need. Cram, Lehn and Pedersen have done some pioneering work in this area and established the following factors which are necessary for accurate molecular recognition<sup>2</sup>:

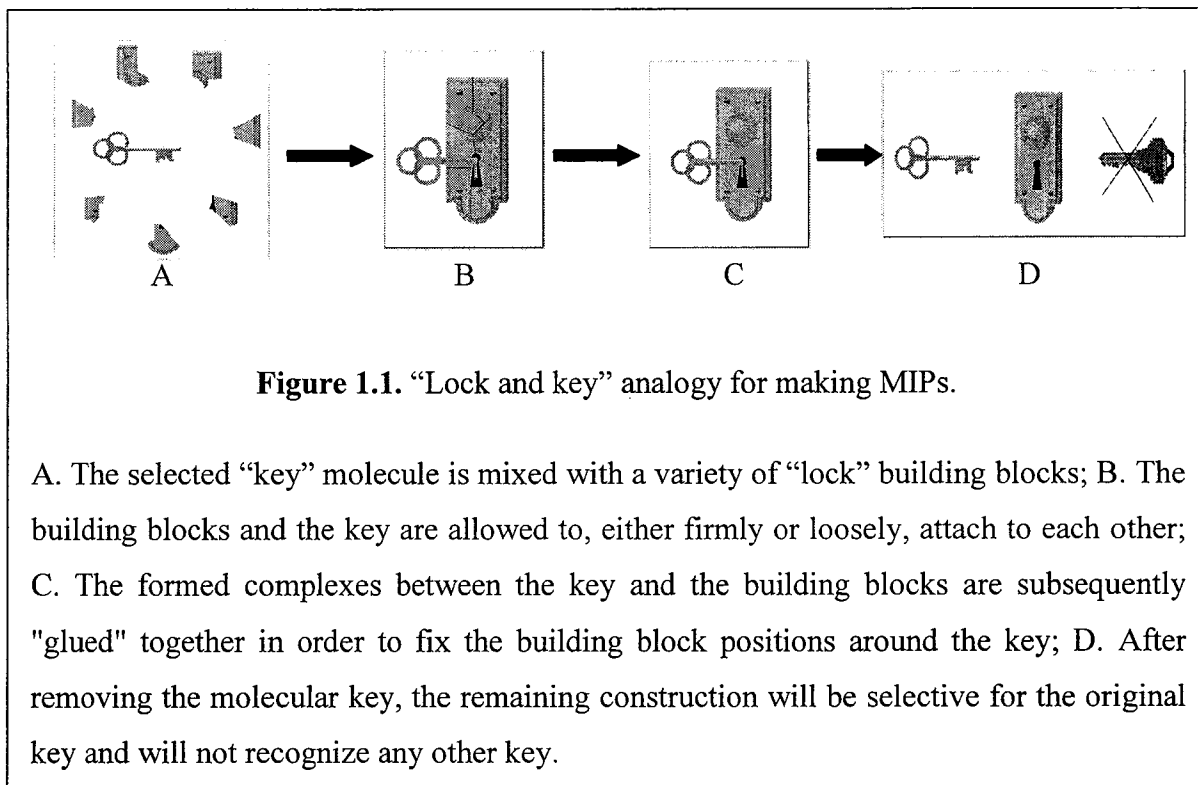
- 1) Functional residues of ligand and receptor are complementary to each other;
- 2) Conformational freedom of both components are minimized;
- 3) Chemical circumstances should be appropriately regulated.

Preparation of the molecular receptor is usually complex and requires multi-step preparative routes, so the overall yield of the final product is low.<sup>3</sup> An attractive simple approach to generate artificial macromolecular receptors is through molecular imprinting. In this method, neither complicated organic synthesis nor precise molecular design is necessary. The only requirements are functional monomers, templates, solvents and crosslinking agents. Polymerization and the subsequent template removal can result in a molecular “memory” imprinted on the polymer, which is capable of selectively binding the template.

Molecular imprinting has attracted wide interests in the scientific community. In 1972, Wulff<sup>4</sup> and Klotz<sup>5</sup> independently reported the preparation of organic polymers with predetermined ligand selectivities, which marked the start of molecular imprinting technology as we know it today.

## **1.2. Scheme to make molecularly imprinted polymers (MIPs)**

The procedure of making MIPs is usually described by making an artificial “lock” for a molecular “key” (Figure 1.1). The “lock and key” hypothesis<sup>6</sup> is often used to explain the catalytic behavior of enzymes. The enzyme has clefts and depressions complementary to the shape of the substrate. Thus, the substrate fits like a key into the lock of the enzyme's active sites.



Following the “lock-and-key” analogy, the general procedure of making MIPs has three steps (see Figure 1.2):

Step 1. Formation of the complex of a template molecule and a functional monomer. The functional monomer is defined as the monomer molecule having the functional groups responsible for the complex formation with the template molecule;

Step 2. Polymerization of such complex with crosslinking agent;

Step 3. Removal of the template from the polymeric matrix.

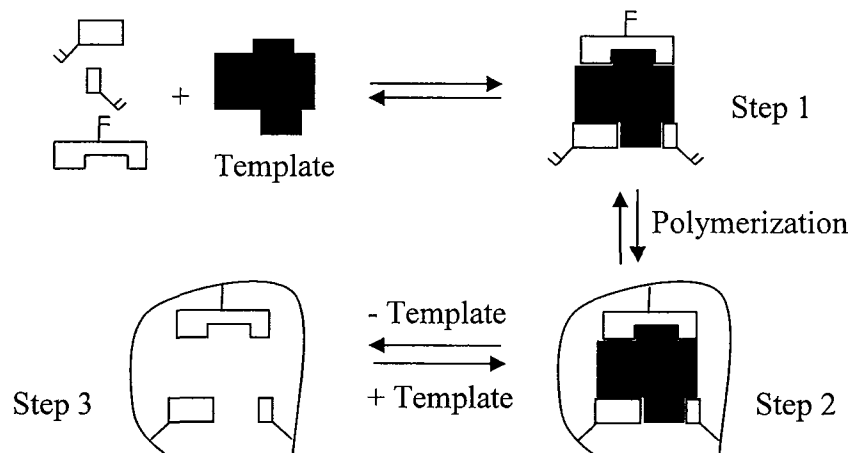


**Figure 1.2.** Scheme of making MIPs.

### 1.2.1. Principle of making MIPs

There are two basic approaches to make MIPs based on the interactions between the template molecules and the functional monomers. One is the pre-organized approach mainly developed by Wulff and his colleagues.<sup>7</sup> The template and monomer species are bonded together covalently and this template-monomer complex remains intact during the polymerization. Such covalent bonds need to be reversible in order to control the template in and out of the MIPs.

Another approach is the self-assembly approach mainly developed by Mosbach and coworkers.<sup>8,9</sup> Instead of covalent bonds, non-covalent bonds are used, such as hydrogen bonds, hydrophobic interactions, van der Waals interactions, and Coulomb interactions between ionized groups. In these cases, the template-monomer complex can be obtained simply by adding the components to a reaction mixture.

In covalent imprinting, although the polymerization conditions are not restricted and the structures of imprinted sites can be probed in detail, the synthesis of a monomer-template complex is necessary. The ligand binding and release are relatively slow due to the formation and cleavage of the covalent linkage. The resulting covalent system lacks flexibility because of the limits of the choices of monomers and templates. The non-covalent imprinting system is simple and convenient. Monomer-template complex formation and the template removal can be performed easily. But the non-covalent interaction is weak, so an excess of the functional monomer is needed, sometimes resulting in the formation of multiple types of binding sites with different affinities.

The above two approaches can be combined to take advantage of the favorable aspects of both. In this “hybrid approach”<sup>10</sup>, the MIPs are designed by covalent imprinting but the ligand binding takes place by non-covalent interactions.

The superior advantages of non-covalent imprinting methodology significantly broaden the scope of molecular imprinting, and it is this approach that will be discussed in detail.

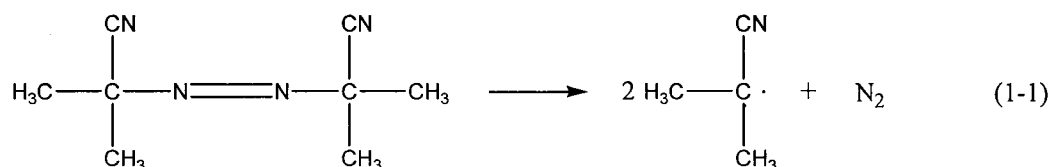
### *1.2.2. Non-covalent imprinting preparation of MIPs*

Most MIPs are prepared by free radical polymerization of functional monomers and crosslinking agents which have vinyl or acrylic groups. Depending on the template, the functional monomers can be complementarily designed to have appropriate functional groups, such as carboxyl, amino, pyridinyl, hydroxyl and amide groups, *etc.*, for the non-covalent linkage.

To preserve the integrity of the cavity in the resultant MIP, a very high degree of crosslinking (70-90%) is necessary. Ethylene glycol dimethacrylate (EGDMA) is one of the most widely used crosslinking agents. The reactivity of the crosslinking agent should be similar to that of the functional monomer to ensure the functional monomer and the crosslinking agent's sufficient copolymerization. In addition, by choosing an appropriate crosslinking agent and the suitable mole ratio of crosslinking agent to functional monomer, the functional groups, which are responsible for the monomer-template complex formation, can be distributed in the polymer network.

The solvent used in the reaction is also called porogen. It plays an important role in the molecular imprinting process especially in the self-assembly system. Besides helping to dissolve the agents for polymerization and dispersing the heat generated during the reaction, most importantly, the solvent provides a macroporous structure to determine the polymer morphology and affects the strength of non-covalent interactions.<sup>11</sup> In the recognition step, similar questions about the choice of solvent exist. Since all non-covalent interactions are influenced by the properties of the solvent, non-polar solvents normally lead to the best recognition. Also, the solvent affects the resin's morphology since swelling of the polymers is dependent on the medium. For many systems, swelling is pronounced in chlorinated solvents, such as chloroform and dichloromethane, as compared to solvents like acetonitrile and tetrahydrofuran.<sup>12</sup> This swelling behavior may lead to changes in the three-dimensional configuration of the functional groups taking part in the recognition in the sites resulting in poorer binding capability. So, in order to avoid any swelling problems, the best choice of recognition solvent is generally either the imprinting porogen or similar solvent although this is not necessarily a prerequisite.

Free radical polymerization is most commonly used in the preparation for MIPs not only because of its versatile applicability and experimental ease, but also for economic reasons. Currently it is most widely used in industry.<sup>13</sup> The polymerization can be initiated by thermal decomposition of radical initiators, such as 2,2'-azobis(isobutyronitrile) (AIBN) (Equation (1-1)).

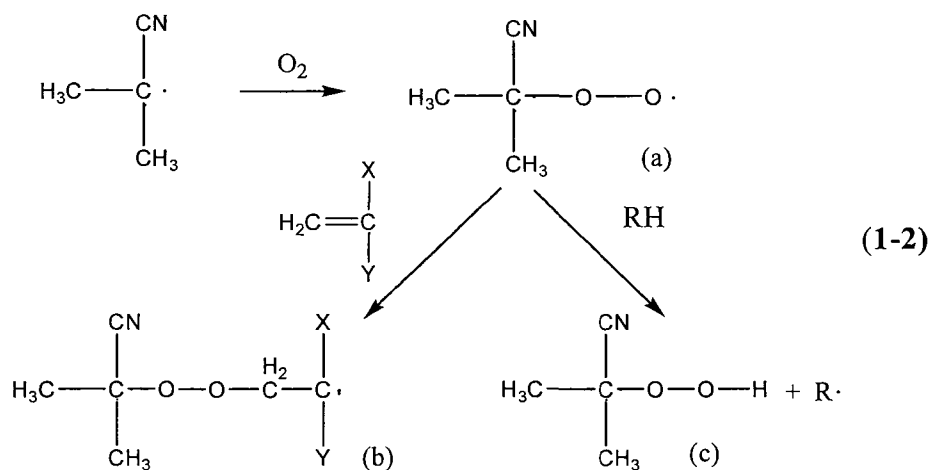


The initiating radical (e.g., alkyl radical from AIBN's decomposition) formed by the decomposition attacks the monomer, producing the propagating radicals. As mentioned above, ideally, the reactivity of the monovinyl functional monomer and the divinyl crosslinking agent should be close, which means the possibility of those two kinds of propagating radicals formation is close. This will ensure the random copolymerization. At the beginning of polymerization, the primary polymer chains are still soluble; as the reaction proceeds, chain growth and cross-linking cause the polymer to separate from the solution. It is important to control the rate of the radical production. If the rate is too high, a large concentration of reactive centers is generated leading to early termination and low molecular weight; if the rate is too low, the polymerization will not be complete within a practicable time frame.

A second method of getting free radicals is through photo initiation. It is used especially in cases where a non-covalent complex between the template and functional monomer is unstable at higher temperatures. In the photochemically initiated

polymerizations, the intensity of the UV light, the distance from the light source and the penetration depth affect the rate of radical production.

In the free-radical polymerization, it is very important to remove oxygen because oxygen can add to the initial free radical to form a hydroperoxy radical (Equation (1-2) (a)). This new formed radical can be a chain transfer agent or a polymerization retardant by either initiating polymerization to form a relatively unstable peroxidic end group (Equation (1-2) (b)) or showing an enhanced tendency to abstract hydrogen from polymer, monomer, or other components in the system (Equation (1-2) (c)).<sup>14</sup> Degassing with nitrogen or argon as well as freeze-and-thaw procedures under reduced pressure are very helpful. In some cases, the low temperature employed in polymerization initiated by UV light helps to stabilize the functional monomer – template complex.



### *1.2.3. Characteristics and applications of MIPs*

Besides the obvious recognition properties of MIPs, their physical and chemical characteristics are highly appealing.<sup>15</sup> Because of their highly crosslinked nature, they exhibit high physical and chemical resistance towards various external-degrading factors. They are typically very stable against mechanical stress, elevated temperatures and high pressures, resistant against treatment with acid, base or metal ions and stable in a wide range of solvents. They can be stored for several years at ambient temperature without apparent reduction in performance. They can be used repeatedly, sometimes in excess of 100 times, without loss of the "memory effect". In comparison with natural biological recognition sites, such as proteins, these properties are highly advantageous.

The preparation of molecular imprinting resins can be simple and inexpensive and MIPs are very stable, which make MIPs ideal for molecular recognition prepared through the rational design. A great variety of chemical compounds have been imprinted successively, including drugs<sup>16,17</sup>, herbicides<sup>18,19</sup>, metal ions<sup>20</sup>, micro-organism<sup>21</sup>, proteins<sup>22,23</sup>, steroids<sup>24,25</sup>, amino acids<sup>26,27</sup>, sugars<sup>28,29</sup>, nucleic acids and their derivatives<sup>30</sup>, and polynuclear aromatic hydrocarbons<sup>31</sup>.

Four main areas of applications for MIPs<sup>11,32</sup> have been developed: (1) separation; (2) sensors; (3) drug development and screening and (4) directed synthesis. Since MIPs possess molecular memory, a Swedish startup company has commercialized them as solid-phase extraction (SPE) materials. MIPs' superior stability makes MIPs candidates for element recognition in sensors' application. Sensors usually consist of a chemically sensitive layer, a transducer and an electronic data collection and processing system. The main components of the MIP sensors are an imprinted sensitive layer and a transducer

which can convert the chemical information into an electrical or optical signal. The selective enrichment of the analyte in the sensitive MIP layer alters the properties of the coating physicochemically so that it changes the sensor response in mass, fluorescence, absorbance, resistance or capacitance. In particular, the quartz crystal microbalance, an acoustic transducer, has become very popular due to its comparatively low price, robustness and ease of use.<sup>33</sup> A high-performance MIP-based assay using chemiluminescence-imaging format as a screening tool was reported, which broadens the drug development and screening.<sup>34</sup> In the study of some enzyme-catalyzed reactions, the enzymes needed to be isolated. The use of MIPs might help to eliminate this step by having MIPs be employed as synthetic receptors or molecular-scale reaction vessels to direct the synthesis.<sup>17,35</sup>

### **1.3. Properties of binding sites in MIPs**

#### *1.3.1. Experimental methods for the characterization of MIPs*

The purpose and glamour of molecular imprinting technique are that after imprinting, the formed polymeric materials contain recognition sites of the predetermined specificity. With hundreds of reports of specific rebinding of the template in MIPs, the properties of binding sites are worthy of study. Basically, there are two experimental methods to study the ligand binding activity of the MIPs, liquid chromatography and batch binding experiments. (Figure 1.3)

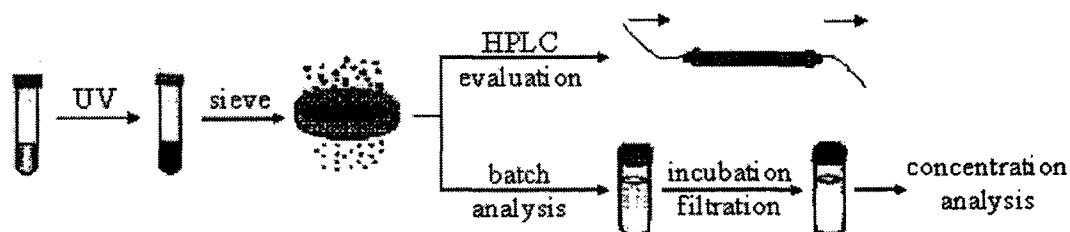


**Figure 1.3.** Two experimental methods to evaluate the binding sites of MIPs.

In the chromatographic method, bulk MIPs are prepared, ground and size selected. Then, the MIPs particles are packed into a stainless steel column and used as the stationary phase for high performance liquid chromatography (HPLC). The binding strength and selectivity of MIPs toward ligand molecules are analyzed in terms of their chromatographic behavior. Successful imprinting selectively promotes the binding of template molecules, increasing their retention time.

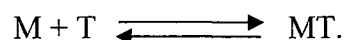
In the batch method, the ligand-binding activity of MIPs can be directly determined in terms of the amount of ligand bound by MIPs. After the extraction of the templates from MIPs, some amount of MIPs is incubated in a ligand solution at various concentrations until the binding reaches equilibrium. After filtration, the concentration of ligand in the liquid phase can be determined by chromatographic, spectroscopic or other analytical methods. By comparing the amounts of different ligands bound in the polymer, the selectivity of the MIPs can be studied. This method was used in this research.

### 1.3.2. Models used for binding evaluation on MIPs

From batch analysis results, adsorption isotherms can be obtained, which provide the information about the number and properties of binding sites. The isotherms can be fitted by some kind of model under different assumptions. Those models are reviewed here.

#### 1.3.2.1. Scatchard analysis

The substrate's binding process is an equilibrium and can be described as:



Define [M] to be the concentration of empty sites in the resin (mmol of empty sites / g of resin); [T], the concentration of substrate in solution (mmol/L); and [MT], the concentration of substrate bound in the resin at equilibrium ( $\mu\text{mol/g}$  of resin), with the latter calculated from the difference between the moles of the free substrate and the initial substrate.

At equilibrium, the equilibrium binding constants can be defined either as an association constant or affinity constant ( $K_a$ ) for MT

$$K_a = \frac{[MT]}{[M][T]}$$

or as a dissociation constant ( $K_d$ )

$$K_d = \frac{[M][T]}{[MT]} = \frac{1}{K_a}.$$

Another property of template-binding site interactions is saturability; that is, only a finite number of specific binding sites exist per unit of resin. The maximum number of the binding sites per unit mass of the resin is designated as  $[MT]_{\max}$ ,

$$[MT]_{\max} = [M] + [MT].$$

Combining this with the definition of  $K_a$  yields

$$\frac{[MT]}{[T]} = -K_a [MT] + K_a [MT]_{\max}. \quad (1-3)$$

This is the Scatchard equation.<sup>36</sup> Thus, plotting the  $[MT]/[T]$  against  $[MT]$  should yield the equilibrium binding constant ( $K_a$ ) and the maximum number of binding sites ( $[MT]_{\max}$ ) from the slope and intercept. The Scatchard equation assumes that all of the binding sites in an MIP are independent and identical, i.e., each with the same intrinsic binding properties.

Not all binding studies reported in the literature yield linear Scatchard plots over the range of concentrations studied. Some data are better represented by a broken line (Figure 1.4 (b)). The binding reported in 17 different systems is summarized in Table 1.1. The Scatchard plots for last eight systems are linear, consistent with only one kind of binding site in the MIP. In the rest of the systems, the Scatchard plots are not linear, but rather have two distinct sections within the plot which can be regarded as two straight lines.

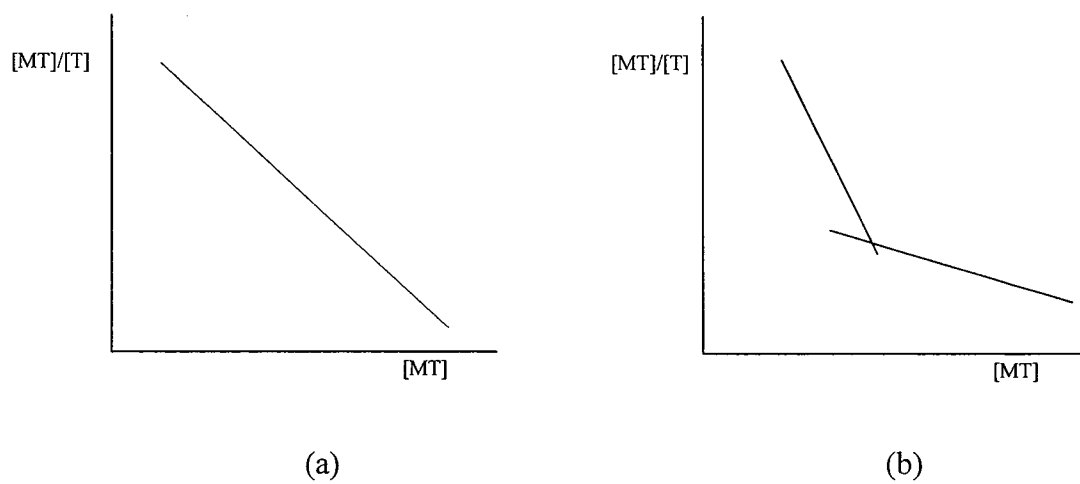


**Figure 1.4.** Two kinds of Scatchard plots shown in literature: (a) and (b).

**Table 1.1.** Summary of Scatchard analyses from the literature.

Template	MIPs Synthesis				Extraction Solvent <sup>d</sup>	Rebinding Solvent <sup>d</sup> , conc (mM)	High Affinity		Low Affinity		Ref
	Mono. <sup>a</sup>	Xlink <sup>b</sup>	M:X:T <sup>c</sup>	Solvent <sup>d</sup>			Ka (L/mmol)	[MT] <sub>max</sub> (μmol/g)	Ka (L/mmol)	[MT] <sub>max</sub> (μmol/g)	
4-aminopyridine	maa	egdma	4:20:1	dmf	ma/aa	membrane; w, 0.1-4.0	1.85	49	0.3	50	37
4-hydroxybenzoic acid	a	egdma	6:30:1	acn	ma/aa	acn, 0-2.5	5.6	9	0.7	22	38
cefalexin	tfmaa	egdma	4:20:1	ma	ma/aa	w, 0.1-4.5	7.1	30	0.4	130	39
cefalexin	tfmaa+4vp	egdma	12:30:1	ma	ma/w	w, 0-4.5	7.1	28	0.36	157	40
norfloxacin	maa	egdma	6:30:1	c/dmf	ma/aa	c/dmf, 0-4.5	11.1	23	0.5	128	41
(5R)-5-benzylhydantoin	a	egdma	4:20:1	acn	ma/aa	acn, 0-30	20	40	7.7	48	42
4-aminopyridine	maa	egdma	4:30:1	c	ma/aa	acn, 0-4.5	161	78	2.3	223	43
/ <sup>e</sup>	bpadma	egdma	1:29:/	c	NaOH/HCl/MeOH	c, 0-1.0	172	10.7	n/a	n/a	44
5,5-diphenylhydantoin	a	egdma	4:20:1	thf	ma/aa	acn, 0.05-4.0	476	17	0.6	104	45
cortisol	maa	egdma	13:65:1	thf	ma/aa	thf, 0.03-20 mg/mL	1.7	0.2	0.6	280	46
corticosterone	maa	egdma	13:65:1	thf	ma/aa	thf, 0.03-20 mg/mL	0.8	0.4	1.3	130	46
2-aminopyridine	maa	egdma	4:30:1	c	ma/aa	acn, 0-4.0	0.4	136	--	--	47
paracetamol	a	egdma	4:40:1	acn	ma/aa	acn, 0-4.5	0.4	126	--	--	48
testosterone	maa	egdma	8:25:1	c	acn	acn, 0-1.5	0.9 (UV), 1.3 (HPLC)	0.6 (UV), 0.4 (HPLC)	--	--	49
trimethoprim	maa	egdma	6:30:1	c	acn/aa	c, 0.5-9.0	5	202	--	--	50
trimethoprim	maa	trim	4:4:1	acn	acn	membrane; acn, 0-4.5	20	290	--	--	51
(-)-cinchonidine	maa	egdma	2.5:75:1	c	acn/ma	dcm; 0-2.0	6.7×10 <sup>3</sup>	4.0	--	--	52
	zp	egdma	2.5:75:1	c	acn/ma	dcm; 0-2.0	1.4×10 <sup>3</sup>	3.8	--	--	
	maa+zp	egdma	3.5:75:1	c	acn/ma	dcm; 0-2.0	1.1×10 <sup>4</sup>	5.3	--	--	

**Table 1.1.** Summary of Scatchard analyses from the literature. (*Continued*)

<sup>a</sup> Monomer abbreviations: a, acrylamide; maa, methacrylic acid; tfmaa, 2-(trifluoromethyl)acrylic acid; bpadma, bisphenol A dimethacrylate; 4vp, 4-vinylpyridine; zp, zinc porphyrin.

<sup>b</sup> Crosslinker abbreviations: egdma, ethylene glycol dimethacrylate; trim, tris(hydroxymethyl) propane trimethacrylate.

<sup>c</sup> Molar proportions of monomer:crosslinker:template.

<sup>d</sup> Solvent abbreviations: aa, acetic acid; acn, acetonitrile; c, chloroform; dmf, dimethyl formamide; dcm, dichloromethane; ma, methyl alcohol; thf, tetrahydrofuran; w, water.

<sup>e</sup> In this paper, covalent imprinting was used in which bisphenol A dimethacrylate was the monomer. Bisphenol A was used for rebinding.

### 1.3.2.2. Model of multiple independent classes of binding sites

Zhou *et al.* firstly used a multisite binding model in a binding study on 5,5-diphenylhydantoin imprinted polymer in which acrylamide was the functional monomer and ethylene glycol dimethacrylate was the crosslinker.<sup>45</sup> From their Scatchard plot, similar to Figure 1.4 (b), two classes of binding sites were postulated for MIPs. To permit quantitative characterization of the polymer, they wrote the equilibrium binding equation as Equation (1-4)

$$[MT] = [MT]_1 + [MT]_2 = \frac{K_{a,1}[MT]_{\max,1}[T]}{1 + K_{a,1}[T]} + \frac{K_{a,2}[MT]_{\max,2}[T]}{1 + K_{a,2}[T]} \quad (1-4)$$

where  $[MT]_{\max,1}$  and  $[MT]_{\max,2}$  are the apparent maximum numbers for two kinds of binding sites, respectively, and  $K_{a,1}$  and  $K_{a,2}$  are the related equilibrium association constants.

The initial binding parameters were obtained in two different concentration ranges by Scatchard analysis (Equation (1-3)) respectively:  $K_{a,1} = 476$  L/mmol,  $[MT]_{\max,1} = 17.2$   $\mu\text{mol/g}$ ;  $K_{a,2} = 0.6$  L/mmol,  $[MT]_{\max,2} = 104$   $\mu\text{mol/g}$ . Using these binding parameter values as initial estimates in Equation (1-4), the fitting curve was in a good agreement with the experimental points. The final estimates for the binding parameters were  $K_{a,1}' = 110$  L/mmol,  $[MT]_{\max,1}' = 10.0$   $\mu\text{mol/g}$ ;  $K_{a,2}' = 0.5$  L/mmol,  $[MT]_{\max,2}' = 94.6$   $\mu\text{mol/g}$ . Zhou and his colleagues thought the values obtained by this model are more reasonable because this method overcame the limit of the ligand concentration used in the experiment.

### 1.3.2.3. Affinity spectrum (AS) method

Other models have been proposed to try to account for the nonlinearity found in many Scatchard plots. The heterogeneity among the binding sites in the MIP resins is presumed. One such method, introduced by Shimizu and coworkers<sup>53,54</sup> use a continuum of affinity constants. Their approach is described next.

Shimizu *et al.* started from the Langmuir-Freundlich (LF) isotherm (Equation (1-5)), also known as the Sips equation<sup>55,56</sup>

$$[MT] = \frac{N_t a [T]^m}{1 + a [T]^m}, \quad (1-5)$$

to describe the relationship between the equilibrium concentration of bound [MT] and free ligand [T] in heterogeneous systems with three fitting coefficients:  $N_t$ , the total number of the binding sites;  $a$ , a variable related to the median binding affinity ( $K_0$ ) via  $K_0 = a^{1/m}$ ;  $m$ , the heterogeneity index which varies from 0 to 1. For a homogeneous system,  $m = 1$ ; for a heterogeneous system,  $m < 1$ . When  $m = 1$ , the LF equation (1-5) changes into the Langmuir isotherm (Equation (1-6))

$$[MT] = \frac{N_t a [T]}{1 + a [T]}. \quad (1-6)$$

In this case, when  $a = K_a$ , it is similar to the Scatchard equation:

$$[MT] = \frac{K_a [MT]_{\max} [T]}{1 + K_a [T]}. \quad (1-7)$$

So the Scatchard analysis (see section 1.3.2.1) is an application of the Langmuir isotherm.

When either  $[T]$  or  $a$  approaches 0, the LF equation reduces to the Freundlich isotherm (Equation (1-8)):

$$[MT] = a[T]^m. \quad (1-8)$$

The Freundlich isotherm is known to be an excellent approximation of the binding behavior of many heterogeneous solid surfaces,<sup>57</sup> provided that the concentration of the ligand is not too high or too low. The Freundlich isotherm fails as the surface approaches saturation because the Freundlich isotherm is a power function and increases indefinitely.

By combining the ability of the Freundlich isotherm modeling heterogeneity with that of the Langmuir isotherm modeling homogeneity, the LF isotherm (Equation (1-5)) is expected to model both homogeneous and heterogeneous systems. The LF model has been successfully used to describe the adsorption behavior of many heterogeneous systems, including gas adsorption onto surfaces,<sup>58</sup> ligand affinity to polyclonal antibodies<sup>59</sup> and adsorption of metal ions to environmental samples.<sup>60</sup>

For heterogeneous binding systems such as the MIP resins that do not exhibit Scatchard behavior, the corresponding affinity distribution  $N(K)$ , for the number of sites having an association  $K$ , was needed. Shimizu *et al.* found this function from the integral of the Langmuir adsorption:

$$[MT] = \int_{-\infty}^{\infty} \frac{N(K)[T]K}{1+[T]K} d(\log K). \quad (1-9)$$

There are many numerical approximation techniques to calculate  $N(K)$ . Shimizu *et al.* selected Hunston's numerical approximation technique to solve the integral.<sup>61</sup> The result was

$$N_i = \left| \frac{(B_1 - B_2)}{2 \log a} - \frac{a[(B_3 - B_4) - 2(B_1 - B_2)]}{2(a-1)^2 \log a} \right|. \quad (1-10)$$

This equation calculates the number of binding sites ( $N_i$ ) having an association constant of  $K_i$  by using the concentration values of bound template molecule interpolated from four points on the experimental isotherm  $B_1, B_2, B_3, B_4$ . They can be calculated from the following relationships, in which the  $B_1, B_2, B_3, B_4$  values are obtained by taking four  $[T]$  values back into the LF isotherm equation:

$$a = \text{constant} > 1.0 \text{ (typically } a = 10^{0.2}\text{)};$$

$$\text{at } [T] = \frac{a}{K_i}, B_1 = [MT];$$

$$\text{at } [T] = \frac{1}{aK_i}, B_2 = [MT];$$

$$\text{at } [T] = \frac{a^2}{K_i}, B_3 = [MT];$$

$$\text{at } [T] = \frac{1}{a^2 K_i}, B_4 = [MT].$$

So the affinity distribution function can be resolved as

$$N_i = N_i a m \frac{\left(\frac{1}{K_i}\right)^m}{\left[1 + a\left(\frac{1}{K_i}\right)^m\right]^4} \left[1 + 2a\left(\frac{1}{K_i}\right)^m + a^2\left(\frac{1}{K_i}\right)^{2m} + 4a\left(\frac{1}{K_i}\right)^m m^2 - a^2\left(\frac{1}{K_i}\right)^{2m} m^2 - m^2\right].$$

(1-11)

Equation (1-11) is a general function for the affinity distribution for the LF binding model. It calculates the number of binding sites ( $N_i$ ) having association constant ( $K_i$ ) by using the LF fitting parameters  $a$ ,  $m$  and  $N_t$ .

An affinity distribution obtained from the AS method is a plot of the number of binding sites ( $N$ ) against those binding sites' association constant ( $K$ ). Shimizu pointed out that this method can more appropriately model heterogeneity as a continuous distribution of binding affinities. The resulting affinity distribution could give not only a quantitative measure of the number of binding sites with respect to binding affinity, but also a measure of the breadth of the heterogeneity for comparison.

The AS method does not require any change on the experimental procedure of batch analysis. Shimizu also mentioned that the AS method is limited by the analytical window due to the ligand solubility, sensitivity of the concentration measurement, etc., as well as the Scatchard analysis<sup>62</sup> while calculating the concentration of binding sites. It should be noted that, in the numerical approximation, only four points are selected in the whole initial ligand concentration range. Hopefully they can best approximate the result besides simplifying the whole resolving process. In addition, the selection for the value of  $a$  is arbitrary.

#### **1.4. Motivation for this work from previous studies**

In summary, many studies of molecular imprinting have been reported in the literature. Most have focused on the utility of the method, addressing its effectiveness as

a tool for separation and identification<sup>16-32</sup>. There have been occasional attempts to understand the phenomenon of molecular imprinting by modeling<sup>45,53,54,62</sup>. Most commonly, these approaches have employed the Scatchard method, either the simple form in which only one kind of binding site is identified<sup>47-52</sup> or a Scatchard-like treatment of two independent classes of binding sites<sup>37-46</sup>. In the second case, the analyses have treated one kind of binding over one range of concentration and the second kind of binding over a different range of concentration, rather than both over the continuum of concentrations. In another attempt to model molecular imprinting, the affinity-spectrum approach by Shimizu heavily emphasizes the distribution of binding affinities among the sites in an MIP resin and results in a complex mathematical model employing parameters that do not have obvious relationships to the chemical system being examined<sup>45,53,54,62</sup>. Finally, notwithstanding the important fact that the nonimprinted resins (NIPs) also bind solute species, only rarely have investigators included the NIP as a reference in their binding studies of imprinted systems<sup>63-65</sup>. One study<sup>63</sup> that recognized binding at NIP sites reported only binding isotherms for MIP and NIP without further analysis. Other research<sup>64,65</sup> that considered NIP sites divided the concentration range into two distinct regions. In each region the NIP isotherm was subtracted from the MIP isotherm to yield separate  $K_d$  values for binding in each concentration range without a clear explanation for why the equilibrium constant might differ at different concentrations.

The studies conducted for this dissertation incorporate the effects of binding that are found in NIP as well as in MIP resins. They also correct the Scatchard-like treatment of two independent classes of binding sites so that both classes of binding sites are operative over the full range of concentrations.

### 1.5. Proposal for this study

The molecular imprinting technique has been widely accepted in various disciplines for a long period with most of the research mainly focused on the synthesis and more practical purposes. However, in the recognition-based applications of MIPs, a notable difficulty is the low yield of high affinity binding sites. Other difficulties reside in the understanding and characterization of the binding sites in MIPs. The selectivity and affinity of MIPs are mainly affected by the properties of the monomers and templates and the interactions between them. Therefore, an understanding of the physical and chemical processes governing the formation of monomer-template complexes in the imprinting process and the subsequent recognition is fundamental for the design of MIPs.

In this study, three template molecules 4-hydroxybenzoic acid, 3-hydroxybenzoic acid and 6-methoxy- $\alpha$ -methyl-2-naphthaleneacetic acid ((*S*)-naproxen) were imprinted respectively. Based on the different functional groups attached to the template molecule, either 4-vinylpyridine or acrylamide was selected as the functional monomer to noncovalently bond with the template. In order to understand the mechanism underlying the formation and recognition of MIPs, the monomer-template complexes before each polymerization were characterized by different spectroscopic analyses. The behavior of the binding in each MIP was studied by batch analyses between the template itself and its structure related molecules. A summary of the principle components of the experiments is shown in Figure 1.5.

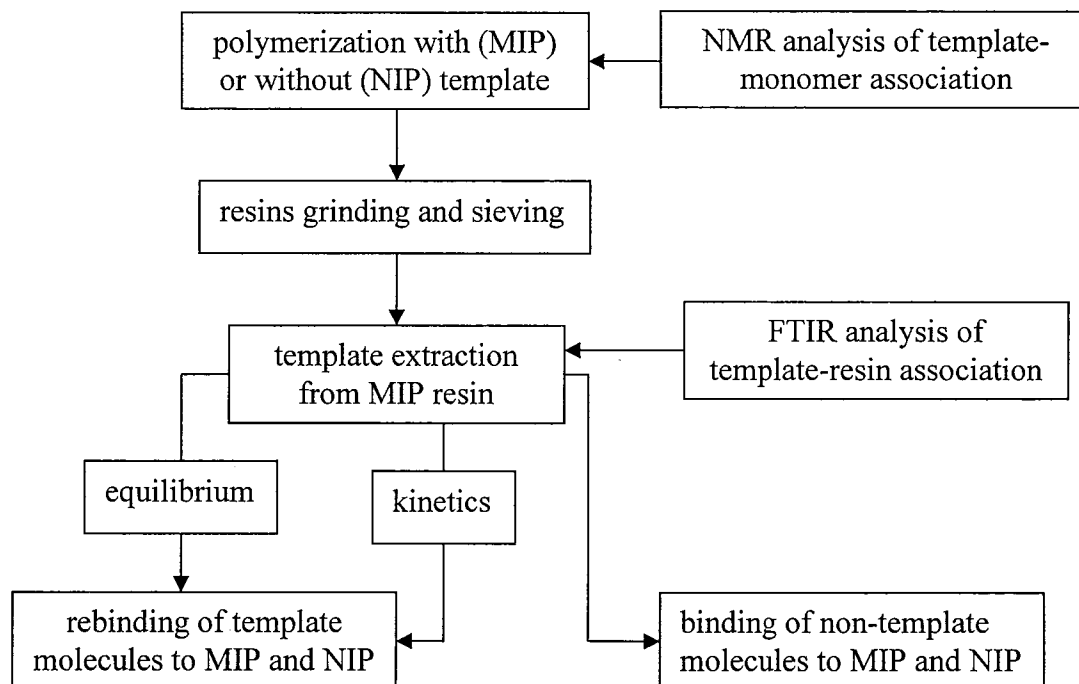


**Figure 1.5.** The experimental scheme used in this study to make MIPs and NIPs.

**REFERENCES**

1. Stryer, L. *Biochemistry*; 3rd ed.; W. H. Freeman and Co.: New York, 1988.
2. Lehn, J. M. *Supramolecular Chemistry*; VCH: Weinheim, 1995.
3. Maeda, M.; Bartsch, R. A. In *Molecular and ionic recognition with imprinted polymers*, 1998; Vol. 703.
4. Wulff, G.; Sarhan, A. *Angew. Chem.* **1972**, *84*, 364.
5. Takagishi, T.; Klotz, I. M. *Biopolymers* **1972**, *11*, 483.
6. Garrett, R. H.; Grisham, C. M. *Biochemistry*; 2nd ed.; Saunders College Publishing, 1998.
7. Wulff, G.; Grobe-Einsler; Sarhan, A. *Makromol. Chem.* **1977**, *178*, 2817.
8. Arshady, R.; Mosbach, K. *Makromol. Chem.* **1981**, *182*, 687.
9. Vlatakis, G.; Andersson, L. I.; Muller, R.; Mosbach, K. *Nature* **1993**, *361*, 645.
10. Whitcombe, M. J.; Rodriguez, M. E.; Villar, P.; Vulfson, E. N. *J. Am. Chem. Soc.* **1995**, *117*, 7105.
11. Hu, Y. Master Thesis, College of William and Mary, 2001.
12. Sellergren, B.; Shea, K. J. *Chromatogr.* **1993**, *635*, 31.
13. Komiyama, M.; Takeuchi, T.; Mukawa, T.; Asanuma, H. *Molecular Imprinting: From Fundamentals to Applications*; WILEY-VCH: New York, 2002.
14. Moad, G.; Solomon, D. H. *The Chemistry of Free Radical Polymerization*; Elsevier Science Ltd, 1995.
15. Ramström, O.; Ansell, R. *J. Chirality* **1998**, *10*, 195.
16. Mosbach, K.; Ye, L. In *PCT Int. Appl.*; (Swed.). Wo, 2003; 2003027047; 25 pp.
17. Yu, Y.; Ye, L.; Haupt, K.; Mosbach, K. *Angew Chem.* **2002**, *41*, 4460.

18. Zhu, Q.; Degelmann, P.; Niessner, R.; Knopp, D. *Environmental Science and Technology* **2002**, *36*, 5411.
19. Zhu, Q.; Haupt, K.; Knopp, D.; Niessner, R. *Analytica Chimica Acta* **2002**, *468*, 217.
20. Murray, G. M. In *U.S. Pat. Appl. Publ.*; (USA). Us, 2003; 2003113234; 15 pp.
21. Aherne, A.; Alexander, C.; Payne, M. J.; Perez, N.; Vulfson, E. N. *J. Am. Chem. Soc.* **1996**, *118*, 8771.
22. Fu, Q.; Sanbe, H.; Kagawa, C.; Kunimoto, K.; Haginaka, J. *Anal. Chem.* **2003**, *75*, 191.
23. Martin, M. T. In *U.S. Pat. Appl. Publ.*; (USA). Us, 2003; 2003100000; 43 pp.
24. Dong, H.; Tong, A.; Li, L. *Spectrochimica Acta, Part A: Molecular and Biomolecular Spectroscopy* **2003**, *59A*, 279.
25. Hishiya, T.; Asanuma, H.; Komiyama, M. *J. Am. Chem. Soc.* **2002**, *124*, 570.
26. Titirici, M. M.; Hall, A. J.; Sellergren, B. *Chemistry of Materials* **2003**, *15*, 822.
27. Kondo, Y.; Morita, Y.; Fujimoto, A.; Tounai, M.; Kimura, S.; Yoshikawa, M. *Chirality* **2003**, *15*, 498.
28. Liu, X.; Dordick, J. S. *J. of Poly. Sci., Polym. Chem. Ed.* **1999**, *37*, 1665.
29. Haginaka, J. *Bioseparation* **2002**, *10*, 337.
30. Turkewitsch, P.; Wandelt, B.; Darling, G. D.; Powell, W. S. *Anal. Chem.* **1998**, *70*, 2771.
31. Dickert, F. L.; Tortschanoff, M.; Fischerauer, G.; Bulst, W. E. *Anal. Chem.* **1999**, *71*, 4559.
32. Haupt, K. *Anal. Chem.* **2003**, *377A*.

33. Dickert, F. L.; Hayden, O.; Lieberzeit, P. A.; Palfinger, C. In *Materials Research Society Symposium Proceedings*, 2002; Vol. 723, p 25.
34. Surugiu, I.; Danielsson, B.; Ye, L.; Mosbach, K.; Haupt, K. *Anal. Chem.* **2001**, *123*, 2901.
35. Mosbach, K.; Yu, Y.; Andersch, J.; Ye, L. *J. Am. Chem. Soc.* **2001**, *123*, 12420.
36. Yamamura, H. I.; Kuhar, M. J. *Neurotransmitter, Receptor Binding*; 2nd ed.; Raven Press: New York, 1985.
37. Guo, H.; He, X.; Liang, H. *Fresenius J. Anal. Chem* **2000**, *368*, 763.
38. Zhang, T.; Liu, F.; Chen, W.; Wang, J.; Li, K. *Anal. Chim. Acta* **2001**, *450*, 532.
39. Guo, H.; He, X. *Fresenius J. Anal. Chem.* **2000**, *368*, 461.
40. Guo, H.; He, X. *Chinese J. Anal. Chem.* **2000**, *28*, 1214.
41. Guo, H.; He, X.; Zhou, J.; Liang, H. *Chinese J. Anal. Chem.* **2001**, *29*, 128.
42. Zhou, J.; He, X.; Li, Y. *Anal. Commun.* **1999**, *36*, 243.
43. Guo, H.; He, X.; Jing, Y.; Liang, H. *Chem. J. Chinese Univ.* **2001**, *22*, 739.
44. Ikegami, T.; Mukawa, T.; Nariai, H.; Takeuchi, T. *Analytica Chimica Acta* **2004**, *504*, 131.
45. Zhou, J.; He, X.; Li, Y. *Anal. Chim. Acta* **1999**, *394*, 353.
46. Ramström, O.; Ye, L.; K., M. *Chemistry & Biology* **1996**, *6*, 471.
47. Zhou, J.; He, X. *Anal. Chim. Acta* **1999**, *381*, 85.
48. Guo, H.; He, X.; Deng, C.; Li, Y. *Chem. J. Chinese Univ.* **2000**, *21*, 363.
49. Cheong, S.; Rachkov, A. E.; Park, J.; Yano, K.; Karube, I. *J. Polym. Sci.: Part A: Polym. Chem.* **1998**, *36*, 1725.
50. Zhou, J.; He, X.; Zhao, J.; Shi, H. *Chem. J. Chinese Univ.* **1999**, *20*, 204.

51. Guo, H.; He, X.; Gan, Y.; Li, W.; Liang, H. *Acta Chim. Sinica* **2001**, *59*, 262.
52. Takeuchi, T.; Mukawa, T.; Matsui, J.; Higashi, M.; Shimizu, K. D. *Anal. Chem.* **2001**, *73*, 3869.
53. Umpleby, R. J., II; Bode, M.; Shimizu, K. D. *Analyst* **2000**, *125*, 1261.
54. Umpleby, R. J., II; Baxter, S. C.; Chen, Y.; Shah, R. N.; Shimizu, K. D. *Anal. Chem.* **2001**, *73*, 4584.
55. Sips, R. *J. Chem. Phys.* **1948**, *16*, 490.
56. Sips, R. *J. Chem. Phys.* **1950**, *18*, 1024.
57. Khan, A. R.; Riazi, M. R.; Al-roomi, Y. A. *Sep. Purif. Technol.* **2000**, *18*, 273.
58. Charmas, B.; Leboda, R. *J. Chromatogr. A* **2000**, *886*, 133.
59. Larrson, A. *Mol. Immunol.* **1988**, *25*, 1239.
60. Ardebrant, H.; Pugh, R. J. *Colloids Surf.* **1991**, *53*, 101.
61. Hunston, D. L. *Anal. Biochem.* **1975**, *63*, 99.
62. Umpleby, R. J., II; Shimizu, K. D. *Polymer Preprints* **2001**, *42*, 671.
63. Mosbach, K.; Te, L.; Yu, Y. In *PCT Int. Appl.*; (Smithkline Beecham P.L.C., UK).  
Wo, 2002; 2002022846; 21 pp.
64. Quaglia, M.; Chenon, K.; Hall, A. J.; De Lorenzi, E.; Sellergren, B. *J. Am. Chem. Soc.* **2001**, *123*, 2146.
65. Shea, K. J.; Spivak, D.; Sellergren, B. *J. Am. Chem. Soc.* **1993**, *115*, 3368.

## CHAPTER 2. BINDING STUDIES ON RESINS IMPRINTED WITH HYDROXYBENZOIC ACID ISOMERS

### 2.1. Hydroxybenzoic acid isomers

MIPs have been widely used to identify and separate optical and positional isomers. The research described here includes an investigation of molecular imprinting using resins imprinted with isomers of hydroxybenzoic acid and related compounds.

The *ortho* isomer of hydroxybenzoic acid is salicylic acid (SA), whose structure is shown in Figure 2.1. SA has considerable commercial importance. Its major use is for the preparation of its ester derivative, such as aspirin, fragrance of wintergreen, food flavorings, antiseptic and antipyretic medicines etc.<sup>1</sup> SA is synthesized by heating sodium phenolate with carbon dioxide in an organic phosphine oxide solvent to form sodium salicylate, followed by the treatment of sulfuric acid. An undesirable byproduct of this synthesis is the *para* isomer, 4-hydroxybenzoic acid (4HBA). Thus, it is important to be able to separate the isomers. The manufacturing process controlling the ratio of SA and 4HBA involves varying the mole ratio of the organic phosphine oxide to the alkali metal phenolate from 1 to 4, with the higher ratio favoring 4HBA.<sup>2</sup>

4-Hydroxybenzoic acid (4HBA), 3-hydroxybenzoic acid (3HBA), salicylic acid (SA) and benzoic acid (BA) (Figure 2.1) are a series of structure-related molecules. They

have a broad range of applications from paper coatings and liquid crystal preparations to drugs.<sup>2</sup> They are also a class of preservatives, commonly used as antimicrobial agents in cosmetics and hygiene products.<sup>3</sup> They also are found in fruits such as grape, apple, orange, plums and berries etc. They may possess anticarcinogenic and other health-promoting effects as antioxidants.<sup>4</sup>

Because of MIPs' easy preparation and low cost, they have potential applications in these areas.

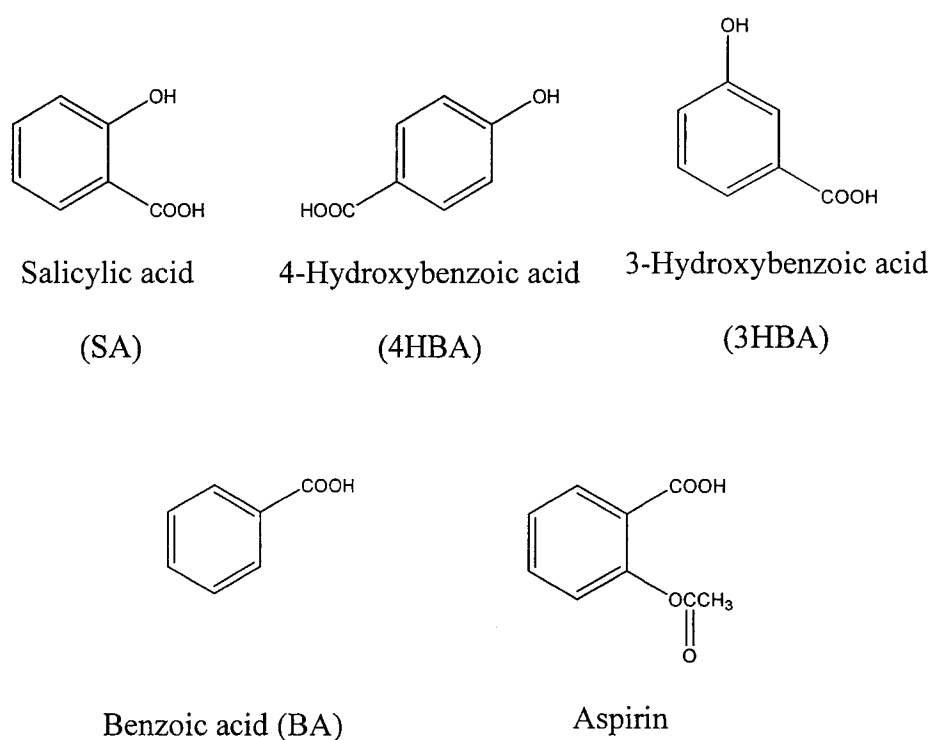


**Figure 2.1.** Chemical structures of the structural related molecules.

There is a strong intramolecular hydrogen bonding in the SA molecule (Figure 2.2), which affects the imprinting procedure. In the 4HBA molecule, the distance

between the hydroxyl group and the carbonyl group makes such intramolecular hydrogen bonding impossible. Although there is intermolecular hydrogen bonding in 4HBA molecules, it does not play a significant role in dilute 4HBA solutions. Ideally, resins imprinted with 4HBA should have the highest selectivity and absorption capacity for 4HBA instead molecules structurally related to it.

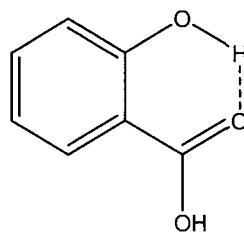


**Figure 2.2.** Intramolecular hydrogen bonding in SA.

For our study, 4HBA and 3HBA were selected as the template molecules respectively; acrylamide (AA) was selected as the functional monomer. An NMR titration technique was used to study the interaction in monomer-template complex in order to attain insight into molecular recognition. Acetonitrile was selected as the porogen for polymerization because some studies showed that the surface area of MIP made in acetonitrile was 23 times that of the same MIP made in chloroform.<sup>5</sup> The higher the surface area is, the higher the binding capacity is.

## 2.2. Experimental

### 2.2.1. Materials

4-Hydroxybenzoic acid (4HBA), 3-hydroxybenzoic acid (3HBA), benzoic acid (BA), ethylene glycol dimethacrylate (EGDMA) and 2,2'-azobisisobutyronitrile (AIBN) were purchased from Aldrich. Acrylamide (AA) was purchased from Bio-Rad Laboratories. Acetonitrile used in the polymerization was of HPLC grade. All the other reagents were of analytical grade.

In order to remove inhibitor, EGDMA was washed three times with 15% aqueous sodium hydroxide solution and then washed with saturated sodium bicarbonate solution. After it was dried over calcium chloride for 12 hours and subsequently with calcium hydride for 24 hours, the EGDMA was distilled in a *vacuo* from calcium hydride. The purity was checked by gas chromatography / mass spectroscopy (GC/MS) (Appendix A), using a Hewlett-Packard 5890 Series II GC instrument in conjunction with a 5971A Mass Selective Detector.

AIBN was recrystallized from methanol and acetonitrile was dried over 4A molecular sieves before use.

### 2.2.2. Preparation of molecularly imprinted polymer with 4HBA (MIP4HBA) and non-imprinted polymer (NIP)

#### 2.2.2.1. Interaction study between 4HBA and AA by titration experiment via $^1\text{H-NMR}$

Stock solutions of 4HBA (0.1 mol/L) and AA (1.6 mol/L) were prepared in deuterated acetonitrile ( $\text{CD}_3\text{CN}$ ). 0.40 mL of the 4HBA solution was pipetted into NMR

tubes, and different volumes of AA and CD<sub>3</sub>CN were added to yield ratios of AA (varied concentration) to 4HBA (0.05 M) ranging from 2 to 16 in a total volume of 0.80 ml. Also for controls, the proton spectra were obtained from a series of solutions containing only AA in CD<sub>3</sub>CN at the same concentrations as the ones in the 4HBA-AA solutions. All <sup>1</sup>H-NMR spectra were obtained at normal probe temperature through a Gemini NMR 400 and the chemical shifts were reported in ppm (δ) with TMS as an internal reference.

#### 2.2.2.2. Preparation of MIP4HBA and NIP

After 4HBA (the template; 0.1380 g, 1.0 mmol) had been dissolved in 5.00 mL acetonitrile, AA (the monomer; 0.4260 g, 6.0 mmol), EGDMA (the crosslinker; 5.70 mL, 30.0 mmol), and AIBN (the initiator; 0.0301 g, 0.18 mmol) were combined in a 50-mL flask. Then another 5.00 mL acetonitrile was added. The mixture was transferred into an 18 mm OD × 180 mm long borosilicate glass tube containing a small Teflon coated magnet. After it was sparged with nitrogen for 20 minutes, the sample was degassed three times by alternately submerging the tube in liquid nitrogen, holding it at 0.06 Torr for at least 15 minutes and then thawing. While thawing, a magnetic rod was used to move the small magnet up and down for the removal of bubbles from the solution. Following the above treatments, the tube was sealed at low pressure.

Another tube was prepared according to the same procedure but without the 4HBA template. The resulting resin is designated NIP. The amount of functional monomer used for synthesis of NIP was the same as that for the MIP to ensure that the differences in selectivity would not result from differences in functional groups concentrations.

The two sealed tubes were cooled to 4°C, agitated for 20 minutes, and then irradiated simultaneously for 48 hours with UV light from an ACE 7825-34 mercury vapor UV lamp (450 watts). During this period, the tubes were kept at 4°C and rotated slowly.

After polymerization, the tubes were opened and the bulk polymer that formed was ground in short repeated cycles using an electric mill. Between each grinding cycle, the products were dry sieved through a 38- $\mu\text{m}$  screen. The particles which passed through the sieve were collected and added to acetonitrile. The mixture was sonicated. After 30 minutes of sitting undisturbed, the component which remained suspended in the liquid was decanted and discarded while the sediment was saved. This was repeated three times. The sedimented particles were dried in a *vacuo* at room temperature for 8 hours.

A thin layer of fine MIP particles was spread on the top of a stub, then a sputter coater machine produced a gold coating by the argon plasma under *vacuo*. The scanning electron micrographs of MIP particles were obtained from an Amray model 1810 scanning electron microscope.

#### 2.2.2.3. *Template extraction by Soxhlet extraction*

The MIP was transferred to a cellulose Soxhlet thimble, and the template and a small amount of other soluble residue were extracted from the resin for 24 hours using 100.00 mL acetonitrile-acetic acid (4:1, v/v). A second Soxhlet extraction with 100.00 mL acetonitrile was performed for another 24 hours. The washing solutions were saved for analyses by a Perkin-Elmer Lambda 35 UV/VIS spectrophotometer and the polymers

were obtained for further study after drying in *vacuo* at room temperature for 10 hours. This procedure was then repeated for the NIP resin.

#### 2.2.2.4. 4HBA, 3HBA and BA binding experiments

Portions of the MIP4HBA after extracting the template were added one at a time to acetonitrile solutions of 4HBA, 3HBA and BA at various concentrations. The phase ratio was a commonly used one: 0.01 g solid / mL solution.<sup>6-9</sup> This process was repeated with NIP for comparison. In separate experiments, pure solvent was also added to MIP4HBA and NIP to determine the (trace) amount of any template remaining after the extraction. Each resin mixture was stirred for 24 hours at room temperature. After centrifugation for 20 minutes at 3500 rpm, the supernatant was transferred into a scintillation vial through a 0.45- $\mu$ m syringe filter. Because 4HBA, 3HBA and BA acetonitrile solutions have the maximum UV absorbance ( $\lambda_{\text{max}}$ ) at 251 nm, 294 nm and 225 nm respectively (Appendix B), the concentration of free 4HBA in the supernatant was determined by measuring its UV absorbance at 251 nm; 3HBA, at 294 nm; and BA, at 225 nm.

#### 2.2.2.5. Kinetic study of 4HBA binding experiment

In each of eight centrifuge tubes, 0.1g MIP4HBA or NIP was mixed with 10.00 mL, 0.1 mM 4HBA acetonitrile solution. All the solutions were stirred at room temperature. After 0.5, 1, 2, 4, 6, 8, 10, 20, 22, 24 and 36 hours, a different tube was centrifuged. The supernatant which formed on centrifugation was transferred into a

scintillation vial through a 0.45- $\mu\text{m}$  syringe filter and its concentration of free 4HBA in the supernatant was determined by measuring its UV absorbance at 251 nm.

### *2.2.3. Preparation of molecularly imprinted polymer with 3HBA (MIP3HBA) and non-imprinted polymer (NIP')*

#### *2.2.3.1. Preparation of MIP3HBA and NIP'*

3HBA (the template; 0.0690 g, 0.5 mmol) was dissolved in 2.50 mL acetonitrile. Before another 2.50 mL acetonitrile was added, AA (the monomer; 0.2133 g, 3.0 mmol), EGDMA (the crosslinker; 2.85 mL, 15.0 mmol), and AIBN (the initiator; 0.0150 g, 0.09 mmol) were combined. The mixture was transferred into a 14 mm OD  $\times$  180 mm long borosilicate glass tube containing a small Teflon-coated magnet. Following the previous treatments of MIP4HBA (see section 2.2.2.2. *Preparation of MIP4HBA and NIP*), the tube was degassed and sealed at low pressure. Another tube was prepared according to the same procedure but without template. This resin is designated NIP'. The two sealed tubes were slowly rotated in a 4°C water bath and the solutions were polymerized under the UV light for 48 hours.

After polymerization, the bulk polymer was repeatedly ground and dry sieved through a 38- $\mu\text{m}$  screen. The template molecules were removed by Soxhlet extraction following the same procedure as the one used in MIP4HBA treatment (see section 2.2.2.3. *Template extraction by Soxhlet extraction*).

### *2.2.3.2. 4HBA, 3HBA and BA binding experiments*

Portions of the MIP3HBA extracting the template were added one at a time to acetonitrile solutions of 3HBA, 4HBA and BA at various concentrations for binding experiments according to the same procedure as the one used in NIP and MIP4HBA binding experiments (see section 2.2.2.4. *4HBA, 3HBA and BA binding experiments*). The concentration of free 3HBA in the supernatant after binding was determined by measuring its UV absorbance at 294 nm; 4HBA, at 251 nm; and BA, at 225 nm.

## **2.3. Results and discussion**

### *2.3.1. Binding studies on 4HBA imprinted polymer system*

#### *2.3.1.1. Interaction between 4HBA and AA before polymerization*

Although the preparation of MIP by the non-covalent method is technically simple, it relies on an association between the template and the functional monomer. Lübke and coworkers proposed<sup>10</sup> that the structure of this complex existing in solution prior to polymerization remains unchanged during polymerization and the resulting sites are not modified by shrinkage upon the template removal.

Comparing the dielectric constant values, the dipole moment values, the boiling points and the heats of vaporization ( $\Delta H_{\text{vap}}$ ) of acetamide and acetic acid (Table 2.1), we found large differences which suggest that the amide group may contribute to stronger intermolecular forces than the carboxylic acid group. Also some MIP studies have shown that in a polar solvent, an amide group is capable of stronger hydrogen bonding than an

acid group.<sup>13,14</sup> So AA was selected instead of methacrylic acid as the functional monomer when using acetonitrile as the porogen in this study.

**Table 2.1.** Physical constants of acetamide and acetic acid.<sup>11,12</sup>

	dielectric constant	dipole moment	boiling point (°C)	$\Delta H_{\text{vap}}$ * (kJ/mole)
acetamide	67.6	3.76 D	222.0	56
acetic acid	6.20	1.70 D	118.1	24

\*  $\Delta H_{\text{vap}}$ , enthalpy of vaporization at boiling point in kJ/mole.

A <sup>1</sup>H-NMR titration experiment was used to study the hydrogen bonding<sup>15,16</sup> between the template and the monomer before the polymerization. A series of 4HBA and AA solutions were diluted according to the desired ratios (Table 2.2). The 4HBA concentration was fixed at 0.05 M and the AA concentration was varied from 0.1 to 0.8 M in deuterated acetonitrile.

**Table 2.2.** Composition in each NMR tube.  
The total volume of 4HBA and AA solution is 0.80 mL.

Conc. ratio of 4HBA : AA in NMR tube	4HBA <sup>a</sup>			AA <sup>a'</sup>		
	(mL) <sup>b</sup>	(mmol) <sup>c</sup>	(M) <sup>d</sup>	(mL) <sup>b'</sup>	(mmol) <sup>c'</sup>	(M) <sup>d'</sup>
<b>1:2</b>	0.40	0.04	0.05	0.05	0.08	0.1
<b>1:4</b>	0.40	0.04	0.05	0.10	0.16	0.2
<b>1:6</b>	0.40	0.04	0.05	0.15	0.24	0.3
<b>1:8</b>	0.40	0.04	0.05	0.20	0.32	0.4
<b>1:12</b>	0.40	0.04	0.05	0.30	0.48	0.6
<b>1:16</b>	0.40	0.04	0.05	0.40	0.64	0.8

a, a'. The initial concentrations of the 4HBA and AA stock solutions were 0.1 M and 1.6 M, respectively.

b, b'. Volume of 4HBA or AA stock solution pipetted into each NMR tube.

c, c'. Mmol of 4HBA or AA in each NMR tube.

d, d'. Final concentration of 4HBA or AA in each NMR tube.

<sup>1</sup>H-NMR spectra of AA, 4HBA and 4HBA-AA (concentration ratio of 4HBA:AA = 1:6) are shown in Figure 2.3, Figure 2.4 and Figure 2.5, respectively. The hydrogens attached to AA and 4HBA were analyzed and marked in each spectrum. In Figure 2.3, broadening of the two amide protons (H<sub>b</sub>) of AA by proton exchange is evident. In addition, in the spectrum of 4HBA-AA mixture, neither new hydrogen peak appears nor any existed hydrogen peak disappears (Figure 2.5).

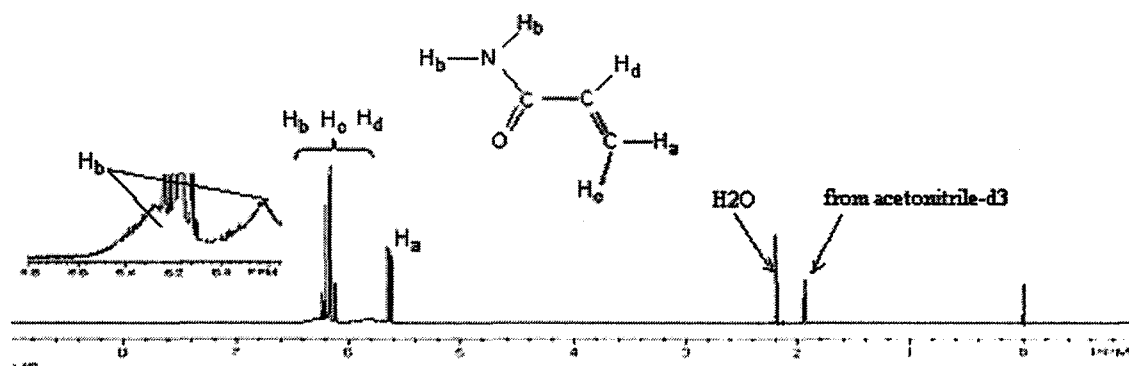


Figure 2.3. <sup>1</sup>H-NMR spectrum of AA in acetonitrile-*d*<sub>3</sub>.

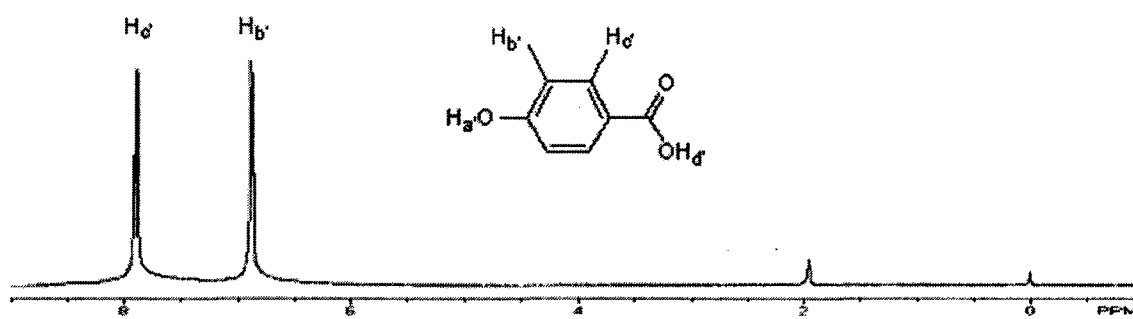


Figure 2.4. <sup>1</sup>H-NMR spectrum of 4HBA in acetonitrile-*d*<sub>3</sub>.

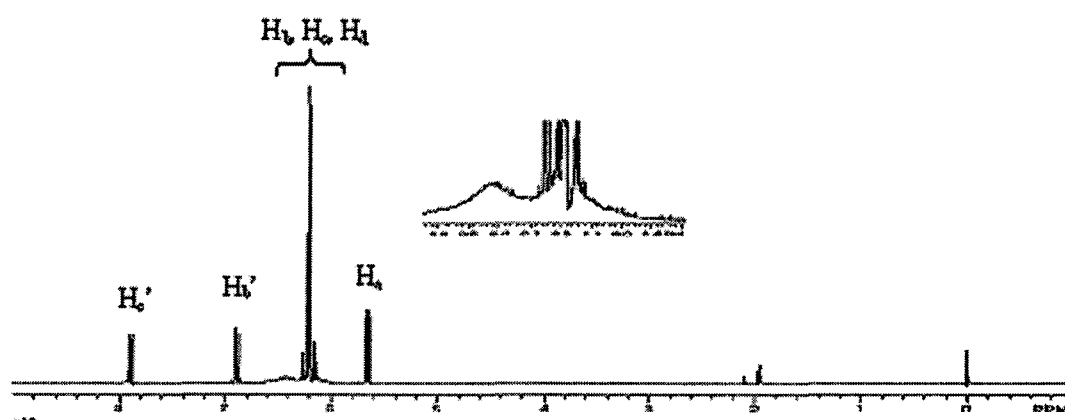
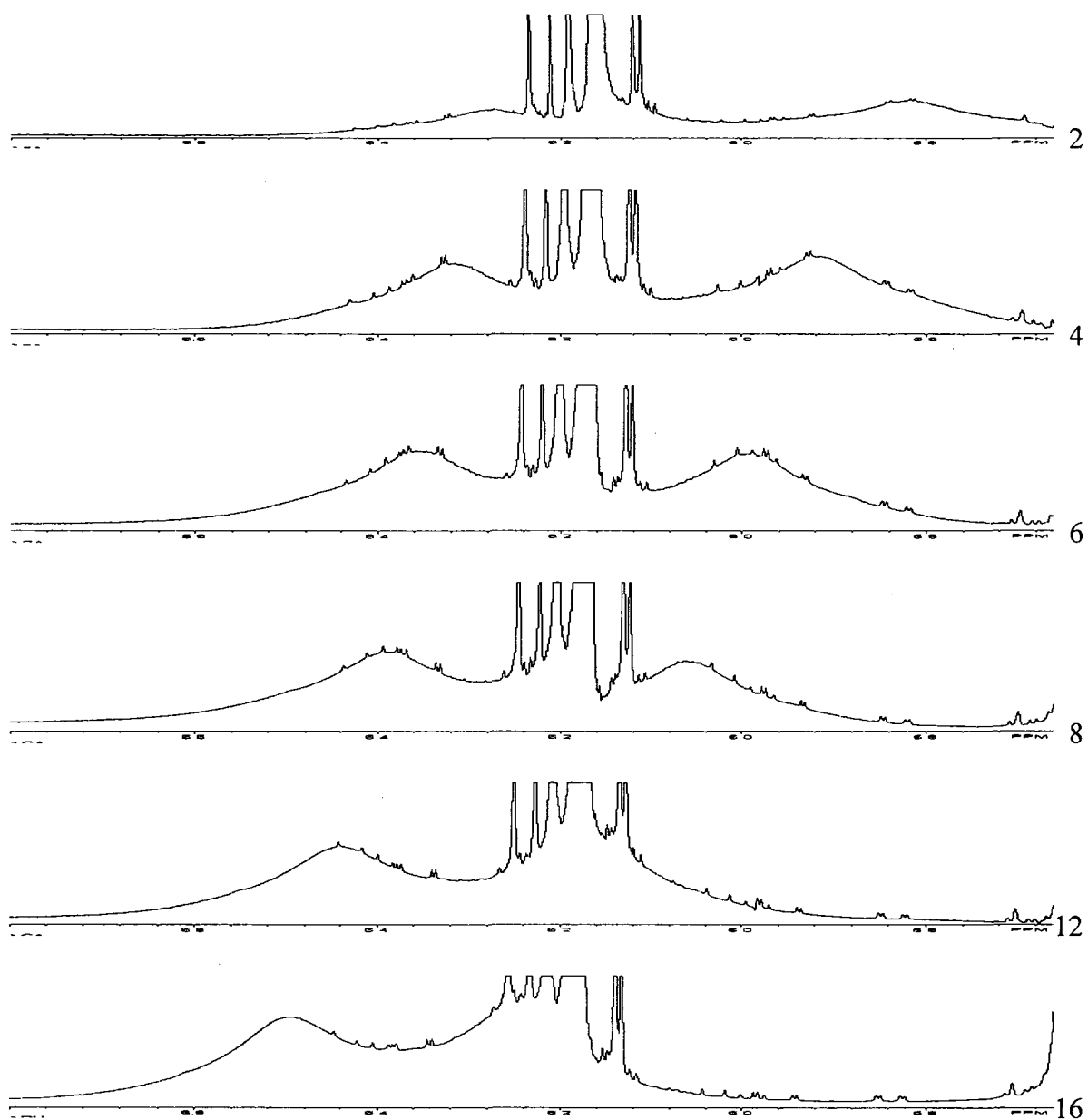


Figure 2.5. <sup>1</sup>H-NMR spectrum of 4HBA and AA in acetonitrile-*d*<sub>3</sub> in which the concentration ratio of 4HBA : AA = 1:6.

The chemical shifts of AA's two amide protons are shown in Figure 2.6 for varying concentrations of AA in deuterated acetonitrile. The full spectra can be found in Appendix C. The increases in the chemical shifts of the amide protons with increasing concentrations of AA are attributed to the increasing amount of hydrogen bonding as the AA solutions become more concentrated. (The reduction in electron density at the proton – a consequence of hydrogen bonding – results in the deshielding of the proton and it resonates at a higher field.)

When 4HBA was added to these solutions (Appendix D and Figure 2.7), the effect is heightened as would be expected if 4HBA hydrogen bonded to the amide protons of AA. Figure 2.8 shows a comparison of the two sets of NMR spectra. Consistent with the conclusion that the 4HBA also forms hydrogen bonds with AA, the effect of adding 4HBA to AA solutions is greatest in dilute solutions where the fraction of hydrogen bonds with 4HBA would be the greatest. Possible hydrogen bonds are shown in Figure 2.9.



**Figure 2.6.** NMR signals from AA's two amide protons at varying concentrations in  $d_3$ -acetonitrile. The concentrations of AA were from top to bottom, 0.1, 0.2, 0.3, 0.4, 0.6, and 0.8 M (see Table 2.2). 4HBA was not present (but see Figure 2.7). These spectra were processed by the software NUTS and zoomed in the same scale from 5.66 ppm to 6.8 ppm.

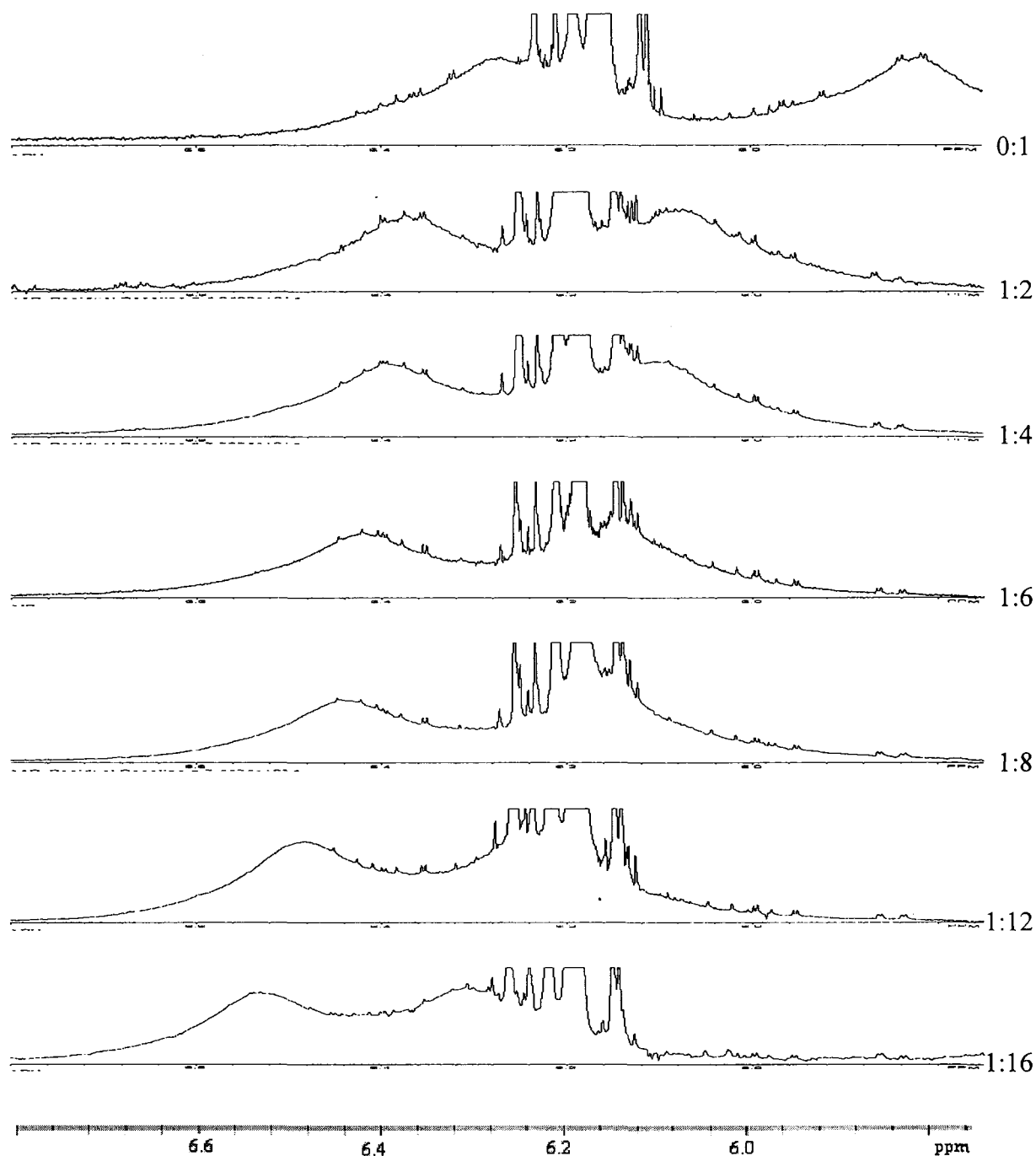


**Figure 2.7.** NMR signals from AA's two amide protons at varying concentrations in the presence of 4HBA in  $d_3$ -acetonitrile. The solvent was  $d_3$ -acetonitrile. The concentration of 4HBA was constant at 0.05 M and the concentration of AA was adjusted to achieve the desired ratio (see Table 2.2 and Figure 2.6). The spectra were processed by the software NUTS and zoomed in the same scale from 5.75 ppm to 6.8 ppm. The ratio indicates the concentration ratio of 4HBA to AA.

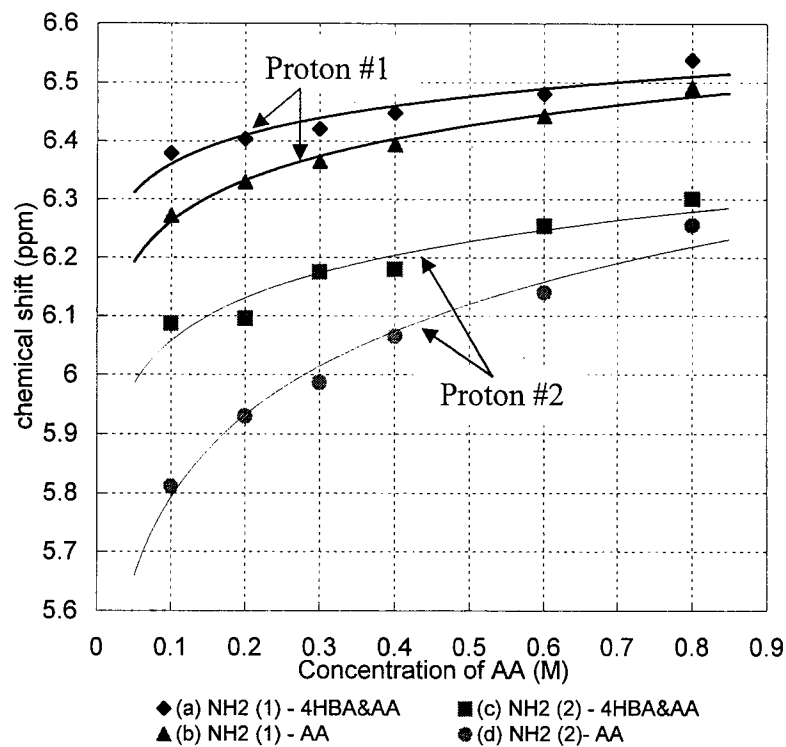


**Figure 2.8.** Chemical shifts for the two amide protons in AA as a function of the concentration of AA. The upper curve (a) for “Proton #1” obtained for 0.05 M 4HBA is compared with the lower curve (b) obtained for AA in the absence of 4HBA. Curves (c) and (d) are the corresponding shifts for “Proton #2”. The lines were drawn arbitrarily through the data points.

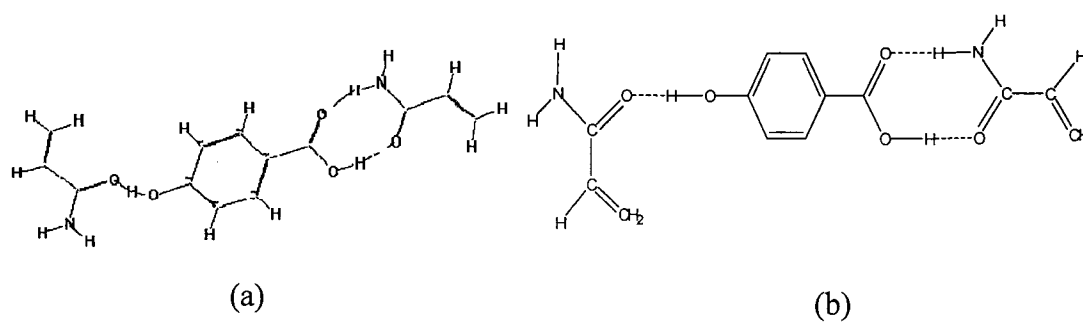


**Figure 2.9.** Probable hydrogen bonding between 4HBA and AA by (a) Serena Software, PC Model (Version 5.13), in which the energy of 4HBA and AA has been minimized and (b) ChemDraw.

### 2.3.1.2. Preparation of MIP4HBA

The MIP resins were prepared using a free-radical polymerization initiated with UV light. A white solid first appeared after the reactants had been irradiated for three hours. In the case of MIP4HBA, 90% of the template that was initially present in the reaction mixture was extracted from the resulting resin, as determined by UV/Vis spectrometry.

Scanning electron micrographs reveal the size and texture of MIP4HBA particles. The particle sizes were controlled by sieving and sedimentation. Their shapes were irregular (Figure 2.10. (a)). MIP4HBA showed a rough surface, the darker areas being pores (Figure 2.10. (b)).

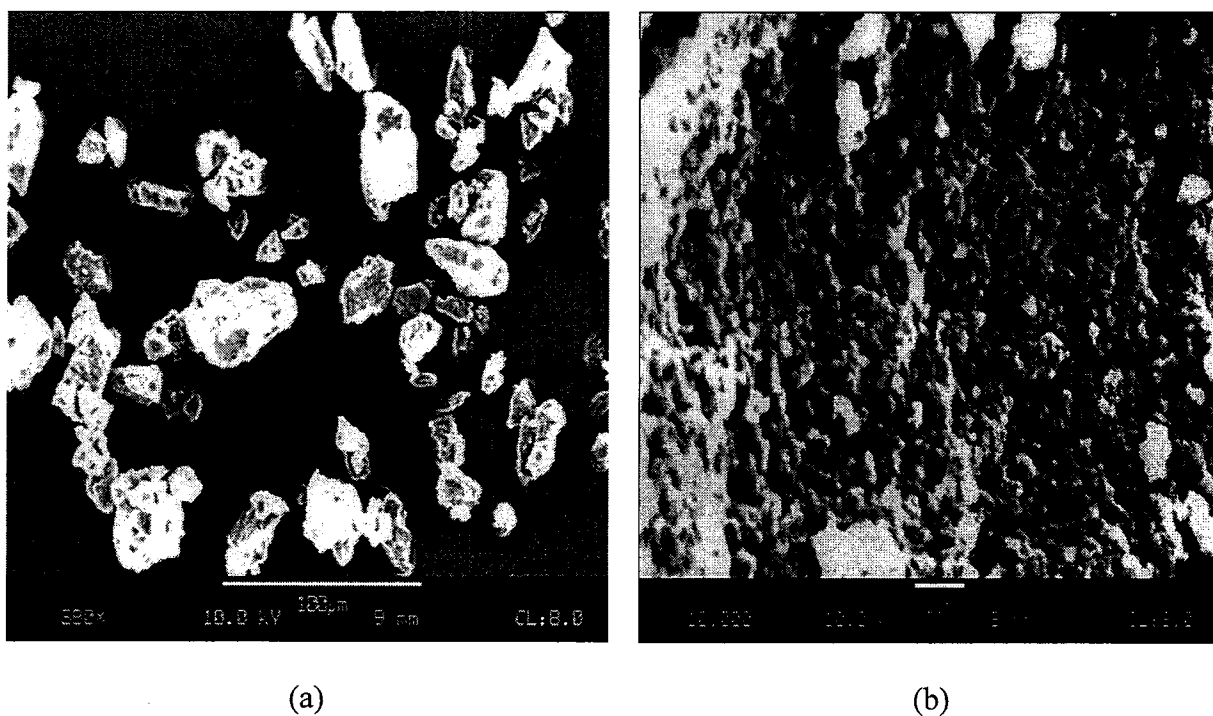


**Figure 2.10.** Scanning electron micrographs of MIP4HBA particles at (a) 380× and (b) 10,000× magnification.

### 2.3.1.3. Binding analyses of MIP4HBA and NIP resins

The affinity for the template species and the site selectivity of the sites were studied using batch analysis. The activity of MIP was compared with the corresponding activity of a non-imprinted resin, which had been prepared under the same conditions as the MIP except for the absence of the template.

The substrate's binding process can be described as an equilibrium:



where  $[M]$  is defined as the concentration of empty sites in the resin (mmol of empty sites / g of resin);  $[T]$ , the concentration of substrate in solution (mmol/L); and  $[MT]$ , the concentration of substrate bound in the resin at equilibrium ( $\mu\text{mol/g}$  of resin), with the latter calculated from the difference between the moles of the free substrate and the initial substrate.

The relationship among these quantities can be expressed as the Scatchard equation<sup>17</sup>:

$$\frac{[MT]}{[T]} = -K_a[MT] + K_a[MT]_{\max} \quad (2-1)$$

with the assumption that all the substrate-binding sites in an MIP are identical.

$K_a = \frac{[MT]}{[M][T]}$  and  $[MT]_{\max}$  represent the association constant for MT and the maximum number of binding sites per unit mass of the resin, respectively.

#### 2.3.1.3.1. Comparison of different polymerizations' binding analyses

In accord with common practice, the porogen acetonitrile used in the polymerization was used as the solvent for the batch analyses.<sup>18,19</sup> After the imprinted

(MIP) and non-imprinted (NIP) resins had been subjected to the extraction, they were immersed in 4HBA-acetonitrile solutions whose concentrations were varied over the range 0-2.5 mM. The binding isotherms for 4HBA in both resins, as determined from the UV-absorbance of the solutions, are compared in Figure 2.11, where the numbers following MIP or NIP represent the date on which the polymerization was performed.

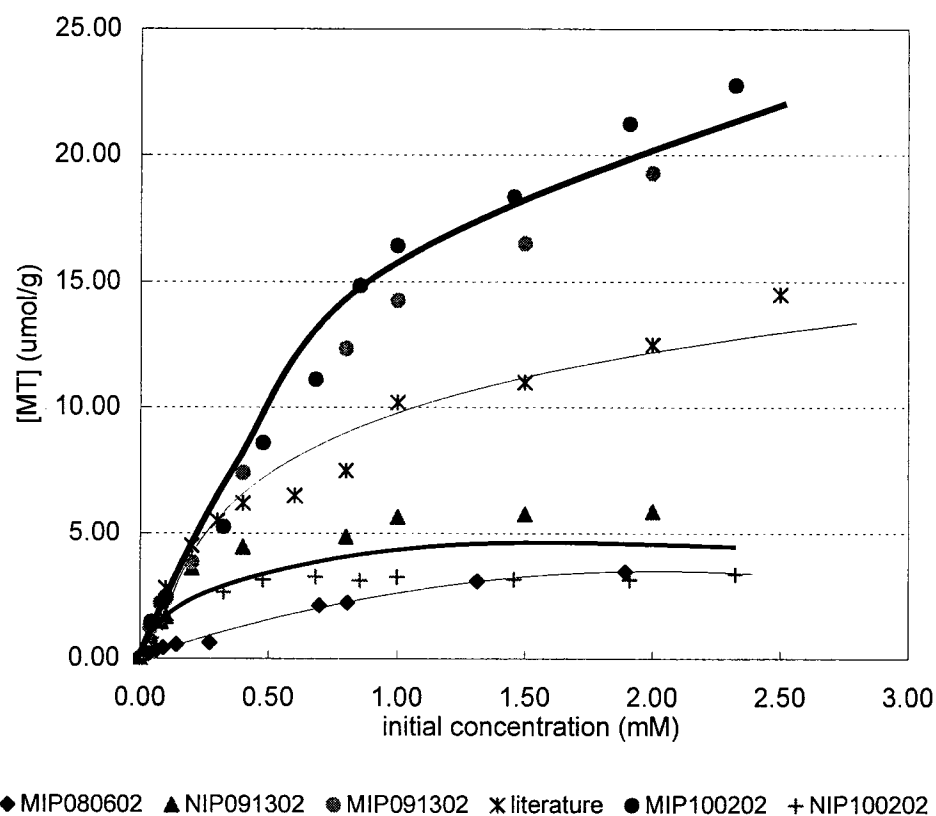


**Figure 2.11.** Binding isotherms for 4HBA on different batches of MIP4HBA and NIP. [MT], concentration of 4HBA bound in 0.1 g resin at equilibrium ( $\mu\text{mol/g}$  of resin);  $t = 25\text{ }^\circ\text{C}$ ; incubation time: 24 hours. The numbers following MIP or NIP symbolized the date on which the polymerization was performed. The result from Zhang's study<sup>8</sup> is identified as "literature".

In Figure 2.11, the plots for MIP091302 and MIP100202 show high absorbances of 4HBA compared to the two reference resins NIP091302 and NIP100202. Even concentrations of 4HBA as great as 2.5 mM apparently did not result in saturation of these two MIPs. These two resins were also 15-80% more absorbent than the resin described by Zhang<sup>8</sup> (*vide infra*).

As is apparent from Figure 2.11, the resin MIP080602 was less effective than MIP091302 and MIP100202 in binding 4HBA from solution. However, the preparation of MIP080602 was different from that of the other two. Its polymerization was carried out in a 125-mL flask which was stationary with respect to the UV source, whereas the other two were synthesized in the sealed small-diameter tubes that were rotated in the UV radiation. It took less than an hour for the MIP091302 and MIP100202 reaction mixtures to become turbid indicating the formation of polymer, while 4 hours had elapsed before the polymer was seen in the MIP080602 preparation.

The data from Zhang's study<sup>8</sup> (identified as literature) were plotted in the same figure for comparison. Although the mole ratio of each component was kept the same in each synthesis, the experimental conditions were different. The polymerization in Zhang's study was performed in a 18 mm OD × 180 mm long borosilicate glass test tube in a 60°C water bath for 24 hours. The template was extracted using acetic acid-methanol (1:4, v/v), then the residual acetic acid was removed using methanol. In the rebinding step, 30 mg MIP was incubated in 3.0 mL 4HBA acetonitrile solution in a 10 mL conical flask for 10 hours at 25°C.

The polymerization MIP080602 was performed in a 125-ml flask and initiated by UV in a 4°C bath for 24 hours. After the first hour's initiation, the solution became more

viscous but still transparent. A white polymer appeared in four hours. Acetic acid-acetonitrile (1:4, v/v) and acetonitrile were used for the template removal in consecutive Soxhlet extractions. In the binding step, 100 mg MIP was mixed in 10 mL 4HBA acetonitrile solution for 24 hours at room temperature. Although MIP080602 showed binding properties similar to the experiment in the literature, its binding capacity is only about 30% of the one in literature. One reason for the low binding capacity might be incomplete polymerization or particle morphology because, unlike the other polymerizations of MIP, some liquid remained in the polymerization flask after the reaction was stopped.

Based on the MIP080602 polymerization, in the next experiments the components for both MIP and NIP were sealed in borosilicate glass test tubes. They were placed near the UV source such that two tubes were equidistant and at the same angle with respect to the UV lamp. The tubes were turned slowly under the control of a motor to ensure that the samples received the UV light evenly. In the polymerizations of MIP091302 and NIP091302, both solutions started to change from clear to turbid after 45 minutes and form the gels in another hour. The stir bar in the MIP091302 tube rotated in the same plane but the one in the NIP091302 tube only vibrated. Also MIP showed less opacity than NIP. Two and half hours later, the stir bar in NIP could not move any more, but the stir bar in MIP continued to vibrate. Both samples were completely opaque by this time. It seemed from the observations that NIP polymerized faster than MIP. In MIP091302's binding analysis, its binding capacity was significantly improved and even more template 4HBA molecules were rebound than what the literature showed.

In the polymerizations of MIP100202 and NIP100202, a smaller OD borosilicate glass tube (14 mm) was used instead of an 18 mm OD tube for the further completion of the reaction. There was a concern that reactants in the interior of the larger tube were receiving significantly less radiation than the material near the surface. After a half hour, both solutions turned white and the stir bars ceased to move; after another half an hour, white solid formed. MIP100202's binding performance was getting improved over that of MIP091302. As will be discussed below, the binding capacity of NIP100202 was significantly less than that of the NIP091302.

To recapitulate, several steps to improve the properties of binding sites in MIP and NIP have been implemented, such as reducing the diameter of the reaction tubes, rotating the tubes during the reaction and modifying the scheme used for the sedimentation of polymerized particles to narrow the distribution of particle sizes. It is apparent from the binding isotherms in Figure 2.11 that the binding capacities of MIP091302 and MIP100202 were improved compared the one in Zhang's study and they were consistent with one another. So those MIPs were selected for the further studies and no additional refinement was attempted.

#### *2.3.1.3.2. Reproducibility of rebinding experiment on MIP4HBA and NIP resins*

Upon finishing the first rebinding of 4HBA, 4HBA molecules were extracted again from MIP091302 and NIP091302 resins, and then the dried resins were stored in the cabinet at the room temperature. After two months, the second rebinding was done with the same resins and under the same experimental conditions for comparison. From

Figure 2.12, two batch analyses on the same resin showed very similar results, showing MIP's stability and robustness.

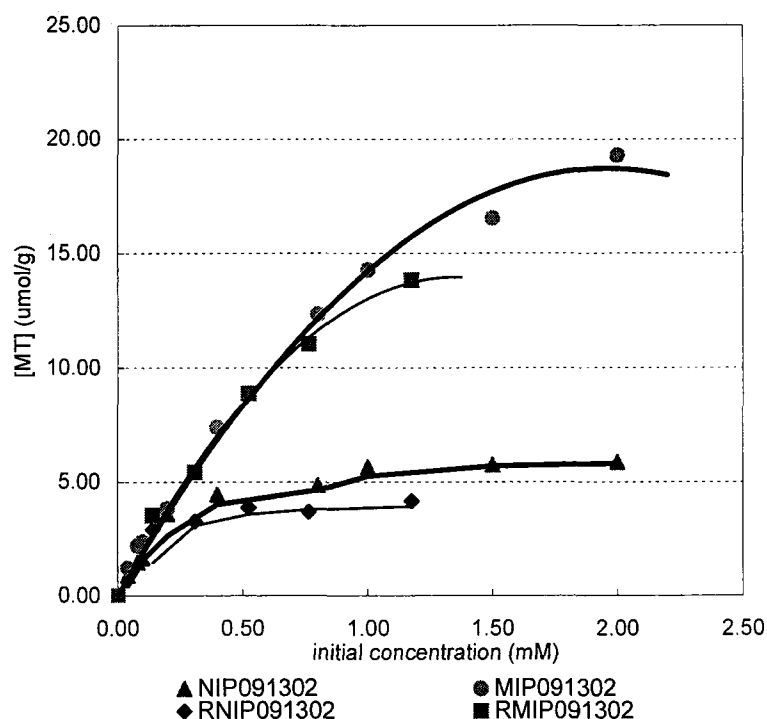


**Figure 2.12.** Reproducibility of 4HBA rebinding on MIP091302 and NIP091302. The second rebinding is shown as RNIP091302 and RMIP091302. [MT], concentration of 4HBA bound in 0.1 g resin at equilibrium ( $\mu\text{mol/g}$  of resin);  $t = 25\text{ }^\circ\text{C}$ ;  $V = 10.0\text{ mL}$ ; incubation time: 24 hours.

#### 2.3.1.3.3. Binding analyses of MIP4HBA and NIP resins

For the later study and comparison, MIP091302 and NIP091302 were selected as the examples for MIP4HBA and NIP. Their first binding isotherms are shown in Figure 2.13. The MIP absorbed more 4HBA than did an equal mass of NIP with the difference increasing with increasing concentrations.

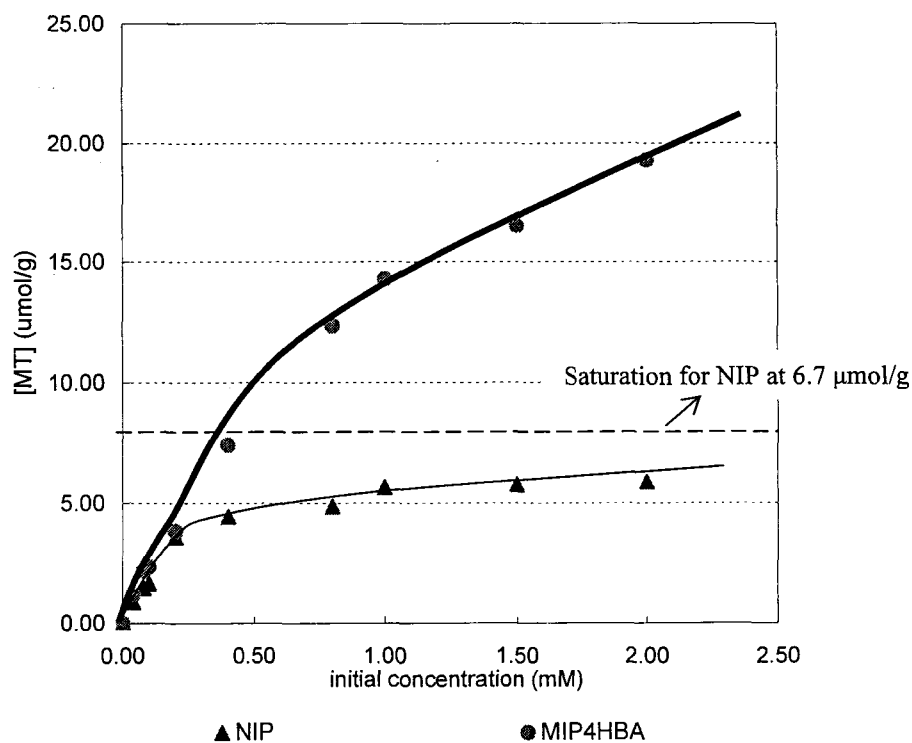


**Figure 2.13.** Binding isotherms for 4HBA on MIP4HBA and NIP.  $[MT]$ , concentration of 4HBA bound in 0.1 g resin at equilibrium ( $\mu\text{mol/g}$  of resin);  $t = 25\text{ }^\circ\text{C}$ ; incubation time: 24 hours. The dashed line at  $[MT] = [MT]_{\text{max},\text{NIP}} = 6.7\text{ }\mu\text{mol/g}$  is the asymptotic limit for NIP as explained in the text.

As shown in Figure 2.14, the percentage uptake from the solution, calculated as the percentage of 4HBA in solution absorbed in the resin while the equilibrium is reached, for the MIP is higher than that for the NIP at the same concentration, but both decrease with an increase of 4HBA's initial concentration.

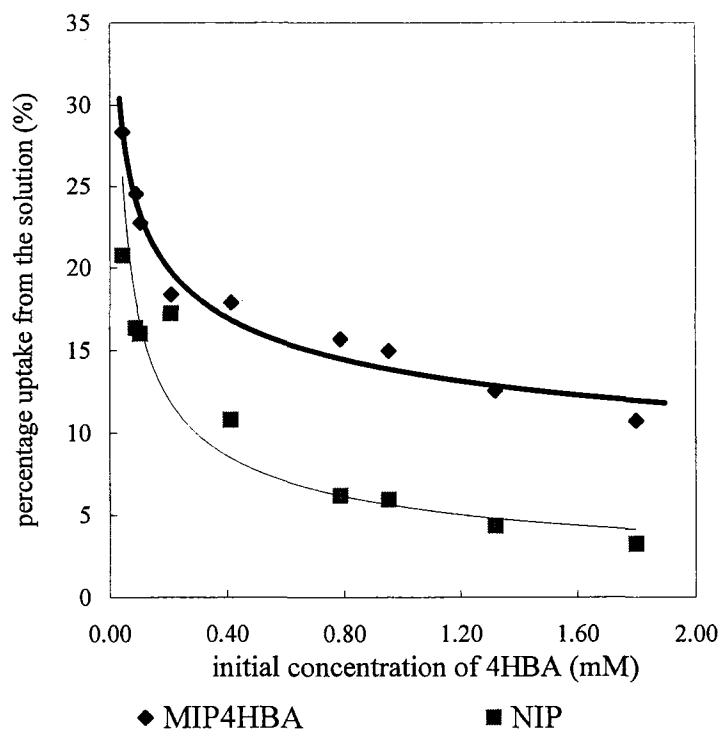


**Figure 2.14.** Percentage uptake from MIP4HBA and NIP binding solutions.

The data in Figure 2.13 are re-plotted in Figure 2.15 with  $[MT]/[T]$  graphed as a function of  $[MT]$  as suggested by Equation (2-1). For the NIP, the ratio  $[MT]/[T]$  is a linear function of  $[MT]$  over the range from  $[MT] = 0$  to the saturation of the resin. The slope and intercept of the line representing these data were determined by the method of least squares, with each point weighted in proportion to the inverse square of its experimental uncertainty<sup>20</sup> (Appendix F). The results yield the equilibrium association constant  $K_{a,NIP} = 4.4 \pm 0.2 \text{ mM}^{-1}$  and the maximum number  $[MT]_{\max,NIP} = 6.7 \pm 0.3 \text{ } \mu\text{mol/g}$ . The data in Figure 2.15 for MIP4HBA solutions are not linear, but concave upwards. The large uncertainties in  $[MT]/[T]$  shown in Figure 2.15 are a consequence of taking the difference between pairs of small concentrations.

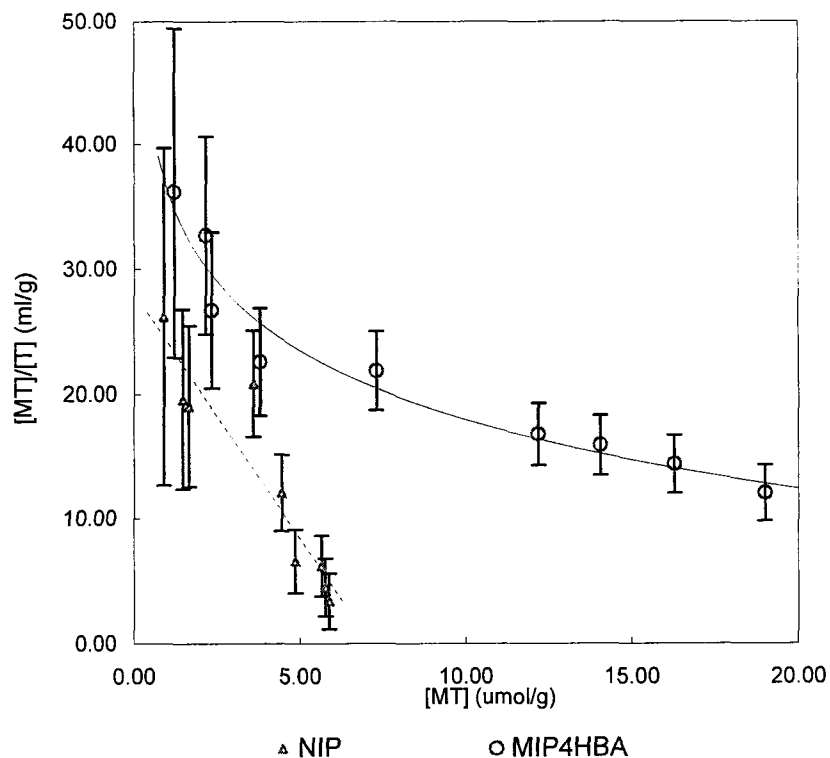


**Figure 2.15.** Scatchard plots of MIP4HBA and NIP for 4HBA.

To take account of the nonlinearity of the MIP4HBA data in Figure 2.15, the MIP4HBA resin was treated as having two kinds of binding sites with different affinities: “general” sites that in this system dominate the behavior at low concentrations of template species and “special” binding sites, dominant at high concentrations. The general binding sites were comparable to those found in the NIP resin. Accordingly, they are assigned the same affinity constant  $K_{a,g} = K_{a,NIP}$  and the same site density  $[MT]_{\text{max},g} = [MT]_{\text{max},NIP}$ .

In this model, some of the bound template is adsorbed on the general sites while the remainder of the bound template is found on the special sites. Thus,

$$[MT]_{total} = [MT]_g + [MT]_s \quad (2-2)$$

The concentration of occupied general binding sites for a given  $[T]$  can be calculated from  $K_{a,g}$  and  $[MT]_{max,g}$  using the results of measurement in NIP and Equation (2-3).

$$[MT]_g = \frac{K_{a,g} [MT]_{max,g} [T]}{1 + K_{a,g} [T]} \quad (2-3)$$

The concentration of occupied special sites  $[MT]_s$  is the difference between  $[MT]_{total}$ , obtained from measurement on MIP, and  $[MT]_g$ .

$$[MT]_s = [MT]_{total} - [MT]_g = [MT]_{total} - \frac{K_{a,g} [MT]_{max,g} [T]}{1 + K_{a,g} [T]} \quad (2-4)$$

According to the Scatchard plot of the special-site data determined from Equation (2-4) (Figure 2.16), the behavior of the special binding sites is also assumed to follow the Scatchard model so that

$$\frac{[MT]_s}{[T]} = -K_{a,s} [MT]_s + K_{a,s} [MT]_{max,s} \quad (2-5)$$

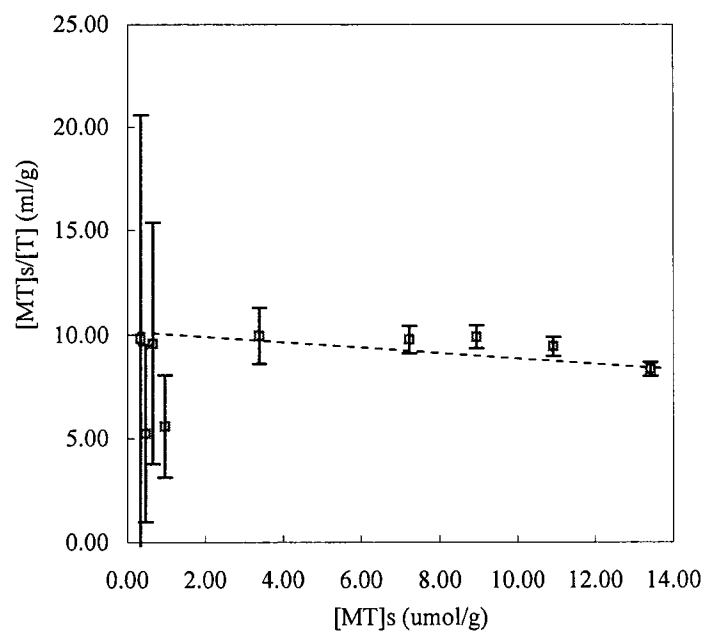


**Figure 2.16.** Scatchard plot for the special binding sites with  $[MT]_s$  determined using Equation (2-5).

From its slope and intercept,  $K_{a,s} = 0.15 \pm 0.01 \text{ mM}^{-1}$  and  $[MT]_{\text{max},s} = 72 \pm 2 \text{ } \mu\text{mol/g}$  were found. These values and those determined from the NIP resin have been substituted in Equation (2-6):

$$[MT]_{\text{total}} = [MT]_s + [MT]_g = \frac{K_{a,s}[MT]_{\text{max},s}[T]}{1 + K_{a,s}[T]} + \frac{K_{a,g}[MT]_{\text{max},g}[T]}{1 + K_{a,g}[T]} \quad (2-6)$$

and the results are plotted as the solid line in Figure 2.17 for comparison with the experimental results. The agreement is very good.

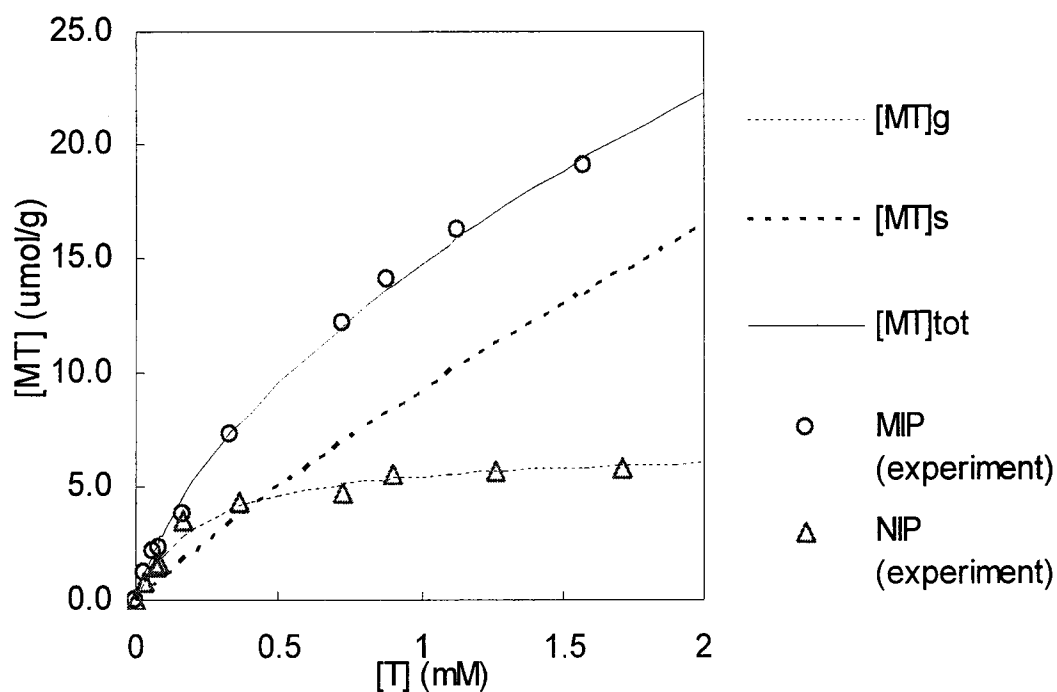


**Figure 2.17.** Representation of the observed binding data using Equation (2-6).  $[\text{MT}]_g$  or  $[\text{MT}]_s$ : the concentration of 4HBA absorbed in the general or special binding sites calculated from its related  $K_a$  and  $[\text{MT}]_{\text{max}}$ ;  $[\text{MT}]_{\text{total}}$ : the concentration of 4HBA absorbed in all binding sites calculated from Equation (2-6); MIP (experiment) or NIP (experiment): the experimental data from binding analysis of MIP or NIP.

#### 2.3.1.4. Kinetic study of 4HBA binding procedure

Batch analyses in these studies were conducted on systems at equilibrium (in contrast to many chromatographic studies reported elsewhere that involve solutions flowing past a stationary resin). The rate of approach to equilibrium was studied by measuring the concentration of 4HBA in the supernatant after 0.5, 1, 2, 4, 6, 8, 10, 20, 22, 24 and 36 hours. Initially, the sorption of 4HBA by MIP increases at a decreasing rate leading to equilibrium after 24 hours (Figure 2.18). On the other hand, 4HBA equilibrated with the NIP resin after 8 hours. Apparently, 4HBA molecules are rapidly adsorbed at the general binding sites until the NIP is saturated. In the MIP resin, besides the general binding sites, there are numerous sites containing functionalities positioned to complement those of the template molecules, and it takes longer for the binding to reach the equilibrium.

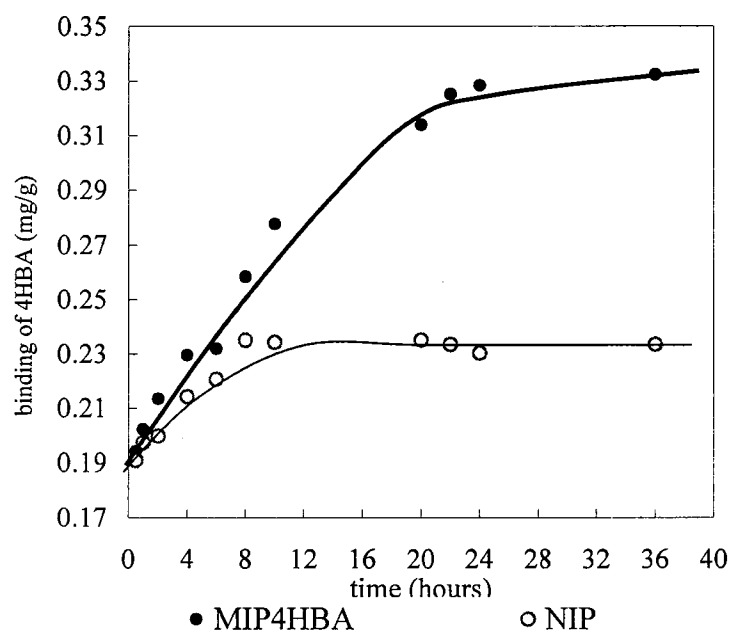


**Figure 2.18.** Kinetic study of 4HBA binding on MIP4HBA and NIP resins.

$m$  (MIP or NIP) = 0.1 g;  $C$  (4HBA) = 0.1 mM;  $V$  = 10.0 mL;  $t$  = 25 °C.

### 2.3.1.5. Substrate selectivity of MIP4HBA and NIP

The selectivity of MIP4HBA for different substrates was studied by measuring the resin's capacity for absorbing 3HBA and BA, both of which are related structurally to the 4HBA template (see Figure 2.19). In carrying out this particular study, batch analyses were performed on MIP4HBA and NIP resins using the same experimental conditions that were employed in the binding of 4HBA by the MIP4HBA resin.

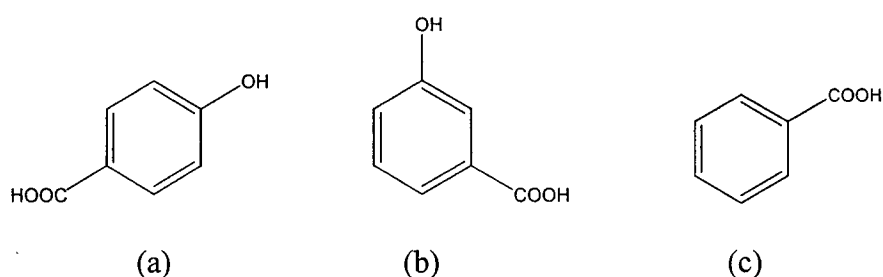


**Figure 2.19.** Structures of the substrates used in this study:

(a) 4HBA; (b) 3HBA and (c) BA.

The effects of molecular structure on binding affinities in MIP are apparent in a comparison of the binding of the three species in Figure 2.19 to NIP and to MIP. 4HBA, 3HBA, and BA bind almost equally to NIP as shown in Figure 2.20 (a). Their saturation concentration on the NIP is about 4  $\mu\text{mol/g}$ . However in experiments with MIP as shown in Figure 2.20 (b), 4HBA (the template) was bound to a greater extent than either 3HBA or BA, with greater binding by BA compared to 3HBA. The MIP was not saturated by any of the three analytes over the ranges of solution concentrations used. The reason for the lower sorption of BA (and 3HBA) by the MIP compared to the NIP is not apparent. For further understanding of the selectivity mechanism of the MIPs, other substrates, for

example, phenol (one hydroxyl group), salicylic acid (the hydroxyl group and the carboxyl group are *ortho* to one another and hydroquinone (*para*-substituted hydroxyl groups) could also be used for the binding experiments.

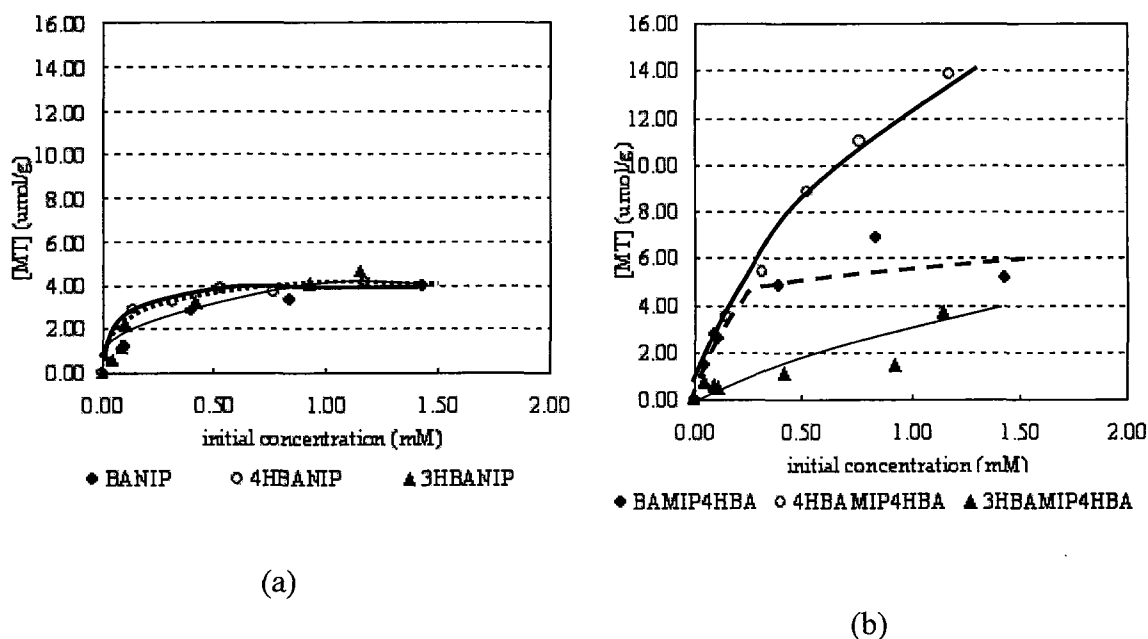


**Figure 2.20.** Binding isotherms of 4HBA, 3HBA and BA on (a) NIP and (b) MIP4HBA. Concentration of resin in solution: 0.01 g / 1.0 mL; binding time: 24 hours;  $t = 25\text{ }^{\circ}\text{C}$ .

### 2.3.1.6. Comparison of batch analyses and chromatographic evaluation

Zhang *et al.*<sup>8</sup> used 4HBA imprinted resin for the stationary phase in a liquid chromatographic separation of 4HBA, 3HBA and BA. This column not only separated 4HBA from the structurally similar compounds, but also had a higher capacity and greater relative retention for 4HBA than for 3HBA and BA (Table 2.3). Values for selectivity and imprinting efficacy from the current equilibrium binding experiments are

compared in the same table. We find evidence for greater selectivity in our equilibrium binding measurements than Zhang *et al.*<sup>8</sup> This is because, in the chromatographic analysis, the absorption-adsorption between the analyte and the binding sites does not reach equilibrium; whereas, in the batch experiment, the binding is an equilibrium process. However, both experiments showed MIP has a significant imprinting performance.

**Table 2.3.** The selectivity factors from MIP4HBA binding experiment and its chromatographic evaluation.<sup>8,a</sup>

Binding evaluation	4HBA	3HBA	BA	Chromatographic evaluation	4HBA	3HBA	BA
$\alpha_{\text{MIP4HBA}}^b$	1	10.71 <sup>c</sup>	2.42	$\alpha'_{\text{MIP4HBA}}^b$	1	2.23	7.26
$\alpha_{\text{NIP}}^b$	1	1.08	3	$\alpha'_{\text{NIP}}^b$	1	0.94	2.29
$\beta^b$	1	9.92	0.81	$\beta'^b$	5.51	2.32	1.74

<sup>a</sup> Experimental conditions: for comparison, the concentration for the binding solution of 0.1 mmol/mL was selected as the same as the injected solution's concentration used for HPLC. 0.1 g MIP or NIP was incubated in 10 mL of 0.1 mM binding solution.

<sup>b</sup> In the binding evaluation, the selectivity factor  $\alpha$  is defined as  $\alpha = (\text{amount of 4HBA absorbed})/(\text{amount of analyte absorbed})$  and the molecular imprinting efficacy factor  $\beta$  is defined as  $\beta = \alpha_{\text{MIP}} / \alpha_{\text{NIP}}$ ; in the chromatographic evaluation, the capacity factor

$k' = \frac{t_R - t_0}{t_0}$ , where  $t_R$  and  $t_0$  are the retention time of the sample and the void marker,

respectively; the relative retention value  $\alpha' = \frac{k'_i}{k'_i}$ , the ratio of capacity factors for any two

substances on the same column; and the molecular imprinting factor  $\beta' = \frac{k'_{MIP}}{k'_{NIP}}$ .

<sup>c</sup> The value  $\alpha = 10.7$  is, by coincidence, the same as the ratio  $[MT]_{\max,s}/[MT]_{\max,g}$  using the values reported above in section 2.3.1.3.3. This coincidence is accidental as follows when it is recognized that the ratio of site densities is independent of the concentration of the solution, whereas  $\alpha$  is not.

### 2.3.2. 3HBA imprinted polymer system

After a thorough study of the 4HBA imprinted system, 3-hydroxybenzoic acid, the *meta* isomer of hydroxybenzoic acid, was selected as the template molecule. A similar methodology was used to study 3HBA imprinted polymer as was used in 4HBA system.

#### 2.3.2.1. Interaction study of 3HBA and AA

As with the 4HBA system, a <sup>1</sup>H-NMR titration experiment was used to study the hydrogen bonding between 3HBA and AA before polymerization. In the spectra (Figure 2.21), both amide proton peaks in AA were shifted downfield as the ratio of AA to 3HBA increased compared with shifts for solutions of AA at the same concentrations (Figure 2.22). So both amide protons in AA are involved in hydrogen bonding formation with 3HBA besides AA's intermolecular hydrogen bonding. The template-monomer complex in acetonitrile can be described in Figure 2.23 by using Serena Software, PC Model (Version 5.13) in which the energy of 3HBA and AA has been minimized.

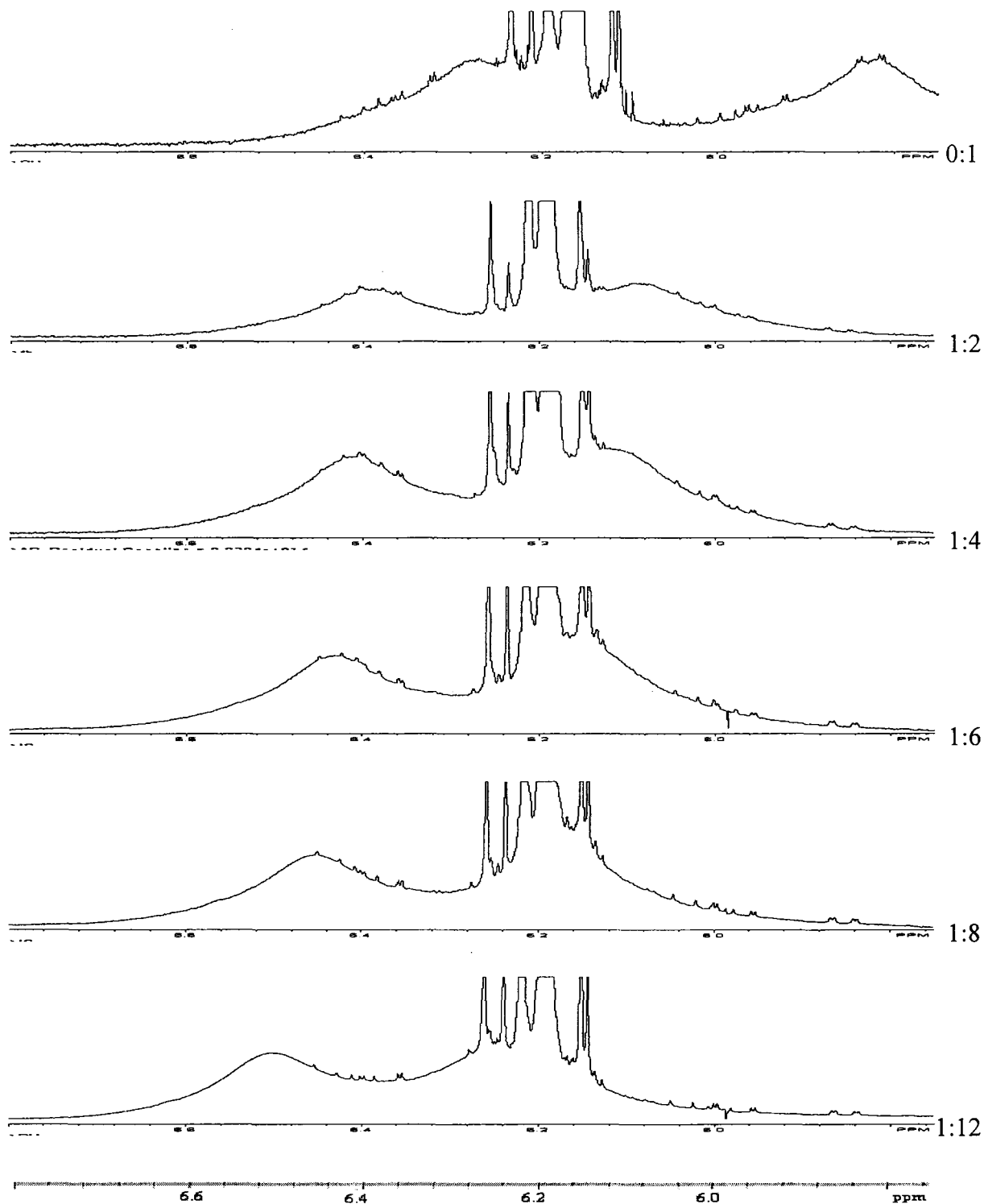


**Figure 2.21.** NMR signals from AA's two amide protons at varying concentrations in the presence of 3HBA in  $d_3$ -acetonitrile. The concentration of 3HBA was constant at 0.05 M and the concentration of AA was adjusted to achieve the desired ratio (similar as shown in Table 2.2). The spectra were processed by the software NUTS and zoomed in the same scale from 5.75 ppm to 6.8 ppm. The ratio indicates the concentration ratio of 3HBA to AA.

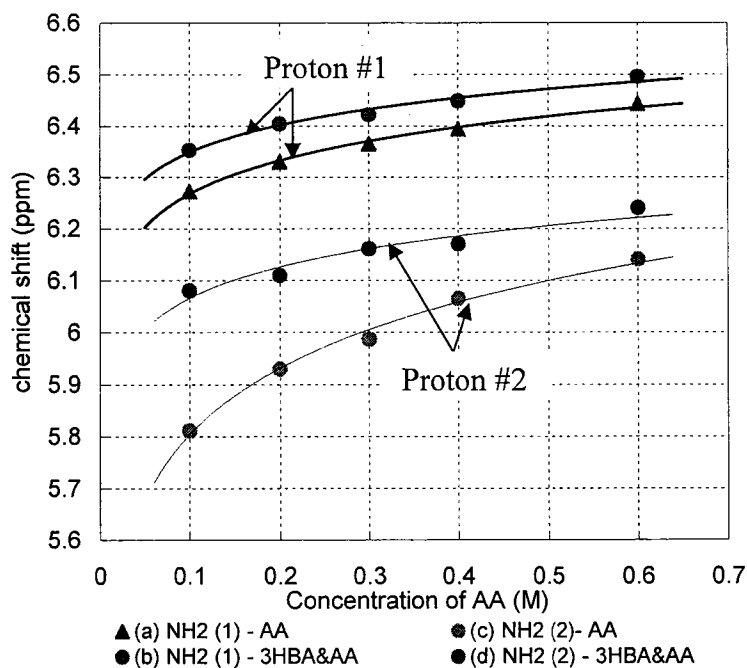


**Figure 2.22.** Chemical shifts for the two amide protons in AA as a function of the concentration of AA. The upper curve (a) for “Proton #1” obtained for 0.05 M 3HBA is compared with the lower curve (b) obtained for AA in the absence of 3HBA. Curves (c) and (d) are the corresponding shifts for “Proton #2”. The lines were drawn arbitrarily through the data points.

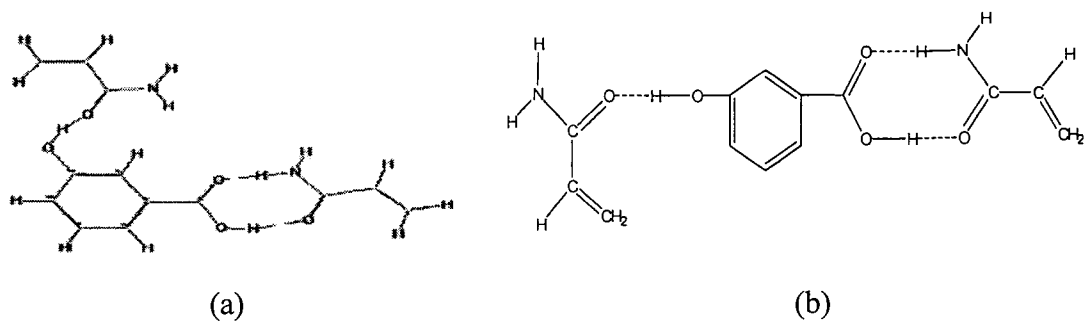


**Figure 2.23.** Probable hydrogen bonding between 3HBA and AA by (a) Serena Software, PC Model (Version 5.13), in which the energy of 4HBA and AA has been minimized and (b) ChemDraw.

### 2.3.2.2. Preparation of MIP3HBA

The same methodology was employed in the preparation of 3HBA imprinted polymer (MIP3HBA) as was employed for MIP4HBA. In MIP3HBA's preparation, a 14 mm OD × 180 mm long borosilicate glass tube was used instead of the 18 mm OD × 180 mm long one used in MIP4HBA's synthesis. Each component used in this set of polymerization is listed in Table 2.4 and compared with the MIP4HBA set. NIP' was prepared as a control without the template. All the other treatments were same as the ones used in the MIP4HBA system.

**Table 2.4.** Composition of each polymerization imprinted with 3HBA and 4HBA.

	Template	Monomer (AA)	Crosslinker (EGDMA)	Porogen (AN)	Initiator (AIBN)
MIP3HBA	3-HBA: 0.0690 g, 0.5 mmol	0.2133 g, 3 mmol	2.85 mL, 15 mmol	5.00 mL	0.0150 g, 0.09 mmol
NIP'	none	0.2133 g, 3 mmol	2.85 mL, 15 mmol	5.00 mL	0.0150 g, 0.09 mmol
MIP4HBA	4-HBA: 0.1380 g, 1 mmol	0.4260 g, 6 mmol	5.70 mL, 30 mmol	10.00 mL	0.0310 g, 0.18 mmol
NIP	none	0.4260 g, 6 mmol	5.70 mL, 30 mmol	10.00 mL	0.0310 g, 0.18 mmol

### 2.3.2.3. Binding analyses of MIP3HBA and NIP'

After the template had been extracted, the imprinted (MIP3HBA) and non-imprinted (NIP') resins were immersed in 3HBA-acetonitrile solutions whose concentrations were varied over the range of 0-1.2 mM. The binding isotherms for 3HBA

in both resins, as determined from the UV-absorbance of the solutions, are plotted in Figure 2.24. The MIP3HBA absorbed more 3HBA than the NIP' with the difference increasing with increasing concentration.

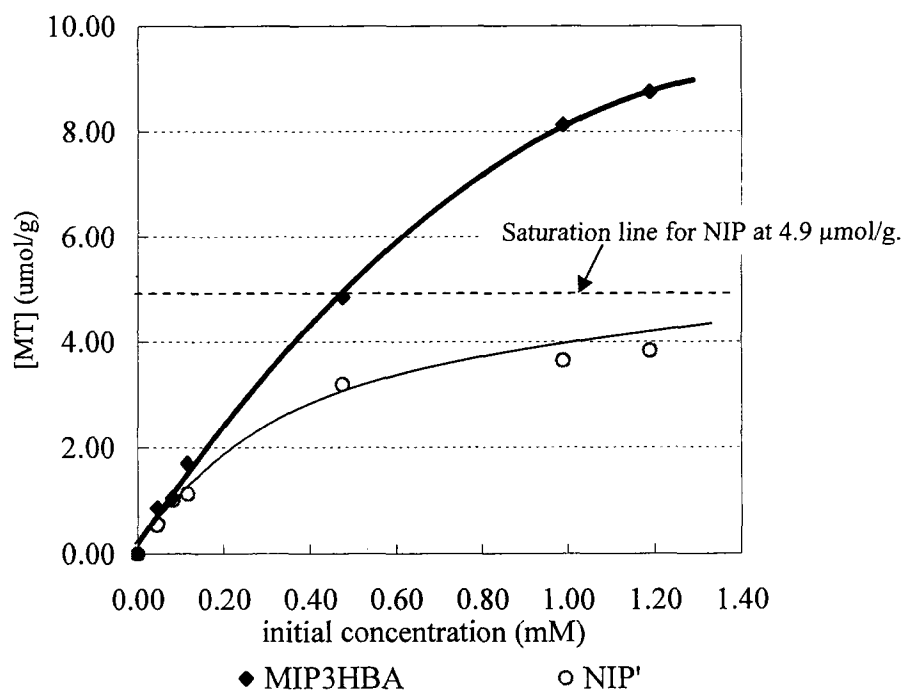


**Figure 2.24.** Binding isotherms for 3HBA on MIP3HBA and NIP'. [MT], concentration of 3HBA bound in the resin at equilibrium ( $\mu\text{mol/g}$  of resin);  $t = 25\text{ }^\circ\text{C}$ ; absorption time: 24 hours. The dashed line at  $[\text{MT}] = 4.9\text{ }\mu\text{mol/g}$  is the asymptotic limit for NIP', as explained in the text.

The data in Figure 2.24 were re-plotted in Figure 2.25 with  $[\text{MT}]/[\text{T}]$  graphed as a function of  $[\text{MT}]$  as suggested by the Scatchard equation. For the NIP', the ratio  $[\text{MT}]/[\text{T}]$  is a linear function of  $[\text{MT}]$  over the range studied, from  $[\text{MT}] = 0$  to  $4.9\text{ }\mu\text{moles / gram}$  of resin. The slope and intercept of the line representing these data were determined by the method of least squares, with each point weighted in proportion to the

inverse square of its experimental uncertainty.<sup>20</sup> The results yield the equilibrium association constant  $K_{a,NIP'} = 3.3 \pm 0.1 \text{ mM}^{-1}$  and the maximum number  $[MT]_{\max,NIP'} = 4.9 \pm 0.2 \text{ } \mu\text{mol/g}$ .

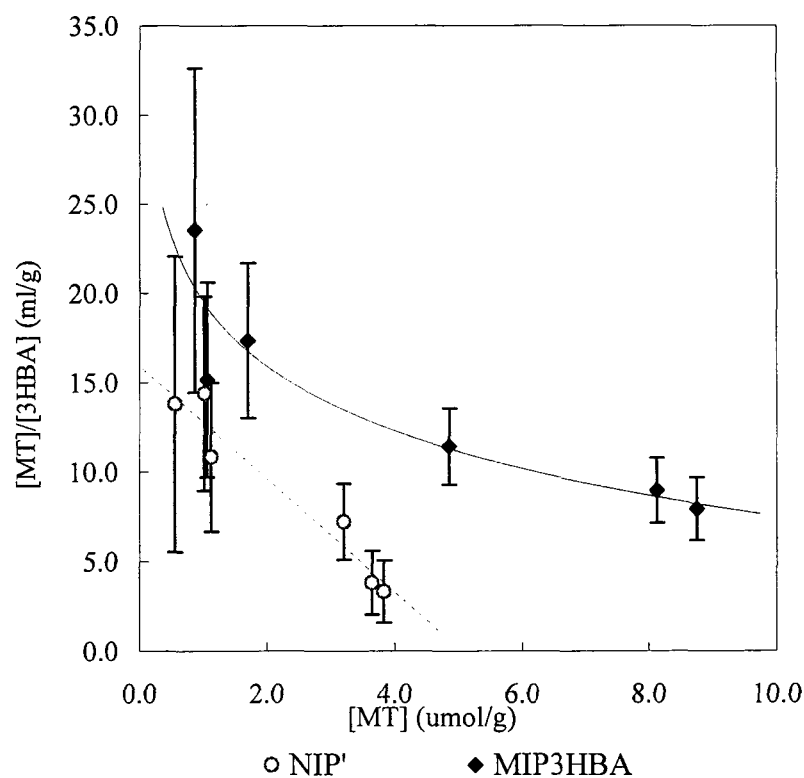


**Figure 2.25.** Scatchard plot of MIP3HBA and NIP' for 3HBA.

Following the previous MIP4HBA study, two kinds of binding sites with different affinities were classified: “general” sites that in this system dominate the behavior at low concentrations of template species and “special” binding sites, dominant at high concentrations. The general binding sites were treated as being the same kind as those found in the NIP' resin. Accordingly, they are assigned the same affinity constant  $K_{a,g} = K_{a,NIP'}$  and the same site density  $[MT]_{\max,g} = [MT]_{\max,NIP'}$ . The concentration of template

at the special sites  $[MT]_s$  is calculated by subtracting the amount attributed to the general sites from the total amount bound  $[MT]_{total}$  according to Equation (2-4) in section 2.3.1.3.3.

A Scatchard plot of the special-site results based on the Equation (2-5) is shown in Figure 2.26. From the slope and the intercept,  $K_{a,s} = 0.04 \pm 0.01 \text{ mM}^{-1}$  and  $[MT]_{\max,s} = 131 \pm 40 \text{ } \mu\text{mol/g}$  were found. These values and those determined from the NIP' resin have been substituted in equation (2-6) in section 2.3.1.3.3 and the results are plotted as the solid line in Figure 2.27 for comparison with the experimental results.

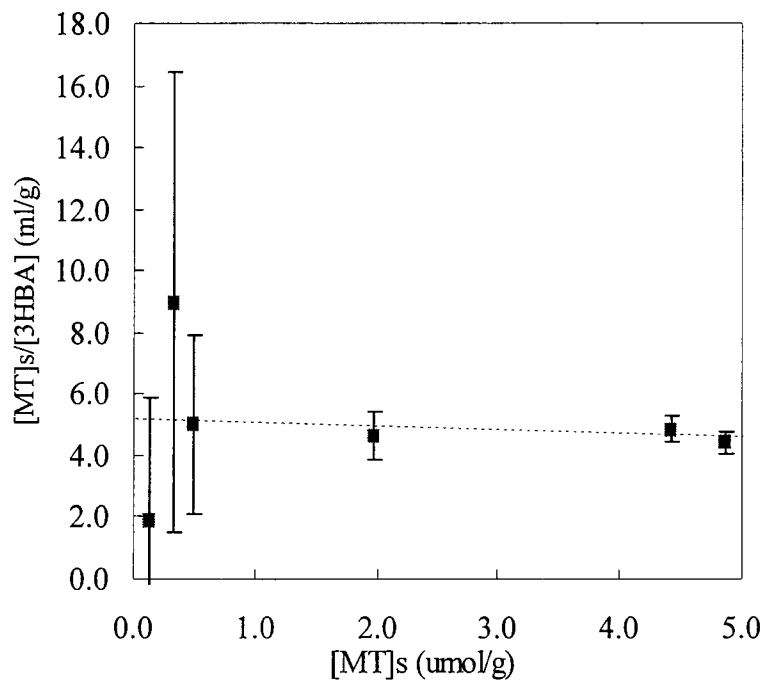


**Figure 2.26.** Scatchard plot for the special binding sites with  $[MT]$  determined using Equation (2-5).

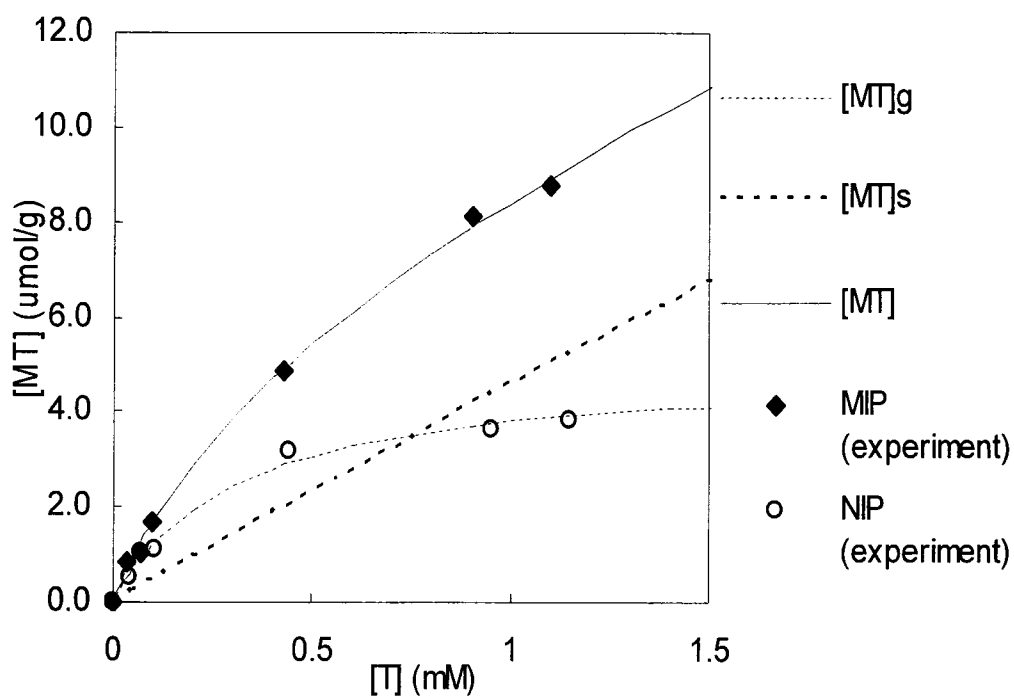


**Figure 2.27.** Representation of the observed binding data using Equation (2-6).  $[MT]_g$  or  $[MT]_s$ : the concentration of 3HBA absorbed in the general or special binding sites calculated from its related  $K_a$  and  $[MT]_{max}$ ;  $[MT]_{total}$ : the concentration of 3HBA absorbed in all binding sites calculated from Equation (2-6); MIP (experiment) or NIP (experiment): the experimental data from binding analysis of MIP or NIP.

#### 2.3.2.4. Substrate selectivity of MIP3HBA and NIP'

The selectivities of MIP for 3HBA and its related compounds 4HBA and BA were compared. Batch analyses were performed on MIP3HBA and NIP' resins respectively under the same experimental conditions. From Figure 2.28, conclusions can be drawn, similar to those in the MIP4HBA case. NIP' showed similar binding capacity for those three analytes. However, in the MIP3HBA binding, 3HBA was bound to a greater extent than both 4HBA and BA, with greater binding by BA compared to 4HBA. The MIP was not saturated by any of the three analytes over the ranges of solution concentrations used.

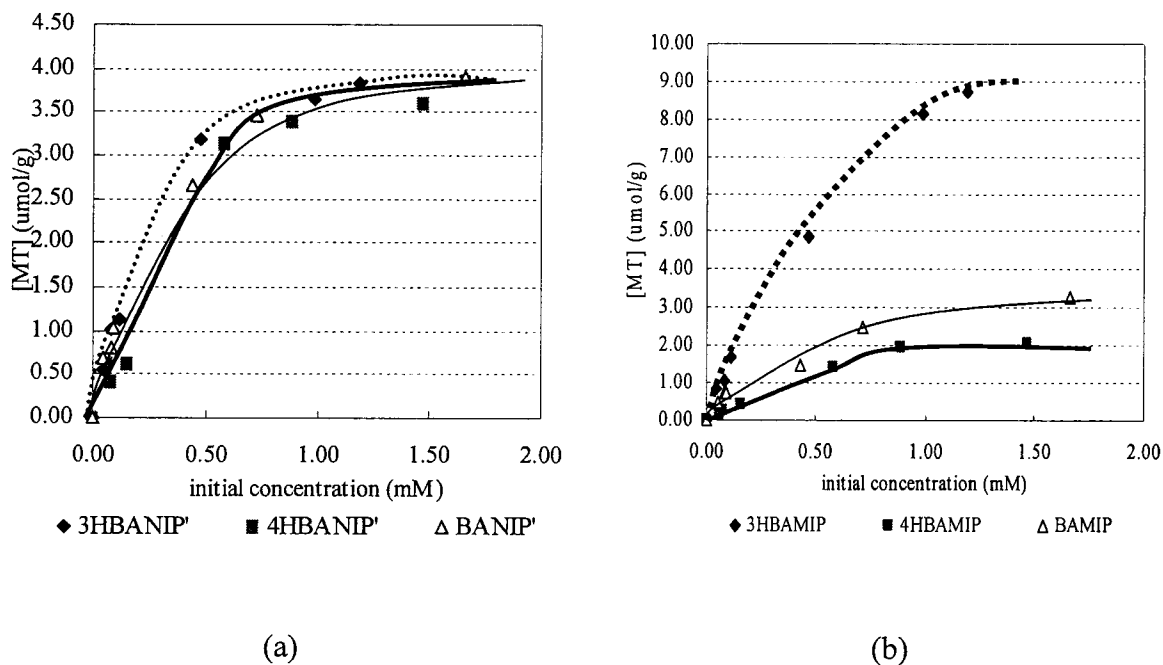


**Figure 2.28.** Binding isotherms of 4HBA, 3HBA and BA on (a) NIP' and (b) MIP. Concentration of resin in solution: 0.01g / 1.0 mL; binding time: 24 hours;  $t = 25\text{ }^{\circ}\text{C}$ .

#### **2.4. Summary**

4HBA and 3HBA were imprinted on the resins respectively and the binding and selectivity properties of 4HBA, 3HBA and BA were studied on each resin in equilibrium binding experiments. Both resins showed better binding performance only on the template molecules which were used in the polymerization. The results were described with a two-site model, the binding sites being designated general and special, in which the general binding sites have very similar binding behavior as is found in NIP. The simulated data from the modified Scatchard equation (Equation (2-6)), which considered both binding sites, fit the experiment results well.

**REFERENCES**

1. *The Columbia Encyclopedia*; Sixth ed.; Columbia University Press, 2001.
2. Kroschwitz, J. I., Ed. *Encyclopedia of Chemical Technology*; John Wiley & Sons, Inc.: New York, 1997.
3. Marengo, E.; Gennaro, M. C.; Gianotti, V. *J. Chromatogr. Sci.* **2001**, *39*, 339.
4. Zuo, Y.; Wang, C.; Zhan, J. *J. Agric. Food Chem.* **2002**, *50*, 3789.
5. Dong, X.; Sun, H.; Lü, X.; Han, J.; Han, B. *Acta chimica Sinica* **2002**, *60*, 2035.
6. Katz, A.; Davis, M. E. *Macromolecules* **1999**, *32*, 4113.
7. Quaglia, M.; Chenon, K.; Hall, A. J.; Lorenzi, E. D.; Sellergren, B. *J. Am. Chem. Soc.* **2001**, *123*, 2146.
8. Zhang, T.; Liu, F.; Chen, W.; Wang, J.; Li, K. *Anal. Chim. Acta* **2001**, *450*, 532.
9. Zhu, Q.; Haupt, K.; Knopp, D.; Niessner, R. *Analytica Chimica Acta* **2002**, *468*, 217.
10. Lübke, C.; Lübke, M.; Whitecombe, M. J.; Vulfron, E. N. *Macromolecules* **2000**, *33*, 5098.
11. Lide, D. R. *CRC handbook of Chemistry and Physics*; CRC Press: Boca Raton, FL, 1994, pp. 6-15 and 9-42.
12. Dean, J. A., Ed. *Lange's Handbook of Chemistry*; 15th ed.; McGraw-Hill, Inc., 1999.
13. Zhou, J.; He, X.; Li, Y. *Anal. Chim. Acta* **1999**, *394*, 353.
14. Yu, C.; Mosbach, K. *J. Org. Chem.* **1997**, *62*, 4057.
15. Yonezawa, Y.; Morishima, I.; Takeuchi, K. *Bull. Chem. Soc. Jpn.* **1976**, *40*, 1807.
16. Rebek, J.; Askew, B.; Killoran, M.; Nemeth, D.; Lin, F. T. *J. Am. Chem. Soc.* **1987**, *107*, 2426.

17. Yamamura, H. I.; Kuhar, M. J. *Neurotransmitter, Receptor Binding*; 2nd ed.; Raven Press: New York, 1985, Chapter 3.
18. Spivak, D.; Gilmore, M. A.; Shea, K. J. *J. Am. Chem. Soc.* **1997**, *119*, 4388.
19. Armstrong, D. W.; Schneiderheinze, J. M.; Hwang, Y. S.; Sellergren, B. *Anal. Chem.* **1998**, *70*, 3717.
20. Garland, C. W.; Niber, J. W.; Shoemaker, D. P. *Experiments in Physical Chemistry*; 7th ed.; The McGraw-Hill Companies, Inc., 2003.

## CHAPTER 3. EXTRACTION AND BINDING STUDIES ON (*S*)-NAPROXEN IMPRINTED POLYMER

### 3.1. Literature review

(*S*)-naproxen is a 2-arylpropionic acid, one of the non-steroidal, anti-inflammatory drugs which can be used to control pain caused by inflammation of muscles, joints and bones. This category of medications includes both prescription and common over-the-counter painkillers such as ibuprofen. Due to the different effects of (*R*)- and (*S*)-naproxen, it is necessary to separate the enantiomers in order to avoid the undesirable side effects.

Several groups have researched MIP with (*S*)-naproxen since 1994. Mosbach's Swedish group was the first to report an MIP study of (*S*)-naproxen.<sup>1</sup> Then between 1997 and 2001 a Japanese group studied the similar system but used a different method to prepare the MIP of (*S*)-naproxen.<sup>2,3</sup>

The Swedish group prepared the MIP by a traditional imprinting method, which was followed by crushing, grinding, and sieving the polymer to produce the packing material for HPLC.

The goal of the Japanese group was to develop an MIP for simultaneous trapping of (*S*)-naproxen and its metabolites in biological fluids. They developed a multi-step swelling and thermal polymerization method with water as the suspension medium

followed by hydrophilic surface modification techniques to make uniformly sized MIP particles.<sup>4</sup> Also, they employed aqueous-rich mobile phase for HPLC. In their multi-step swelling thermal polymerization method, uniform-sized polystyrene (PS) seed particles were prepared as the shape template by emulsifier-free emulsion polymerization. The seed particles, which were about 1  $\mu\text{m}$  in diameter, were swollen in a good solvent that contained the template, EGDMA and 4-vinylpyridine (4VP). Then the polymerization of EGDMA and 4VP was carried out in the swollen PS seed at 50°C under argon with slow stirring following the hydrophilic surface modification. The template was extracted from the resin with THF and methanol. An HPLC column was packed by the traditional slurry packing method, and the retentivity and enantioselectivity of MIPs were studied. By their method, a separation factor of 1.74 for the enantioselectivity of (*S*)-naproxen was obtained, an improvement over the 1.65 of Mosbach.

Here, we focused on understanding how the template molecule (*S*)-naproxen is captured by and released from the MIP during the prearrangement procedure before the polymerization, during the extraction and the rebinding procedures. An outline of the scheme is presented in Figure 3.1. Although it has previously been shown that 4VP is efficient in the preparation of MIPs selective for N-protected amino acids,<sup>4</sup> we had some difficulty getting a decent binding isotherm for (*S*)-naproxen. From the previous experience with MIP4HBA and MIP3HBA systems, acrylamide (AA) was chosen for the functional monomer and other improved experimental techniques were adopted. The two-site model proposed in Chapter 2 was used in this case to simulate (*S*)-naproxen rebinding. It was found that the classification of binding sites, “general” and “special”, is also applicable in this case.

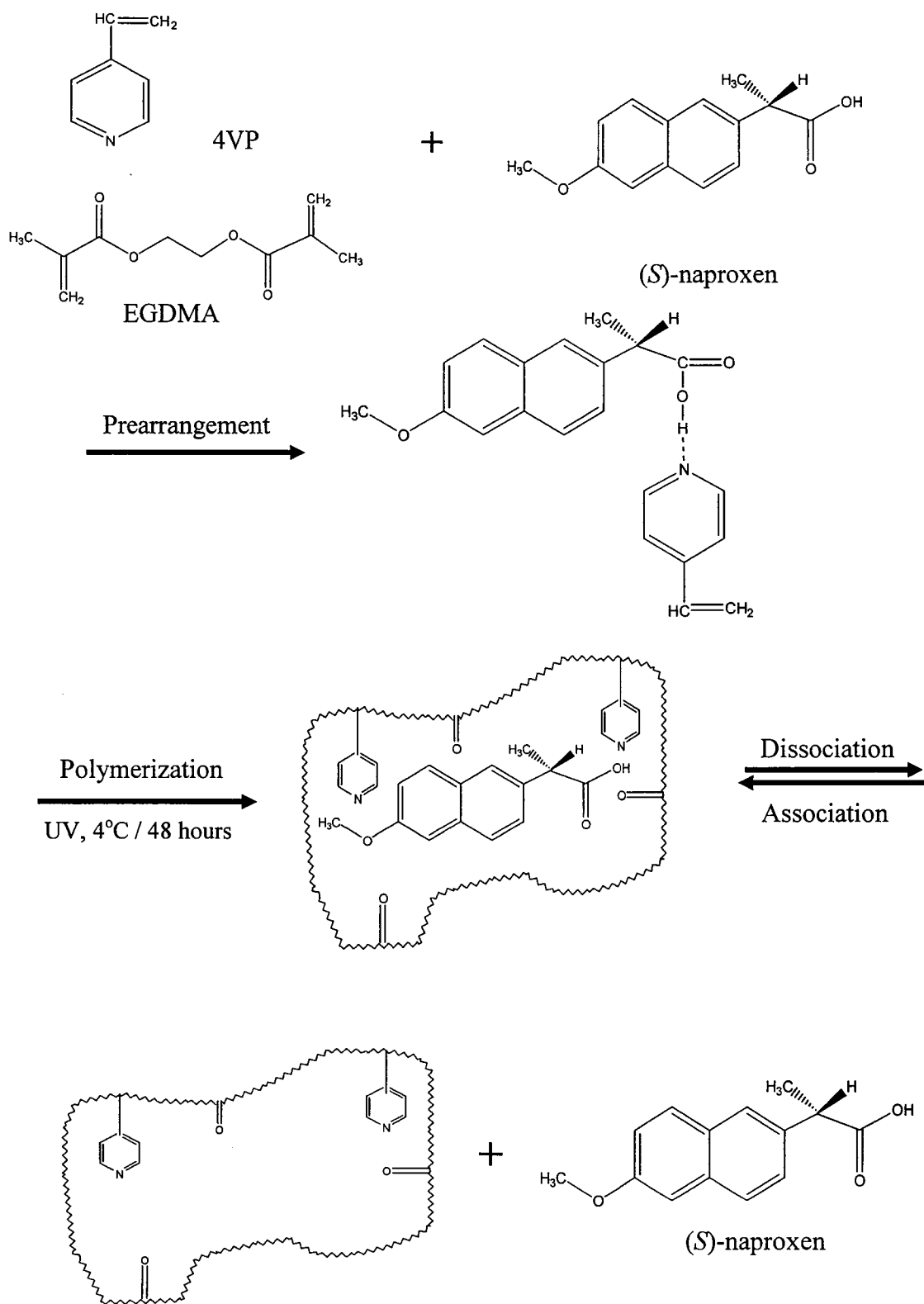


**Figure 3.1.** Scheme of making MIP for (S)-naproxen while 4VP was the monomer.

### 3.2. Experimental

#### 3.2.1. Materials

(*S*)-(+)-6-methoxy- $\alpha$ -methyl-2-naphthaleneacetic acid ((*S*)-naproxen) was purchased from Aldrich and TCI America. 4-Vinylpyridine (4VP), ethylene glycol dimethacrylate (EGDMA) and 2,2'-azobisisobutyronitrile (AIBN) were from Aldrich. Acrylamide (AA) was purchased from Bio-Rad Laboratories. All organic solvents were of analytical or HPLC grade.

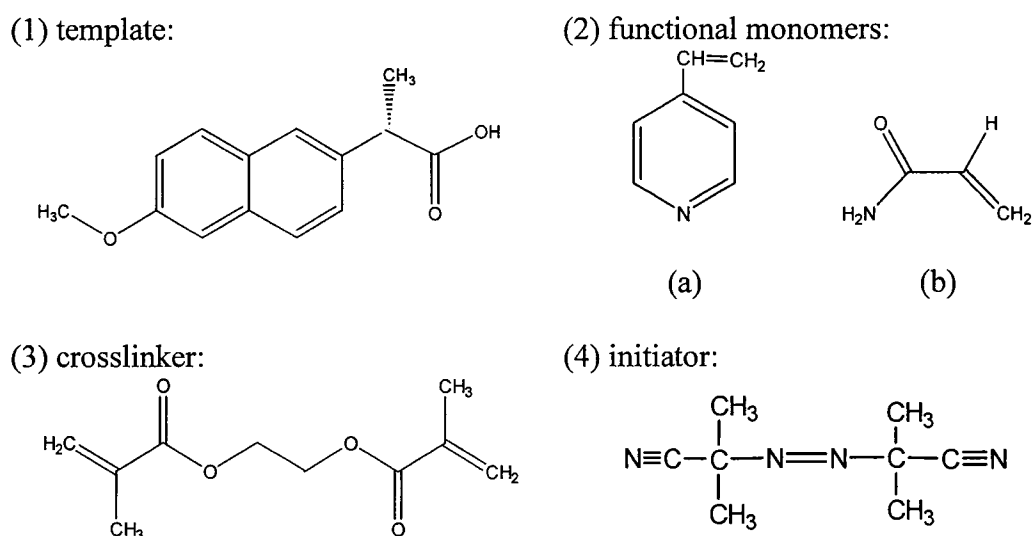


**Figure 3.2.** Structures of the compounds used in the experiment.

(1) template: (*S*)-naproxen; (2) functional monomers: (a) 4VP; (b) AA; (3) crosslinker: EGDMA and (4) initiator: AIBN.

The polymerization inhibitor hydroquinone was removed from 4VP and EGDMA. 4VP was purified by fractional distillation over KOH pellets under reduced  $N_2$  pressure.

EGDMA was distilled under *vacuo* from calcium hydride. AA was used without any pretreatment. AIBN was recrystallized from ethanol.

### 3.2.2. 4VP used in the preparation of non-imprinted polymer (NIP1) and molecularly imprinted polymer with (*S*)-naproxen (4VPMIP <sup>a</sup>)

#### 3.2.2.1. UV study of the interaction between 4VP and (*S*)-naproxen

A series of solutions were prepared with a fixed concentration of (*S*)-naproxen (0.04  $\mu\text{mol/L}$ ) and varying concentrations of 4VP in THF (0.032; 0.16; 0.24; 0.32  $\mu\text{mol/L}$ ). The UV/VIS absorption spectra of these solutions were attained with a Perkin-Elmer Lambda 35 UV/VIS spectrophotometer at a scan speed of 240.0 nm/min.

#### 3.2.2.2. Preparation of NIP1 and 4VPMIP

0.4600 g (*S*)-naproxen (2 mmol), 1.30 mL 4VP (12 mmol) and 11.32 mL EGDMA (60 mmol) were dissolved in 8 mL tetrahydrofuran (THF). The solution was stirred in a 4°C bath for 1 hour. Then 0.1150 g AIBN dissolved in 8 mL THF was added. This mixture was immediately purged with nitrogen for 15 minutes and then irradiated for 48 hours with UV light from an ACE 7825-34 mercury vapor UV lamp (450 watts). The resulting polymer was ground in a ball mill (SPEX 8000) and dry sieved to sizes between 63 and 125  $\mu\text{m}$ . A reference non-imprinted polymer (NIP1) was prepared using the same procedure without addition of the template.

---

<sup>a</sup> 4VPMIP, an abbreviation for the (*S*)-naproxen imprinted polymer in which 4VP was the functional monomer.

### 3.2.2.3. Extraction analyses of NIP1 and 4VPMIP

Approximately 1 g 4VPMIP was stirred with 20 mL THF for 24 hours, thereby removing some template from the resin to THF. After centrifuging, the supernatant was filtered through a 0.45  $\mu\text{m}$  syringe filter. Its UV absorbance was measured at 260 nm. Washing was repeated three more times. The UV absorbance for the solutions was measured after calibrating the absorbance as a function of (*S*)-naproxen concentration over the range for 0.02 to 0.25 mg/mL. A background absorbance was determined in washings of a resin that had been prepared in the absence of template. This correction, which in no case exceeded 4%, was subtracted from the absorbance of the washings in order to eliminate the effects of any non-template UV-absorbing material. These washing experiments were performed on three different 4VPMIP samples.

### 3.2.2.4. Fourier transformation infrared spectra (FT-IR) of 4VPMIP and NIP1

Infrared spectra were obtained for resins 4VPMIP and NIP1. The ground 4VPMIP powders before and after (*S*)-naproxen extraction were dried in a *vacuo* oven at about 70°C to remove the solvent. After 2-3 mg of powder sample was finely ground in a mortar, 150 mg of ground and dried KBr was added to the mortar and quickly mixed with the polymer. Then the mixture was transferred to a die and pressed into a solid disk. After about 1.5 minutes, the two bolts attached to the die were removed, leaving the KBr disk which was mounted in a Perkin-Elmer Spectrum 1600 FT- IR instrument.

The IR spectra were measured between 1000 and 4000  $\text{cm}^{-1}$  with a 4  $\text{cm}^{-1}$  resolution using a Perkin-Elmer Spectrum 1600 FT- IR instrument.

3.2.3. AA used in the preparation of non-imprinted polymer (NIP2) and molecularly imprinted polymer with (*S*)-naproxen (AAMIP<sup>b</sup>)

3.2.3.1. Preparation of NIP2 and AAMIP

After (*S*)-naproxen (the template; 0.2301 g, 1.0 mmol) had been dissolved in 3.00 mL THF, AA (the monomer; 0.1893 g, 2.7 mmol), EGDMA (the crosslinker; 1.26 mL, 6.7 mmol), and AIBN (the initiator; 0.0334 g, 0.2 mmol) were combined in a 50-mL flask. Then another 3.00 mL THF was added. The reaction was performed in a 14 mm OD × 180 mm long borosilicate glass tube. Following the same procedures as MIP4HBA polymerization, the tube was sealed at low pressure. Another tube was prepared according to the same procedure but without template and the resulting resin is designated NIP2.

After UV initiated polymerization for 48 hours, the tubes were broken. The bulk polymer that formed was ground in short repeated cycles using an electric mill. Between each grinding cycle, the products were dry sieved through a 38- $\mu$ m screen. With the same size-selecting technique (refer to the procedure in section 2.2.2.2.), only a small part of qualified particles were saved and dried in a *vacuo* at room temperature for 8 hours.

The template (*S*)-naproxen and a small amount of other soluble residue were extracted from the resin in a cellulose Soxhlet thimble for 24 hours using 100 mL THF-acetic acid (7:3, v/v). A second Soxhlet extraction with 100 mL THF was performed for another 24 hours. The washing solutions were saved for analysis by UV and the polymers were obtained for further study after drying in *vacuo* at room temperature for 10 hours.

---

<sup>b</sup> AAMIP, an abbreviation for the (*S*)-naproxen imprinted polymer in which AA was the functional monomer.

### 3.2.3.2. (*S*)-naproxen binding experiment

Around 0.04 g AAMIP (after the extraction) was added to 4.0 mL of (*S*)-naproxen THF solutions at differing concentrations. This was repeated with NIP2 for comparison. In separate experiments, pure solvent was also added to AAMIP and NIP2 to determine the (trace) amount of any template remaining after the extraction. Each resin mixture was stirred for 24 hours at room temperature. After centrifugation for 20 minutes at 3500 rpm, the supernatant was transferred into a scintillation vial through a 0.45- $\mu$ m syringe filter. The concentration of free (*S*)-naproxen in the supernatant was determined by measuring its UV absorbance at 260 nm.<sup>5</sup>

## 3.3. Results and discussion

### 3.3.1. 4VPMIP system

#### 3.3.1.1. Interaction between monomer and template

The interactions between (*S*)-naproxen and 4VP are important for understanding imprinting and recognition phenomena in MIPs. (*S*)-Naproxen molecule has the carboxyl group, which is the most commonly used hydrogen bonding functional group in molecular imprinting. For amides and carboxylic acids, a number of different hydrogen-bonding complexes have been studied in the gas phase; it was found that O—H $\cdots$ O and N—H $\cdots$ O hydrogen bonds are the strongest among all kinds of hydrogen bonding complexes containing only one hydrogen bond.<sup>6</sup>

The absorption of ultraviolet or visible radiation generally results from excitation of bonding electrons; as a consequence, the wavelengths of absorption peaks can be

correlated with the types of bonds in the species. The UV spectra in Figure 3.3 show the prearrangement interaction between 4VP and (*S*)-naproxen. As the concentration of 4VP was increased, the wavelength  $\lambda_{\text{max}}$  of maximum absorption by (*S*)-naproxen shifted to greater  $\lambda$ , and the maximum absorbance at the maximum wavelength increases with the addition of 4VP.

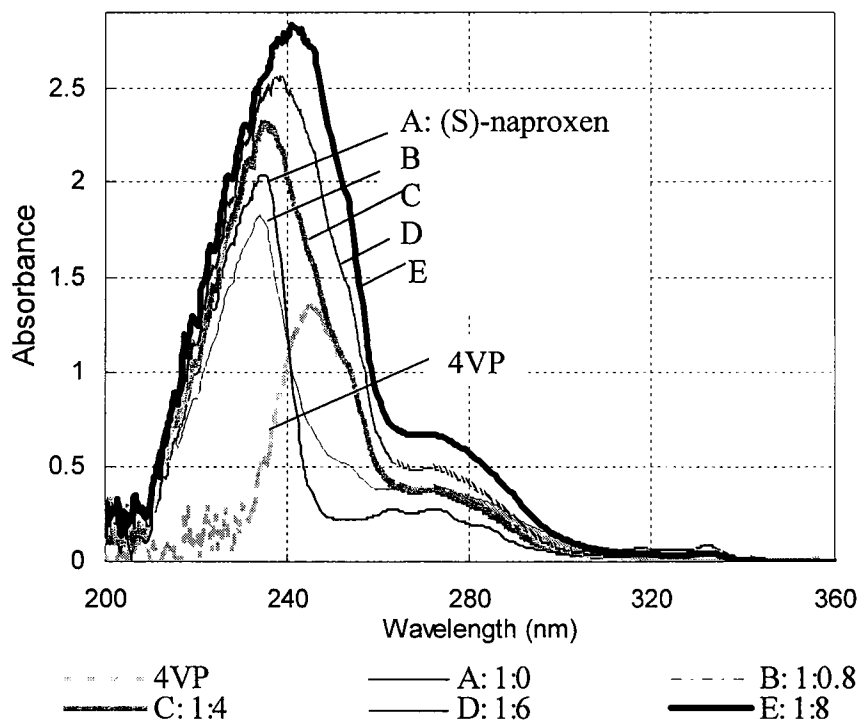


**Figure 3.3.** UV absorption spectra of (*S*)-naproxen and 4VP in THF. Concentration of (*S*)-naproxen is 0.04  $\mu\text{mol/L}$ ; concentration of 4VP ( $\mu\text{mol/L}$ ): B, 0.032; C, 0.16; D, 0.24; E, 0.32.

This result can be explained as the interaction between 4VP and (*S*)-naproxen (Figure 3.4). Due to the addition of 4VP,  $\pi$  electrons of the carbonyl group in (*S*)-naproxen are further delocalized by conjugation. The effect of this delocalization is to lower the energy level of the  $\pi^*$  orbital and give it less antibonding character. As a result,

the absorption maxima associated with  $n \rightarrow \pi^*$  transitions are shifted to longer wavelengths.

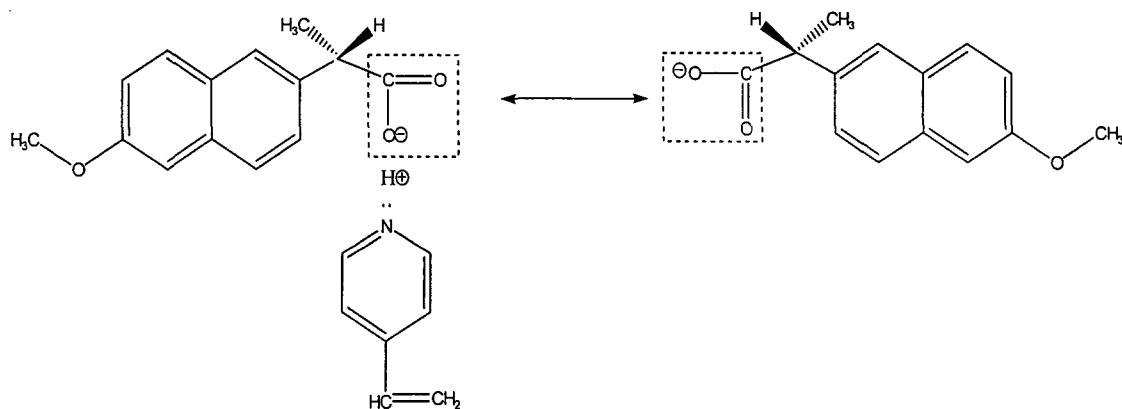


**Figure 3.4.** Delocalization of  $\pi$  electrons in (*S*)-naproxen with the addition of 4VP.

A previous FT-IR study<sup>6</sup> showed that when 4VP was added to (*S*)-naproxen in a THF solution, the stretch absorption of the OH group in (*S*)-naproxen FT-IR spectrum was shifted from  $3501\text{ cm}^{-1}$  to  $3040\text{ cm}^{-1}$ ; the carbonyl stretch absorption was shifted from  $1736\text{ cm}^{-1}$  to a much more broadened band centered around  $1733\text{ cm}^{-1}$ .

In addition, the interaction of template with the solid polymer was tested by FT-IR. The spectra were collected upon resins (A) in the absence of (*S*)-naproxen, (B) with the (*S*)-naproxen in place after polymerization, and (C) after extraction of (*S*)-naproxen. (Figure 3.5) The carbonyl stretch absorption  $\tilde{\nu}_{\text{max}}$  moves from (A)  $1739$  to (B)  $1726$  to (C)  $1734\text{ cm}^{-1}$ .

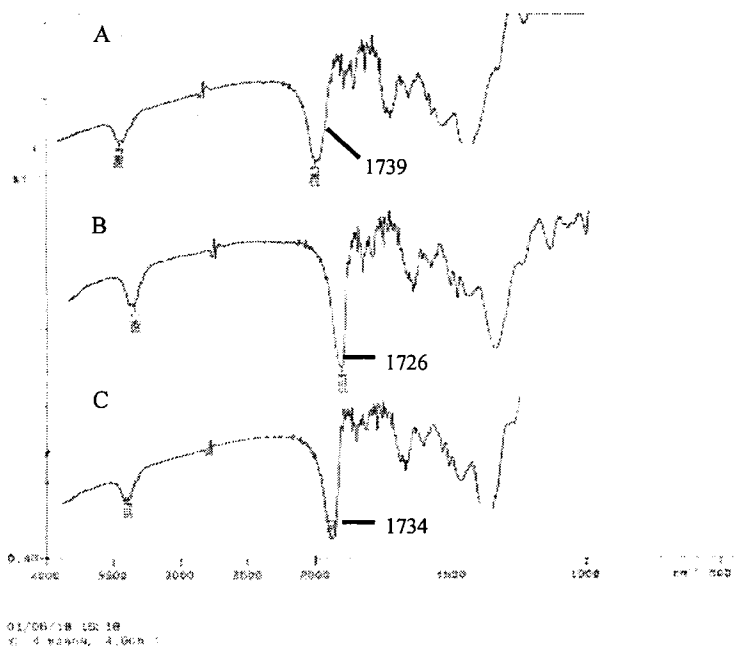


**Figure 3.5.** FT-IR Spectra for (A) NIP1; (B) 4VPMIP before (*S*)-naproxen extraction; (C) 4VPMIP after (*S*)-naproxen extraction. Wave numbers are reported in  $\text{cm}^{-1}$ .

Usually, the carbonyl peak is composed of contributions from both ester ( $1735 - 1750 \text{ cm}^{-1}$ ) and dimerised or hydrogen bonded carboxylic acid functionalities ( $1700 - 1725 \text{ cm}^{-1}$ ) with the apparent, cumulative, absorbance maximum lying between these,  $1730 \text{ cm}^{-1}$ .<sup>7</sup> The dimerisation can be ignored in this case because of the use of a dilute solution. So the hydrogen bonding is responsible for lowering the carbonyl frequency shift by weakening the carbonyl bond and lowering the electron withdrawing potential together with the stretching force constant. This suggests that the template molecule may interact through hydrogen bonding in this 4VPMIP network and the hydrogen bonding may be more responsible for the selectivity of the template.

### 3.3.1.2. Extraction analyses of 4VPMIP resins

Our original study<sup>5</sup> concentrated on a quantitative analysis for (*S*)-naproxen in four successive washings of the 4VPMIP resin to remove the template after polymerization: first with THF, then the following three with a THF-acetic acid solution. The washings were performed in a capped flask with stirring. The concentration of (*S*)-naproxen in each washing was determined by high performance liquid chromatography (HPLC). A 0.025-mL sample was injected and went through a C18-silica reversed phase column (Alltech, econosphere C18 3 $\mu$ , 50 mm  $\times$  4.6 mm) at a flow rate 1.0 mL/min of mobile phase THF/ H<sub>2</sub>O (60:40, v/v). The elution was monitored by UV at 260 nm. The HPLC chromatograph is depicted in Figure 3.6. There was no (*S*)-naproxen in the control experiment; consequently there is no (*S*)-naproxen peak in its HPLC chromatograph. The amount of (*S*)-naproxen washed out was calculated from the peak area and the standardization equation. With successive washings, the amount of (*S*)-naproxen extracted decreased. After the fourth washing, at least 70% of the (*S*)-naproxen had been washed out from the resin. However, some (*S*)-naproxen still remained.

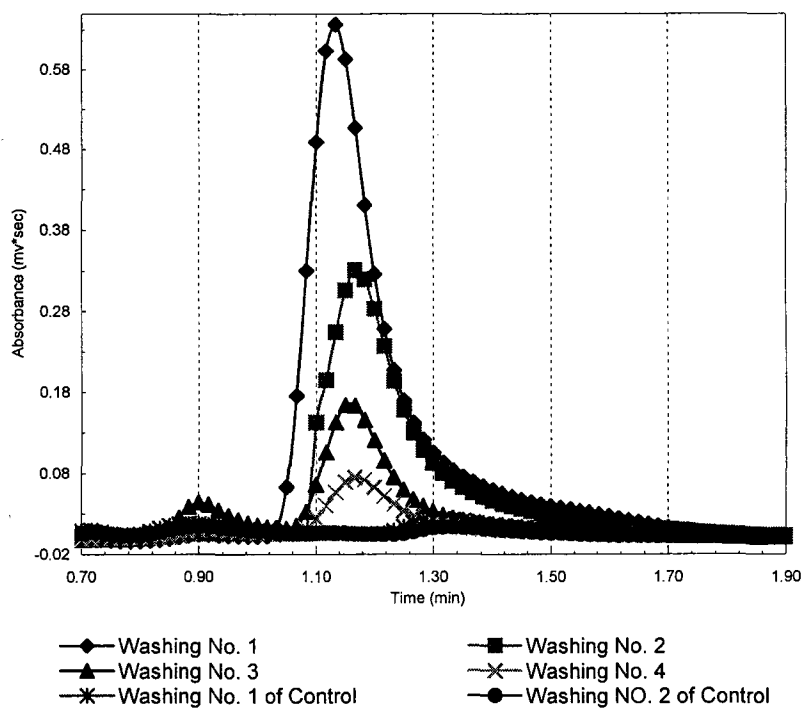


**Figure 3.6.** HPLC chromatograph of four consecutive washings of MIP and its control experiment.

Washing the template from the resin is an important step in preparing MIP system for analytical applications. In the later trials, Soxhlet extraction was used for the continuous washings of (*S*)-naproxen from the template-containing resins with THF. There was no difference found between the treatments with THF / acetic acid and with THF alone. A 90-94% recovery of the template initially present could be reached after four successive THF washings. Small amount of template was apparently trapped in the resin and could not be washed out completely from the MIP.

It is assumed that after each washing, the cavities left have the same properties and only these cavities are considered during each washing procedure. Then the reversible model reaction can be expressed as is shown in Figure 3.7.

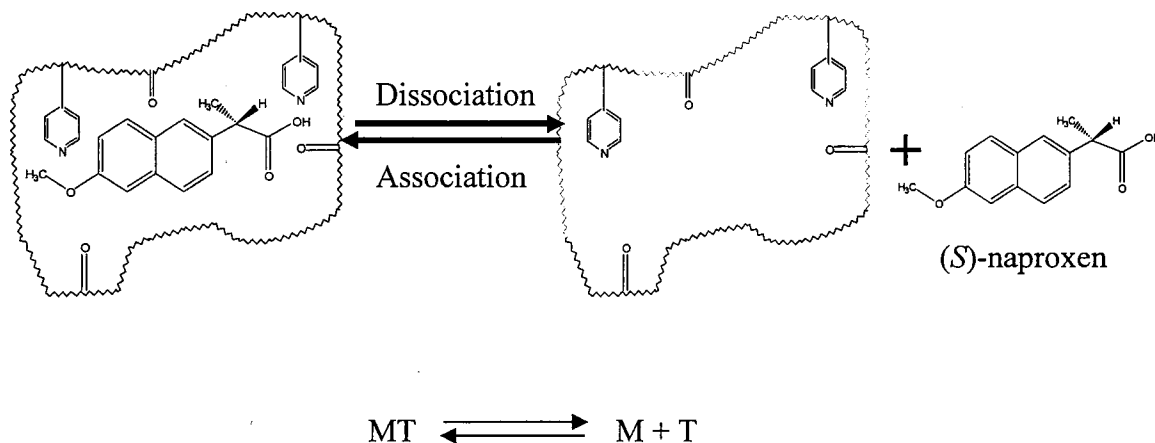


**Figure 3.7.** The reversible model reaction for washing analyses.

Let  $MT$  symbolize the (*S*)-naproxen in the MIP,  $M$  symbolize the empty sites for (*S*)-naproxen in the polymer resin and  $T$  symbolize the template (*S*)-naproxen in the washing solution. The molar concentration of template  $[T]$  in the wash solutions was measured directly from the UV absorbance of those solutions. The amount of (*S*)-naproxen remaining in the resin,  $[MT]$  measured in mmoles per gram of resin, was determined by difference from the amount of (*S*)-naproxen initially present in the polymerizing mixture. The data were fit to the two-site Scatchard Equation

$$[MT] = \frac{n_{\max,H}[T]}{K_{d,H} + [T]} + \frac{n_{\max,L}[T]}{K_{d,L} + [T]}$$

using an iterative spreadsheet procedure that minimized

the sum of the squares of the difference between the measured and calculated concentrations  $[MT]$  of bound (*S*)-naproxen by adjusting the parameters for the maximum number of binding sites  $n_{\max,H}$  and  $n_{\max,L}$  and dissociation constants  $K_{d,H}$  and  $K_{d,L}$ . Here the subscripts H and L refer to the high- and low-affinity binding sites.

Two of these sets of four washings yielded good fits. The third required a negative  $K_{d,H}$  to fit the four data points to the four parameters. The mean values and their spreads for the two good data sets are  $n_{max,H}=13\pm 1$   $\mu\text{moles}$  of sites per gram of resin,  $n_{max,L}=110\pm 30$   $\mu\text{mol/g}$ ,  $K_{d,H}=0.003\pm 0.002$   $\text{mmol/L}$ , and  $K_{d,L}=14\pm 5$   $\text{mmol/L}$ . The data for one set of washings are depicted in Figure 3.8. The two-site Scatchard analysis shows the strong binding sites to be saturated at solution concentrations  $[T]>0.4$   $\text{mmol/L}$ . A more precise value for  $K_{d,H}$  would require more data at concentrations below saturation than were obtained in these washing experiments.

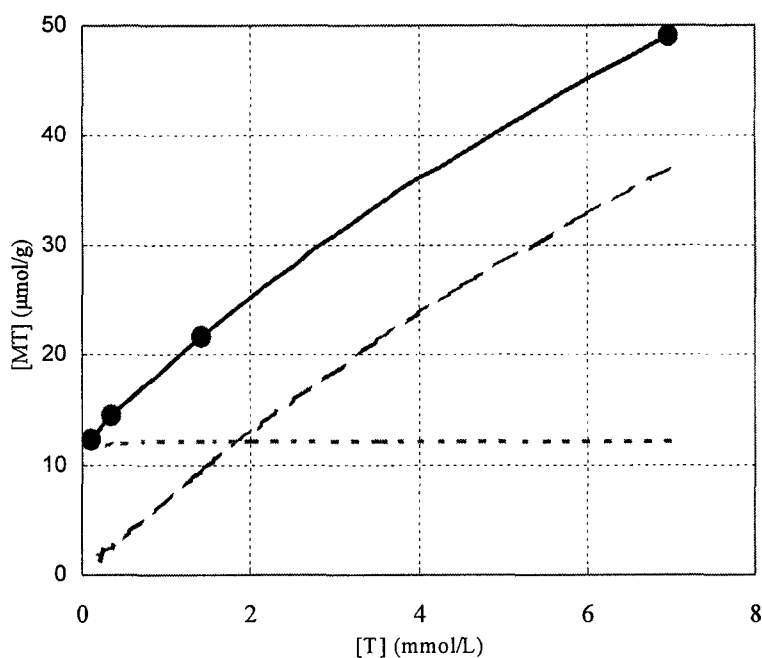


**Figure 3.8.** Two-site Scatchard plot showing the quantity of (*S*)-naproxen absorbed at the weak (dashed line) and strong (dotted line) binding sites. Measured values for the four washings are shown. The solid line is the calculated fit for the total amount bound.

### 3.3.2. AAMIP System

In the MIP extraction procedure, the template molecules should be able to dissociate from the binding sites; in the binding experiment, they should also have the ability to associate into those binding sites. Although the previous UV and FTIR experiments showed that 4VP is a good monomer candidate to imprint (*S*)-naproxen, 4VPMIP did not show significant binding capacity for (*S*)-naproxen. In the interaction study between 4HBA and AA (see section 2.3.1.1), AA formed a stable complex with 4HBA by hydrogen bonds because the acid group in 4HBA plays an important role. From the success of binding experiments in MIP4HBA and MIP3HBA systems, AA was selected as the monomer for (*S*)-naproxen imprinted resin.

#### 3.3.2.1. Preparation of AAMIP

The scheme to use AA as the monomer to prepare MIP is described in Figure 3.9.

Besides the improved techniques, such as sealing the components in the glass tube under *vacuo*, selecting fine particles by a 38- $\mu\text{m}$  screen and extracting template from the resin continuously with a Soxhlet device, etc., the ratio of template to monomer to crosslinker was selected as 3:8(AA):20 instead of 1:6(4VP):30 (Table 3.1). Using a higher monomer concentration has been found to promote high selectivity and affinity in the rebinding step.<sup>8</sup> Also by using a more concentrated pre-polymerization solution, more stable AA-(*S*)-naproxen complexes were expected to form, which will ensure more effective binding sites formed in the later polymerization.

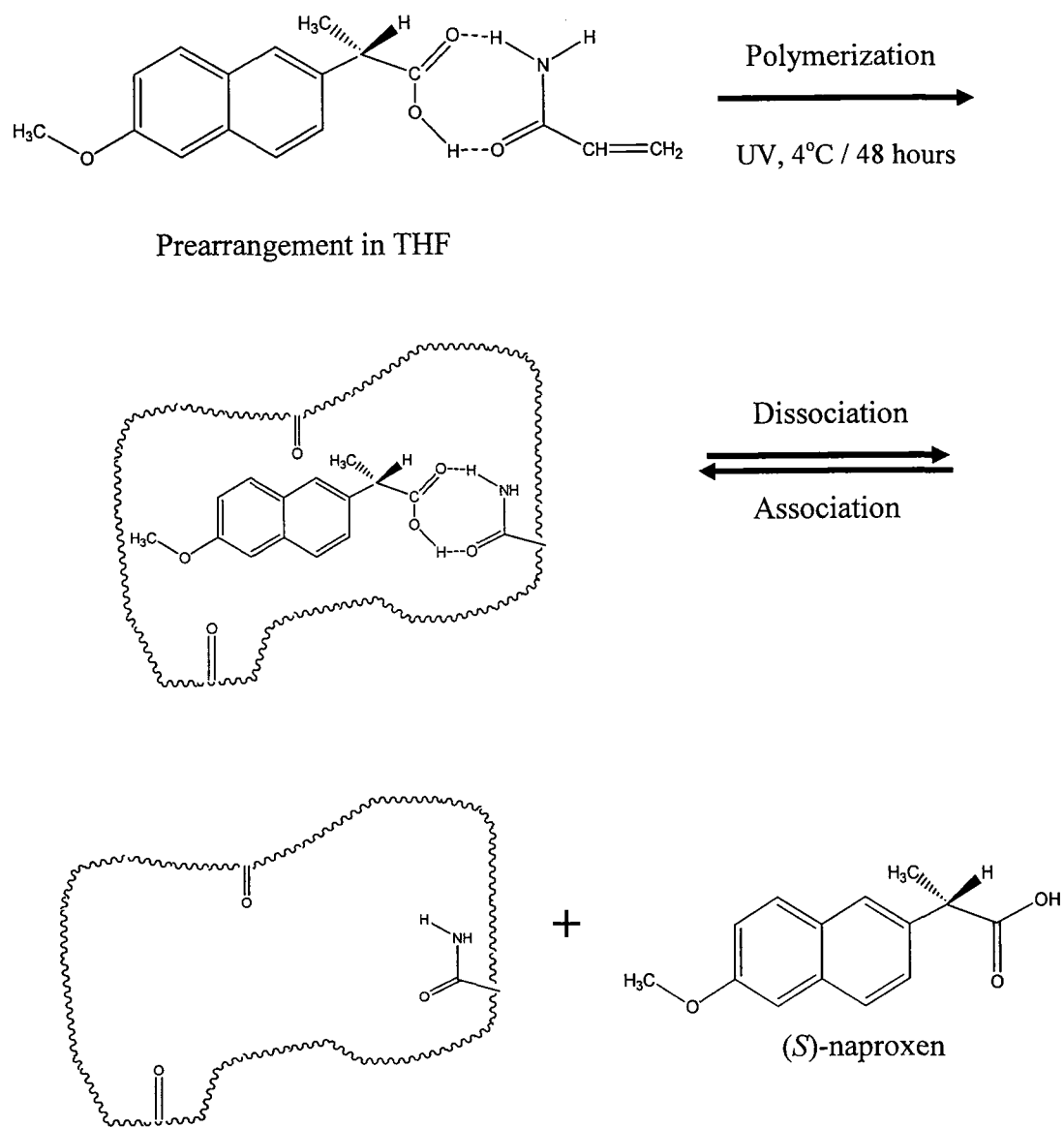


**Figure 3.9.** Scheme of making MIP for (*S*)-naproxen while AA was the monomer.

**Table 3.1.** Composition of each polymerization imprinted with (*S*)-naproxen.

	Template ( <i>S</i> -naproxen)	Monomer	Crosslinker (EGDMA)	Porogen (THF)	Initiator (AIBN)
<i>AAMIP</i>	0.2301 g, 1.0 mmol	<i>AA</i> : 0.1893 g, 2.7 mmol	1.26 mL, 6.3 mmol	6.00 mL	0.0334 g, 0.2 mmol
<i>NIP2</i>	none	<i>AA</i> : 0.1893 g, 2.7 mmol	1.26 mL, 6.3 mmol	6.00 mL	0.0334 g, 0.2 mmol
4VPMIP	0.4600 g, 2 mmol	4VP: 1.30 mL, 12 mmol	11.32 mL, 60 mmol	16.00 mL	0.1150 g, 0.67 mmol
NIP1	none	4VP: 1.30 mL, 12 mmol	11.32 mL, 60 mmol	16.00 mL	0.1150 g, 0.67 mmol

### 3.3.2.2. Binding analyses of *AAMIP* and *NIP2* resins

After the extractions of the imprinted (*AAMIP*) and non-imprinted (*NIP2*) resins, they were immersed in (*S*)-naproxen-THF solutions whose concentrations were varied over the range of 0-2.5 mM. The binding isotherms for (*S*)-naproxen in both resins, as determined from the UV-absorbance of the solutions, are plotted in Figure 3.10. The *AAMIP* absorbed more (*S*)-naproxen than the *NIP2* with the difference increasing with increasing concentrations. The *NIP2* appeared to be close to saturation when the initial concentration of (*S*)-naproxen was  $[T]_0 \geq 1.0$  mM.

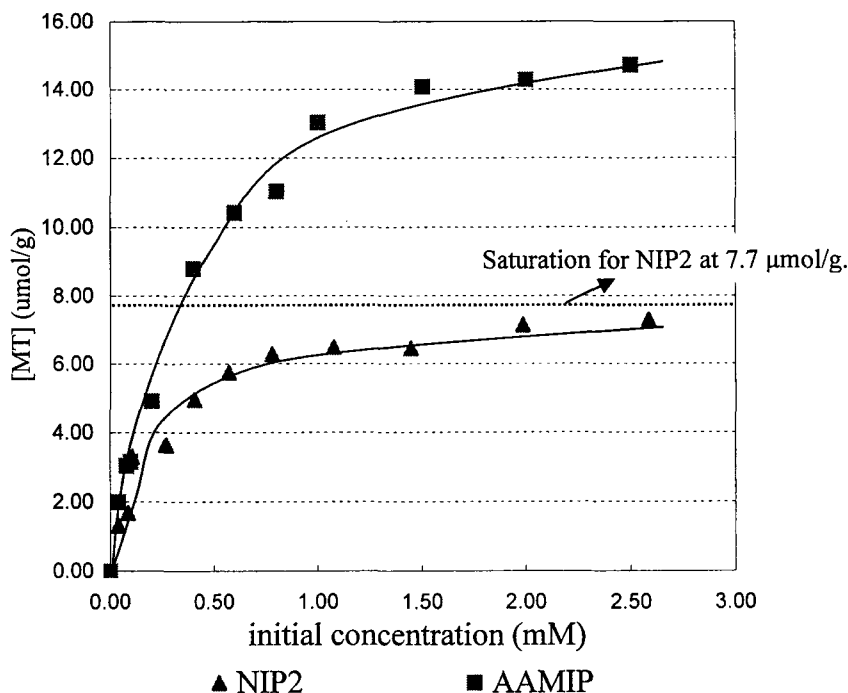


**Figure 3.10.** Binding isotherms for (*S*)-naproxen on AAMIP and NIP2. [MT], concentration of (*S*)-naproxen bound in the resin at equilibrium ( $\mu\text{mol/g}$  of resin);  $t = 25$  °C; absorption time: 24 hours. The dashed line at  $[\text{MT}] = 7.7 \mu\text{mol/g}$  is the asymptotic limit for NIP2, as explained in the text.

The data in Figure 3.10 were re-plotted in Figure 3.11 with  $[\text{MT}]/[\text{T}]$  graphed as a function of  $[\text{MT}]$  as suggested by the Scatchard equation<sup>9</sup>. For the NIP2, the ratio  $[\text{MT}]/[\text{T}]$  is a linear function of  $[\text{MT}]$  over the range from  $[\text{MT}] = 0$  to the saturation of the resin. The slope and intercept of the line representing these data were determined by the method of least squares, with each point weighted in proportion to the inverse square

of its experimental uncertainty.<sup>10</sup> The results yield the equilibrium association constant

$$K_{a,NIP2} = 5.3 \pm 0.3 \text{ mM}^{-1} \text{ and the maximum number } [MT]_{\max,NIP2} = 7.7 \pm 0.5 \text{ } \mu\text{mol/g.}$$

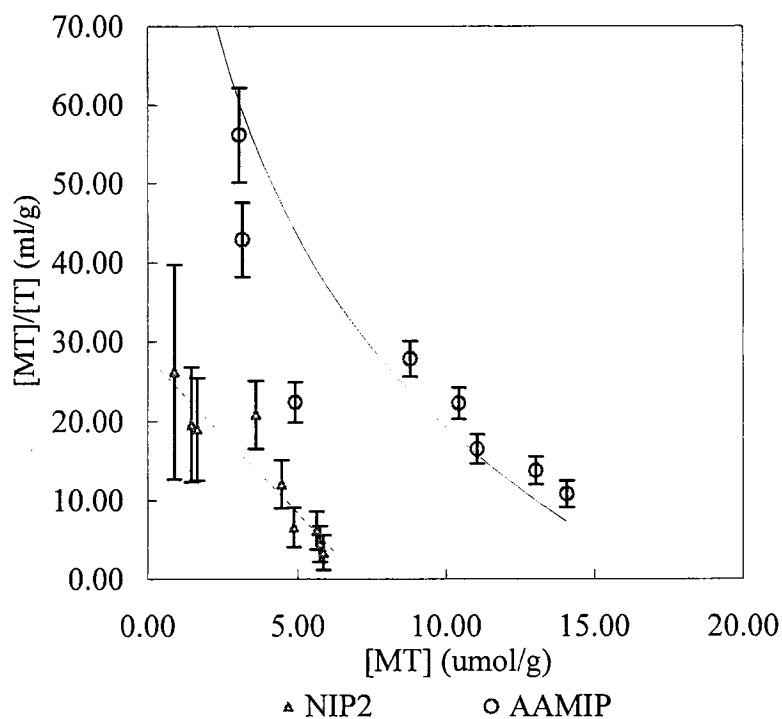


**Figure 3.11.** Scatchard plot of AAMIP and NIP2 for (*S*)-naproxen.

Following the previous MIP4HBA and MIP3HBA study, two kinds of binding sites with different affinities were classified: “general” sites that in this system dominate the behavior at low concentrations of template species and “special” binding sites, dominant at high concentrations. The general binding sites were treated as being the same kind as those found in the NIP2 resin. Accordingly, they are assigned the same affinity constant  $K_{a,g} = K_{a,NIP2}$  and the same site density  $[MT]_{\max,g} = [MT]_{\max,NIP2}$ . The

concentration of template at the special sites  $[MT]_s$ , is calculated by subtracting the amount attributed to the general sites from the total amount bound  $[MT]_{total}$  according to Equation (2-4) in section 2.3.1.3.3.

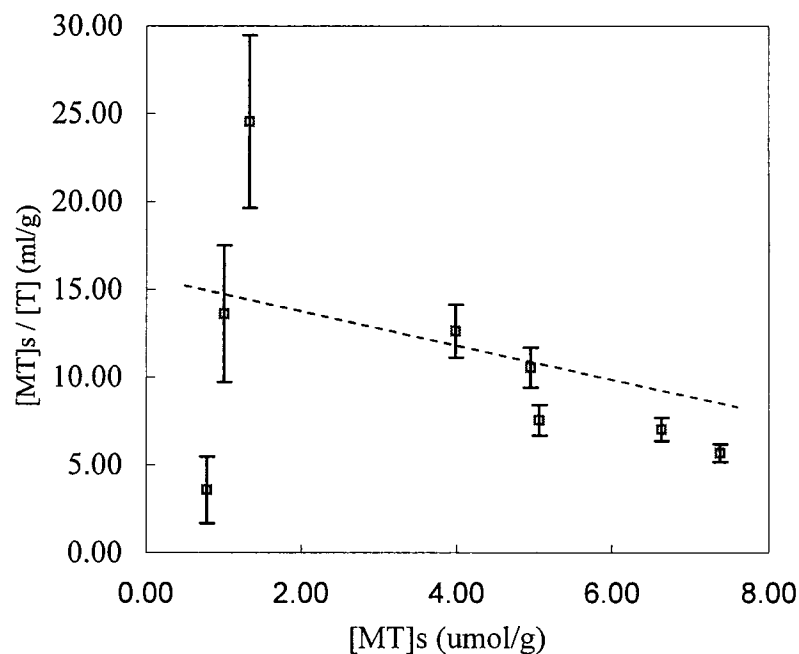


**Figure 3.12.** Scatchard plot for the special binding sites with  $[MT]$  determined using Equation (2-5).

A Scatchard plot of the special-site according to Equation (2-5) in section 2.3.1.3.3 is shown in Figure 3.12. From the slope and the intercept,  $K_{a,s} = 0.84 \pm 0.04 \text{ mM}^{-1}$  and  $[MT]_{\max,s} = 15 \pm 1 \text{ } \mu\text{mol/g}$  were found. These values and those determined from the NIP' resin have been substituted in Equation (2-6) in section 2.3.1.3.3 and the results are plotted as the solid line in Figure 3.13 for comparison with the experimental results.

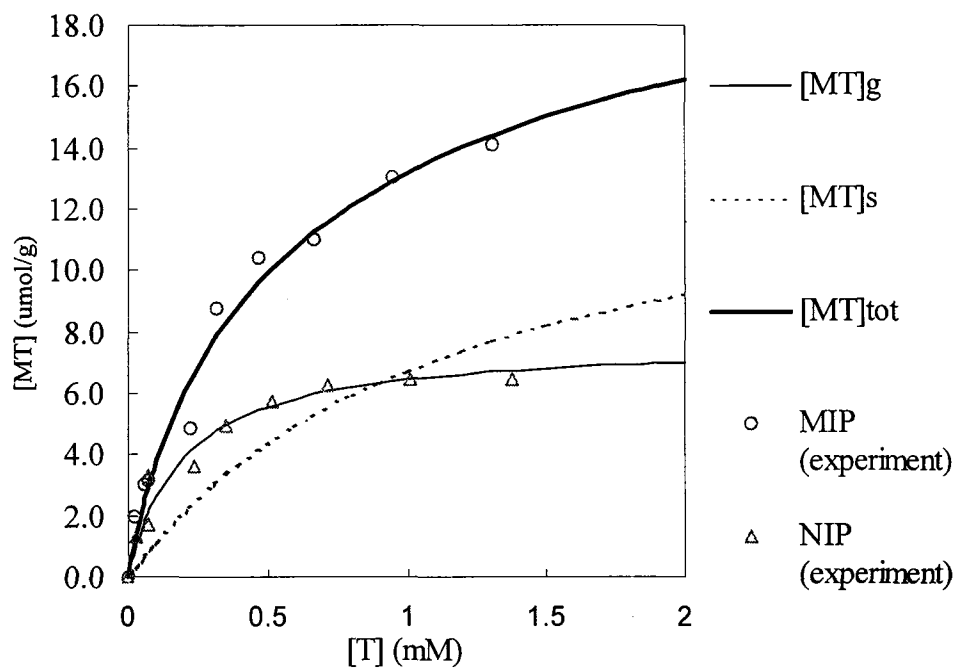


**Figure 3.13.** Representation of the observed binding data using Equation (2-6).  $[MT]_g$  or  $[MT]_s$ : the concentration of (S)-naproxen absorbed in the general or special binding sites calculated from its related  $K_a$  and  $[MT]_{max}$ ;  $[MT]_{total}$ : the concentration of (S)-naproxen absorbed in all binding sites calculated from Equation (2-6); MIP (experiment) or NIP (experiment): the experimental data from AAMIP's binding or NIP2's binding.

### 3.4. Summary

(*S*)-naproxen imprinted polymers have been successfully prepared by using two different kinds of functional monomers 4VP and AA. The monomer-template interaction was proved by UV-Vis and FTIR. The template removal analysis was quantified by HPLC study.<sup>11</sup> In addition, a simple two-binding-site model proposed in hydroxybenzoic acid isomers imprinted resins' study can also be applied in explaining the binding isotherm about (*S*)-naproxen imprinted polymer.

**REFERENCES**

1. Kempe, M.; Mosbach, K. *J. Chromatogr. A*, **1994**, *664*, 276.
2. Haginaka, J.; Takehira, H.; Hosoya, K.; Tanaka, N. *J. Chromatogr. A* **1999**, *849*, 331.
3. Haginaka, J.; Sanbe, H. *Anal. Chem.* **2000**, *72*, 5206.
4. Kempe, M.; Fisher, L.; Mosbach, K. *J. Mol. Recogn.* **1993**, *6*, 25.
5. Hu, Y. Master Thesis, College of William and Mary, 2001.
6. Yu, C.; Mosbach, K. *J. Org. Chem.* **1997**, *62*, 4057.
7. Svenson, J.; Nicholls, I. A. *Anal. Chim. Acta* **2001**, *435*, 19.
8. Sellergren, B.; Dauwe, C.; Schneider, T. *Macromolecules* **1997**, *30*, 2454.
9. Yamamura, H. I.; Kuhar, M. J. *Neurotransmitter, Receptor Binding*; 2nd ed.; Raven Press: New York, 1985, Chapter 3.
10. Garland, C. W.; Niber, J. W.; Shoemaker, D. P. *Experiments in Physical Chemistry*; 7th ed.; The McGraw-Hill Companies, Inc., 2003.
11. Hu, Y.; Orwoll, R. A. In *Materials Research Society Symposium Proceedings*, 2002; Vol. 723, pp 105.

## CHAPTER 4. DISCUSSION

### 4.1. Anatomy of binding sites in MIPs

The glamour of MIPs is that this kind of material is tailor made so that it has the special selectivity and affinity for the template. But when and how do the binding sites form? A closer look at the copolymerization of monovinyl monomers (functional monomers) and divinyl monomers (crosslinking monomers) initiated by free radicals is needed. At the beginning of the reaction, the primary chains form upon the radicals' attack. The pendant double bonds can either remain unreacted or react with another growing chain to form a crosslink or intramolecular cycles.<sup>1</sup> Although the pendant double bonds are half as reactive as the monomeric double bonds on average, only a few percent of the pendant double bonds react by cyclization in bulk polymerization.<sup>1</sup> After a certain number of crosslinks are formed, the polymer's viscosity increases, and then a gel starts to form. In the later stages of the polymerization, the remaining double bonds become less reactive due to the poor accessibility within the highly crosslinked domains of the polymer. So far, the main chain's structure in MIPs is still unknown, because the reactivity of monomers has many influencing factors such as the solvent, the reaction temperature and the presence of template molecules, etc.

Based on the review of the free radical polymerization, two possible mechanisms for the formation of binding sites in MIPs were proposed: "frozen-in" and "step-by-step".

Suppose there are two functional groups A and B attached on the functional monomer M, which have the ability to form a complex with the template molecule in a pre-polymerization solution. If the rate of chain propagation is high, instead of having time to dissociate with the monomer, the template remains assembled with the monomer. As a result, the template-monomer complexes are “frozen” in the polymer matrix. In this case, the amount of crosslinker should be excessive and the formed polymer resin is very rigid (Figure 4.1. (a)). However, if the template has time to dissociate from the monomer before the formation of the three-dimensional sites, the functional group A or B on the monomer will interact with the template step by step while the polymer chain propagates (Figure 4.1. (b)). The majority of the binding sites might form according to this “step-by-step” mechanism. Sellergren gave a similar discussion in the MAA-EGDMA MIP system.<sup>2</sup>

In addition, for the formation of the defined recognition sites, the structural integrity of the monomer-template complexes must be preserved during polymerization to allow the functional groups to be fixed in space in a stable arrangement complementary to the template. This can be achieved by the use of extensive crosslinking. The formed polymer matrix is not only to contain the binding sites in a stable form, but also to provide porosity to allow easy access for the analytes. The concentrations of the functional monomer and template, the temperature and pressure for the polymerization, and the choice of porogen will also affect the recognition properties of MIPs related to the monomer-template complexes.<sup>3</sup>

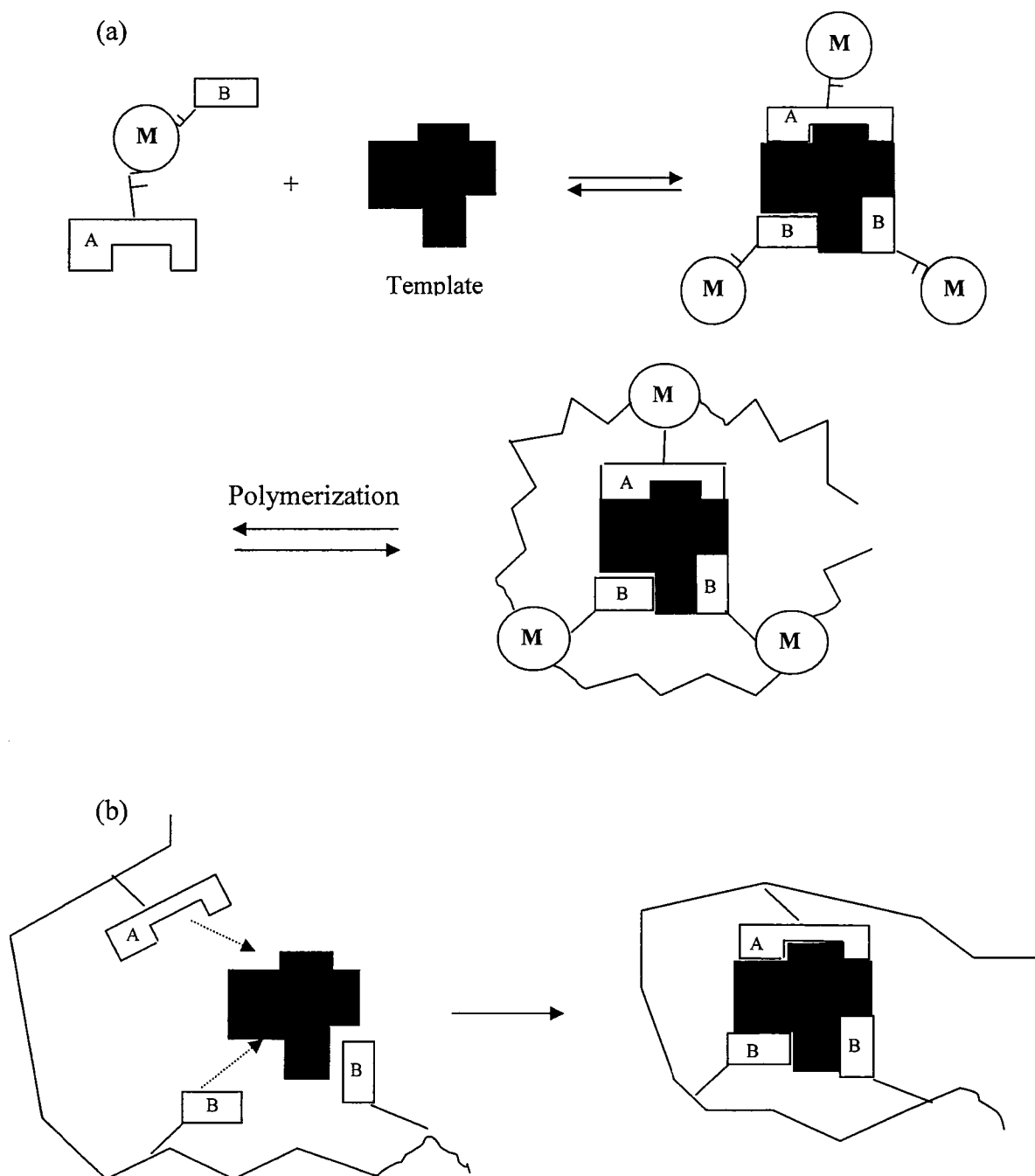


**Figure 4.1.** Mechanisms for the formation of the binding sites in MIPs: (a) "frozen"-in ; (b) step-by-step.

## 4.2. Analyses of the binding sites parameters in MIPs

MIPs with 4HBA were studied previously by Zhang's research group.<sup>4,6</sup> They prepared two main systems based on the functional monomers: 4-vinylpyridine (4VP) and acrylamide (AA). When 4VP was the functional monomer, 4HBA and SA were imprinted separately. Because the complex SA-4VP formed in the pre-polymerization solution is more stable than the complex 4HBA-4VP, SA imprinted polymer showed a higher molecular recognition ability.<sup>6</sup> In another system, AA was the functional monomer. MIPs with SA did not show the imprinting effect because SA-AA cannot form a sufficiently stable complex,<sup>5</sup> but MIP with 4HBA showed selectivity.<sup>4</sup>

In our study, AA was selected as the functional monomer with the template 4HBA or 3HBA. NMR showed that both AA's amide protons were involved in the hydrogen bond interaction with 4HBA or 3HBA. The stability of such interactions played a major role in the later recognition procedure.

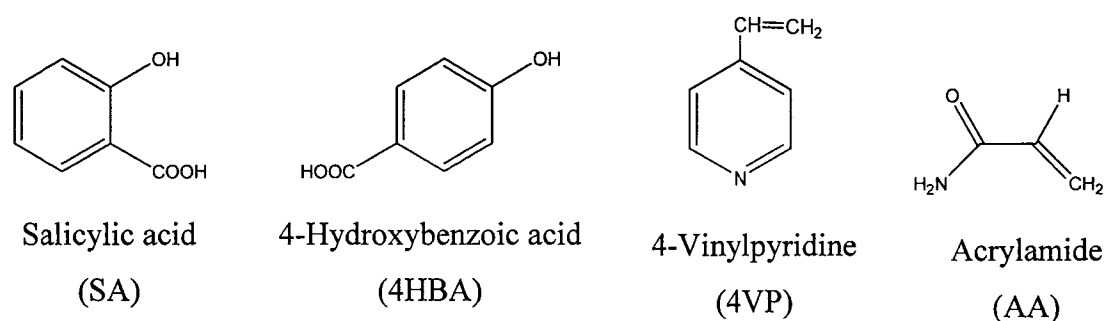


**Figure 4.2.** Structures of templates and functional monomers used in Zhang's research.

When Zhang *et al.* estimated the binding parameters, the equilibrium association constant and the number of the affinity binding sites, they used the traditional Scatchard analysis. From a plot, similar to the one in Figure 1.4. (b) with two distinct sections, two kinds of binding sites were assigned over the range of concentrations studied: one with high affinity dominating the lower concentration of the ligand bound in the MIP ([MT]) and the binding was described with a larger value for  $K_a$ ; the other with low affinity dominating the higher [MT] and the binding was described with a smaller  $K_a$ . Based on those two distinct sections within the Scatchard plot, they were regarded as the straight lines and the binding parameters could be calculated according to the Scatchard equation. The results were listed in Table 4.1.

**Table 4.1.** Binding parameters derived from the Scatchard analysis.<sup>4,5,7</sup>

template	MIP Synthesis				High Affinity		Low Affinity	
	Mono. <sup>a</sup>	Xlink <sup>b</sup>	M:X:T <sup>c</sup>	Solvent <sup>d</sup>	$K_a$ (mM <sup>-1</sup> )	[MT] <sub>max</sub> (μmol/g)	$K_a$ (mM <sup>-1</sup> )	[MT] <sub>max</sub> (μmol/g)
4HBA <sup>4</sup>	AA	EGDMA	6:30:1	AN	5.7	9	0.7	22
SA <sup>5</sup>	4VP	EGDMA	6:30:1	AN	13.2	26.5	0.3	168.7
SA <sup>7</sup>	MAA	PETRA	4:4:1	AN	11.4	18.5	0.5	150.4

<sup>a</sup>Monomer abbreviations: AA, acrylamide; MAA, methacrylic acid; 4VP, 4-vinylpyridine.

<sup>b</sup>Crosslinker abbreviations: EGDMA, ethylene glycol dimethacrylate;

PETRA, pentaerythritol triacrylate.

<sup>c</sup>Molar proportions of monomer:crosslinker:template.

<sup>d</sup>Solvent abbreviations: AN, acetonitrile.

When the Scatchard plot with a broken line is analyzed, as Zhang has done, the contribution of the lower affinity binding sites to the binding capacity of MIPs at lower

concentrations of substrate is not considered in the determination of higher affinity binding parameters. Similarly, at a high concentration of substrate, the binding capacity of higher affinity binding sites is ignored in the determination of lower affinity binding parameters. The binding behavior of the control polymer, prepared without a template (i.e., NIP), is not considered either in Zhang's study.

In our study, the binding behaviors of both MIP and NIP resins were considered and compared. From the binding isotherms, a simple two-binding-site model with one kind of sites special for the template and the other kind being more general with similar affinities as the control polymer is proposed. Instead of classifying the binding sites based on two different concentration ranges, the whole derivation of the simple two-binding-site model considers the whole concentration range. From the similar binding behavior of the control polymer and MIPs at the lower concentration range, they were treated as having similar affinities and defined as the "general" binding sites. The other type was defined as the "special" binding sites. The properties of "general" and "special" binding sites were found quite similar to what Zhang *et al.* described as the "high" and "low" affinity binding sites respectively (Table 4.2). In another words, the general sites, which are treated here as existing in both the MIP and NIP resins, have a *greater* binding affinity than the special sites. That is,  $K_{a,g} > K_{a,s}$ .

**Table 4.2.** Comparison of binding parameters in three MIP systems.

MIP4HBA <sup>a</sup> (Zhang)	High Affinity		Low Affinity	
	K <sub>a</sub> (mM <sup>-1</sup> )	[MT] <sub>max</sub> (μmol/g)	K <sub>a</sub> (mM <sup>-1</sup> )	[MT] <sub>max</sub> (μmol/g)
	5.7	9	0.7	22
MIP4HBA (This work)	General Binding		Special Binding	
	K <sub>a</sub> (mM <sup>-1</sup> )	[MT] <sub>max</sub> (μmol/g)	K <sub>a</sub> (mM <sup>-1</sup> )	[MT] <sub>max</sub> (μmol/g)
	4.4 ± 0.2	6.7 ± 0.3	0.15 ± 0.01	72 ± 2
MIP3HBA (This work)	General Binding		Special Binding	
	K <sub>a</sub> (mM <sup>-1</sup> )	[MT] <sub>max</sub> (μmol/g)	K <sub>a</sub> (mM <sup>-1</sup> )	[MT] <sub>max</sub> (μmol/g)
	3.3 ± 0.1	4.9 ± 0.2	0.04 ± 0.01	131 ± 40

a. results of Zhang *et al.*<sup>6</sup>

The special sites are viewed as molecular sized cavities usually with two or more functional groups that can participate in strong intermolecular interactions such as hydrogen bonding. Special sites exist because a template was present during the polymerization and then subsequently removed. For an analyte molecule to bind to a special site, it must have a unique combination of size, shape and correctly positioned functionalities that are complementary to the resin's functionalities at that site. This accounts for the selectivity which is characteristic of MIPs. Because the analyte molecules must also be positioned and orientated within very strict limits in order to bind at a special site, there is a large loss of entropy associated with the transfer of molecules from solution to special binding sites.

To get a sense of entropy loss, we consider the thermodynamics of the binding of a template species T with a site in the matrix M



The equilibrium constants reported in Table 4.2 for both 3HBA and 4HBA correspond to a greater decrease in free energy  $-\Delta G_g = RT \ln K_{a,g}$  when the template binds to the general sites than when it binds to the special sites. That is, for the equilibrium shown above

$$-\Delta G_g > -\Delta G_s.$$

For 4HBA, the free energy of binding at the general sites is 8 kJ/mol less than at the special sites; for 3HBA, it is 11 kJ/mol less.<sup>a</sup> This is an unexpected result, since the presumption is that binding is favored at the special sites where there apparently are more polar units such as carbonyl groups in the correct position for binding. If the attractive energy of binding is stronger for the special sites, then for the binding “reaction” above

$$\Delta H_g > \Delta H_s$$

Consequently,

$$\Delta S_g > \Delta S_s$$

or the entropy loss in transferring analyte from the liquid solution to the binding sites is greater for the specific sites than for the general sites. This is consistent with the understanding that the analyte molecule has greater freedom at a general site than at a special site.

---

<sup>a</sup> The free energy difference at room temperature between 4HBA or 3HBA’s binding at the special sites and the general sites is calculated according to

$$\Delta G_s - \Delta G_g = (-RT \ln K_{a,s}) - (-RT \ln K_{a,g}) = -RT \ln \frac{K_{a,s}}{K_{a,g}}.$$

If there were no energetic difference between the two sites, *i.e.*,  $\Delta H_g = \Delta H_s$ , then the difference in the entropy loss,  $(\Delta S_g - \Delta S_s)/R$ <sup>b</sup>, would be 3 for 4HBA and 4 for 3HBA.<sup>c</sup> Since it is expected that  $\Delta H_g > \Delta H_s$ , these values would be the lower limits.

The number of special binding sites was found to be greater than the number of general sites. It may be that a majority of the potential sites for hydrogen bonding, etc. is inaccessible owing to the rigidity of the structure and other sites that might otherwise be accessible are already interacting (*e. g.*, hydrogen bonding) with units in the resin.

These  $[MT]_{\max}$  and  $K_a$  values can be compared with other data. For example, the potential density of the binding sites in the MIP's resin ( $[MT]_{\max, \text{ideal}}$ ) is 163  $\mu\text{mol/g}$  based on the quantities of starting material, compared to 72 (MIP4HBA) and 131 (MIP3HBA)  $\mu\text{mol/g}$  calculated from the two-binding-site-model. Also the calculated  $K_a$  can be compared with the  $K_a$  derived from the NMR binding studies.<sup>9</sup> Whitecombe and coworkers<sup>10</sup> found  $K = 0.03 \pm 0.01 \text{ mM}^{-1}$  from the chemical shift of acrylamide N-H

<sup>b</sup> From  $\Delta G_g - \Delta G_s = (-RT \ln K_{a,g}) - (-RT \ln K_{a,s})$  and  $\Delta G = \Delta H - T\Delta S$ ,  
 $(\Delta H_g - T\Delta S_g) - (\Delta H_s - T\Delta S_s) = -RT \ln(K_{a,g} / K_{a,s})$  can be derived.

When  $\Delta H_g = \Delta H_s$ ,  $(\Delta S_g - \Delta S_s)/R = \ln(K_{a,g} / K_{a,s})$ .

<sup>c</sup>  $\Delta_{\text{fus}}H$  is defined as the enthalpy change at equilibrium between the liquid phase and the most stable solid phase at the transition temperature which is normally the melting point  $t_m$ .  $\Delta_{\text{fus}}S$  (J/mol·K) at  $t_m$  can be calculated as  $\Delta_{\text{fus}}S = \Delta_{\text{fus}}H / t_m$  at the equilibrium ( $\Delta_{\text{fus}}G = 0$ ). From Table 4.3, the entropy values of fusion ( $\Delta_{\text{fus}}S/R$ ) of water, acetic acid and benzoic acid are comparable with the entropy change for 4HBA and 3HBA.

Table 4.3. The thermophysical properties<sup>8</sup> of water, acetic acid and benzoic acid at the equilibrium of solid and liquid.

name	$t_m$ (K)	$\Delta_{\text{fus}}H$ (kJ/mol)	$\Delta_{\text{fus}}S$ (J/mol·K) at $t_m$	$\Delta_{\text{fus}}S/R$ at $t_m$
water	273	6.01	22.01	2.6
acetic acid	290	11.73	40.50	4.9
benzoic acid	396	18.02	45.58	5.5

resonance against the concentration of added butyric acid in an NMR titration experiment. This is the same order of magnitude as  $K_a = 0.15 \pm 0.01$  (MIP4HBA) and  $0.04 \pm 0.01$  (MIP3HBA)  $\text{mM}^{-1}$  as derived from the two-binding-site-model.

Other models have been employed to analyze binding by MIPs. For example, Shimizu *et al.* proposed a heterogeneous binding model based on the Freundlich isotherm<sup>11</sup> assuming a continuous distribution of binding sites (see section 1.3.2.3). The data from 4HBA binding on MIP4HBA resin were re-plotted in Figure 4.3. (a) according to the Freundlich equation:

$$\log[MT] = m \log[T] + \log a .$$

From the linear regression fit of the isotherm, two parameters  $a$  and  $m$  can be derived, which were used to generate the corresponding affinity distribution

$$N = 2.3am(1 - m^2)K^{-m} .$$

It relates the number of binding sites ( $N$ ) for each class of binding sites having an association constant ( $K$ ). Although 4HBA binding on MIP4HBA could be fitted to the affinity distribution well (Figure 4.3. (b)), unlike the proposed two-binding-site model, the heterogeneous binding model is complex and involves arbitrary parameter.

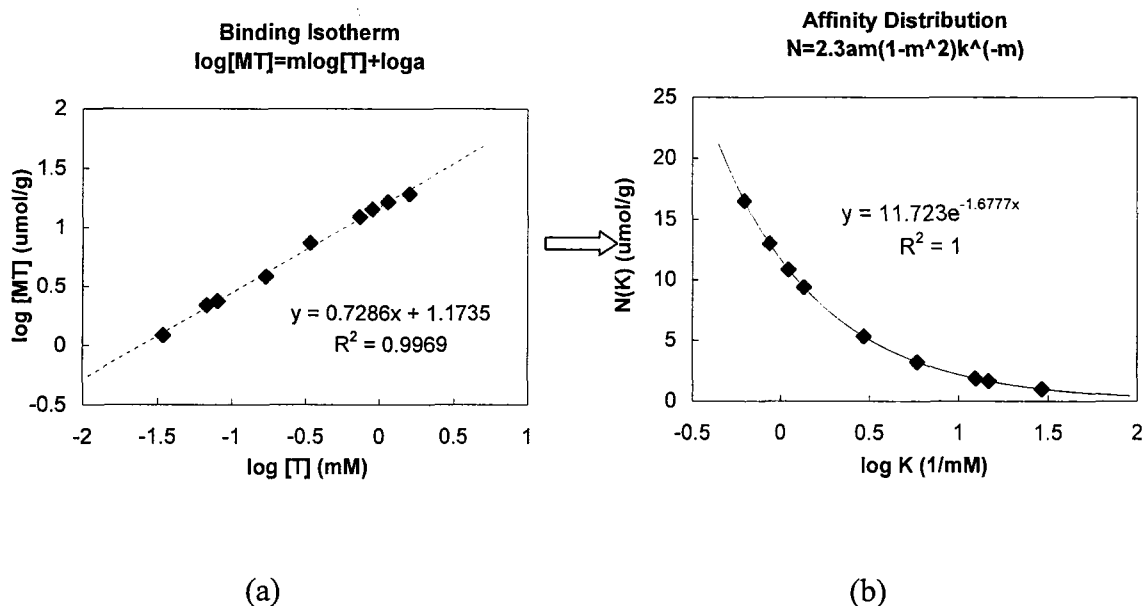


**Figure 4.3.** Binding isotherm (a) for MIP4HBA and the corresponding affinity distribution (b) according to Shimizu.<sup>11</sup>

#### 4.3. MIPs in the bulk format

The molecular imprinting studied here takes place in the bulk of the resin rather than on its surface.<sup>2,12</sup> Several pieces of evidence from this study support that conclusion. (1) Each analyte species (4HBA, 3HBA, and (*S*)-naproxen), when used as the template in the synthesis of MIPs, was dispersed uniformly throughout the resin when the resin was prepared. Yet the template was removed by solvent extraction with recovery efficiencies in excess of 90%. In the case of surface phenomena, only a much smaller fraction of the template would be recovered. (2) The number of special binding sites was determined from the uptake of the template molecule in rebinding studies. This number is comparable to the number of template molecules in the polymerization, i.e., 163  $\mu\text{mol/g}$

for both MIP4HBA and MIP3HBA. (3) Equilibration in the binding experiments (Figure 2.18) from a well stirred solution required at least 8 hours in the case of NIP and a day for MIP. These times are comparable to the times used for equilibration in swelling equilibria experiments on *lightly* crosslinked polymers (24 hours for 1-mm thick butyl rubber swollen by xylene)<sup>13</sup> and in other MIP systems' studies<sup>3,14,15</sup>. The longer time for equilibration of the MIP compared to the NIP in the binding studies of 4HBA depicted in Figure 2.18 can be attributed to the greater difficulty of the analyte molecule in situating itself in the special sites than in the general sites.

**REFERENCES**

1. Landin, D. T.; Macosko, C. W. *Macromolecules* **1988**, *21*, 846.
2. Sellergren, B.; Hall, A. J. In *Molecularly Imprinted Polymers: Man-made mimics of antibodies and their applications in analytical chemistry*; Sellergren, B. Ed.; Elsevier, 2001, p 21.
3. Sellergren, B. In *Molecularly Imprinted Polymers: Man-made mimics of antibodies and their applications in analytical chemistry*; Sellergren, B. Ed.; Elsevier, 2001, p 113.
4. Zhang, T.; Liu, F.; Chen, W.; Wang, J.; Li, K. *Anal. Chim. Acta* **2001**, *450*, 532.
5. Zhang, T.; Liu, F.; Wang, J.; Li, N.; Li, K. *Chromatographia* **2002**, *55*, 447.
6. Zhang, T.; Liu, F.; Wang, J.; Li, K. *Huaxue Xuebao* **2001**, *59*, 1623.
7. Dong, X.; Sun, H.; Lü, X.; Han, J.; Han, B. *Acta chimica Sinica* **2002**, *60*, 2035.
8. Lide, D. R. *CRC Handbook of Chemistry and Physics*; 83rd ed.; CRC Press: Boca Raton, FL, 2002.
9. Connors, K. A. *Binding Constants*; John Wiley & Sons Publication: New York, 1987.
10. Whitcombe, M. J.; Martin, L.; Vulfson, E. N. *Chromatographia* **1998**, *47*, 457.
11. Shimizu, K. D. In *Materials Research Society Symposium Proceedings*, 2004; Vol. 787, p 17.
12. Guyot, A. In *Synthesis and separations using functional polymers*; Sherrington, D. C.; Hodge, P. Eds.; John Wiley & Sons Ltd., 1988, p 1.
13. Flory, J. J.; Rehner, J. J. *J. Chem. Phys.* **1944**, *12*, 412.
14. Kriz, D.; Mosbach, K. *Anal. Chim. Acta* **1995**, *300*, 71.
15. Takeuchi, T.; Fukuma, D.; Matsui, J. *Anal. Chem.* **1999**, *71*, 285.

## CHAPTER 5. SUMMARY AND CONCLUSIONS

In this study, 4HBA, 3HBA and (*S*)-naproxen imprinted resins were successfully prepared. Based on the functional groups on the template molecule, a suitable monomer, either acrylamide or 4-vinylpyridine, was selected to form the template-monomer complex by non-covalent bonding. <sup>1</sup>H-NMR, UV-Vis and FTIR spectroscopies provided evidence for hydrogen bonding, which is the key for the whole imprinting.

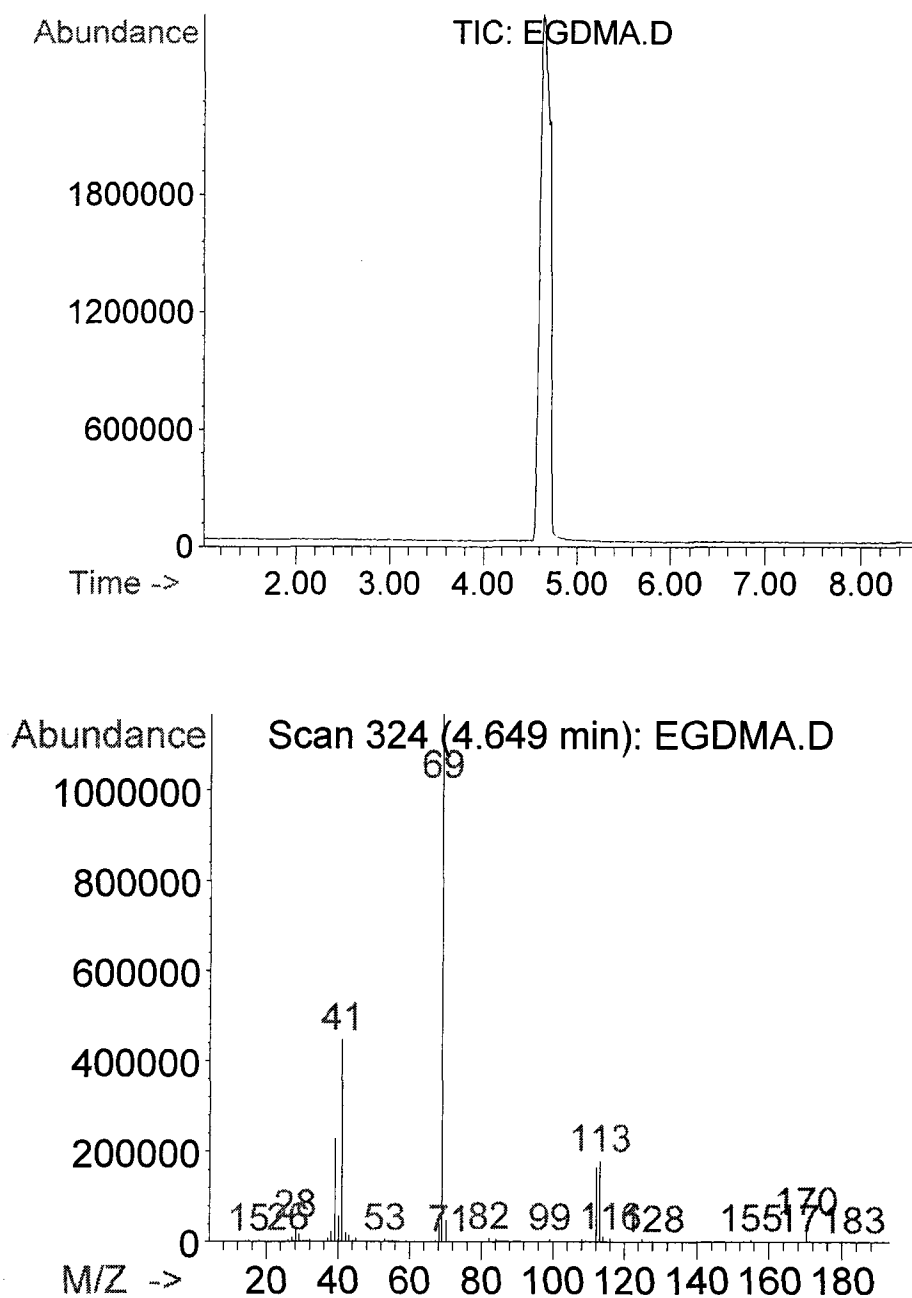
After polymerizing monomer and crosslinker in the presence of template, the template was recovered with a greater than 90% yield. The binding results for template molecule and its structure related molecules showed the MIPs possess the predesigned affinity and selectivity.

Although some studies reported the results in terms of a simple Scatchard plot (Equation (1-3) and Figure 1.4 (a)) and Shimizu recognizes that there can be a distribution function that sheds little light on the nature of the MIP system, with rare exception, the capacity of the control polymer (NIP) was not taken into account. The studies described here incorporate effects of binding that are found in NIP as well as in MIP resins. From the template's binding isotherms, a simple two-binding-site model is proposed based upon the Scatchard equation. Upon considering the binding behavior of

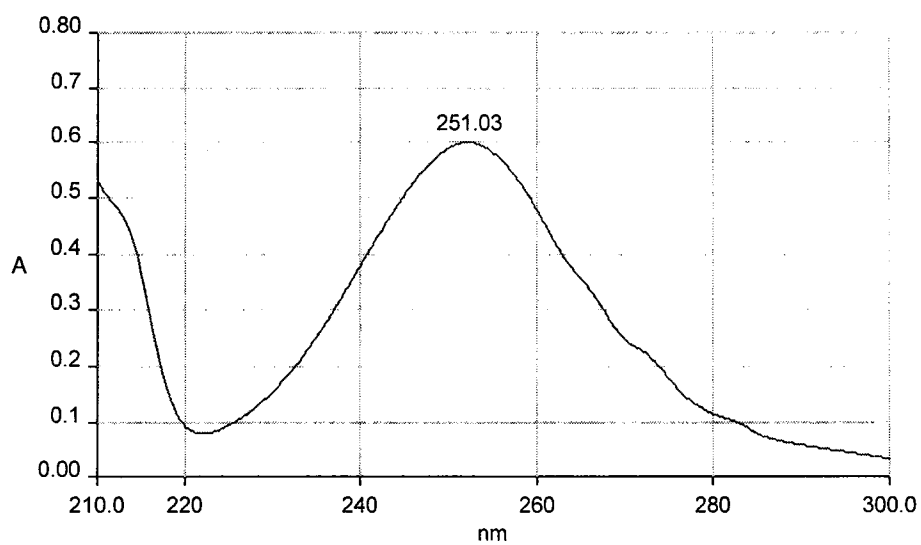
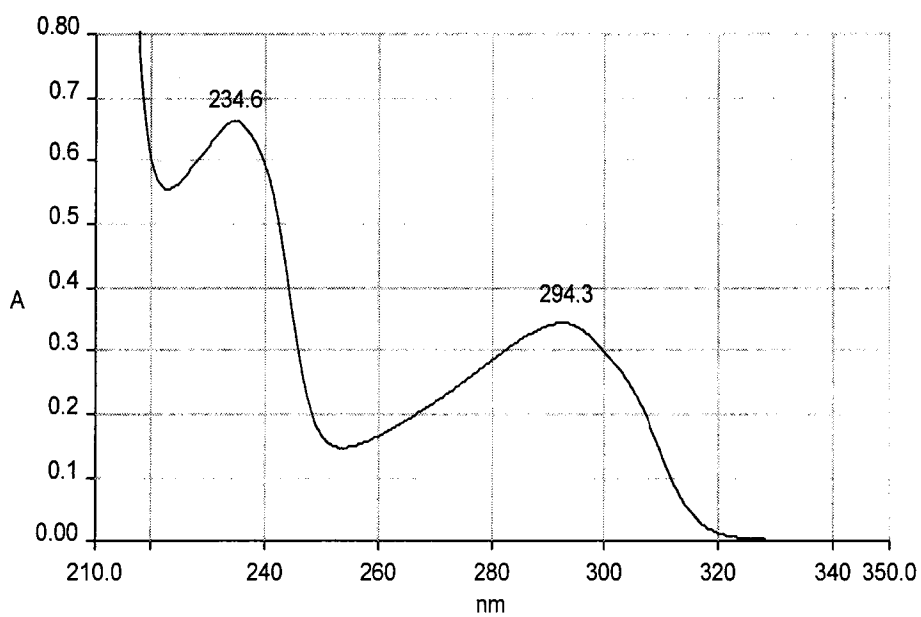
NIP, it successfully describes the binding behavior of three different MIPs studied in this thesis. Two kinds of binding sites are defined as “general” and “special”. The binding to general sites, which are common to both NIP and MIP, was found to have similar affinity to the analytes. They are stronger than the binding to the “special” imprinted sites in the MIP. However, the “special” imprinted sites are more numerous than the “general” sites, which determined the selectivity of MIPs. Compared with other models reviewed in section 1.3.2, this model corrects the Scatchard-like treatment of two independent classes of binding sites so that classes of binding sites are operative over the full range of concentration and its format is simple with no arbitrary parameters involved for the derivation.

## APPENDICES

## Appendix A. GC-MS spectra of EGDMA.



**Figure A.1.** GC-MS spectra of EGDMA which was purified under vacuum distillation.

**Appendix B. UV spectra of 4HBA, 3HBA and BA in acetonitrile.****Figure B.1.** UV spectrum of 4HBA acetonitrile solution.**Figure B.2.** UV spectrum of 3HBA acetonitrile solution.

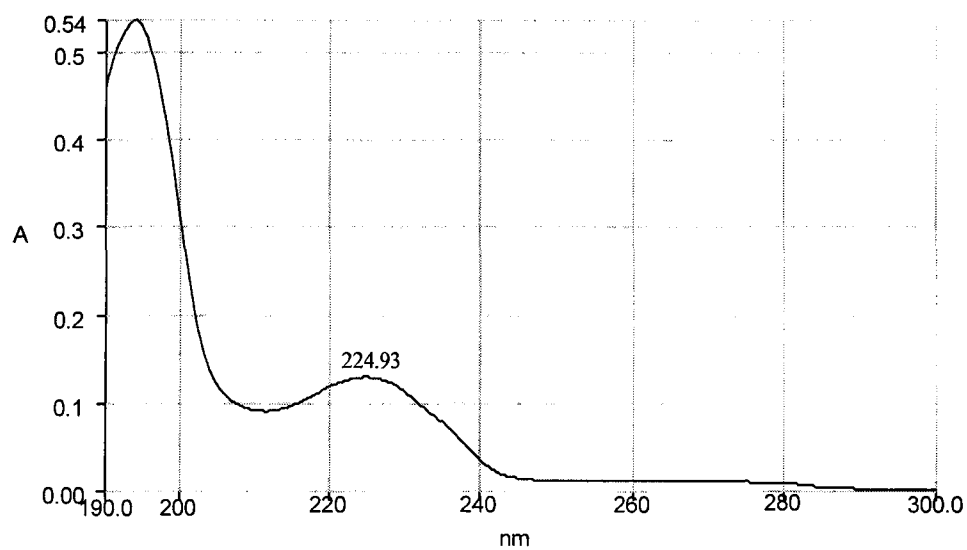


**Figure B.3.** UV spectrum of BA acetonitrile solution.

**Appendix C.  $^1\text{H-NMR}$  spectra of AA in acetonitrile- $d_3$ .**

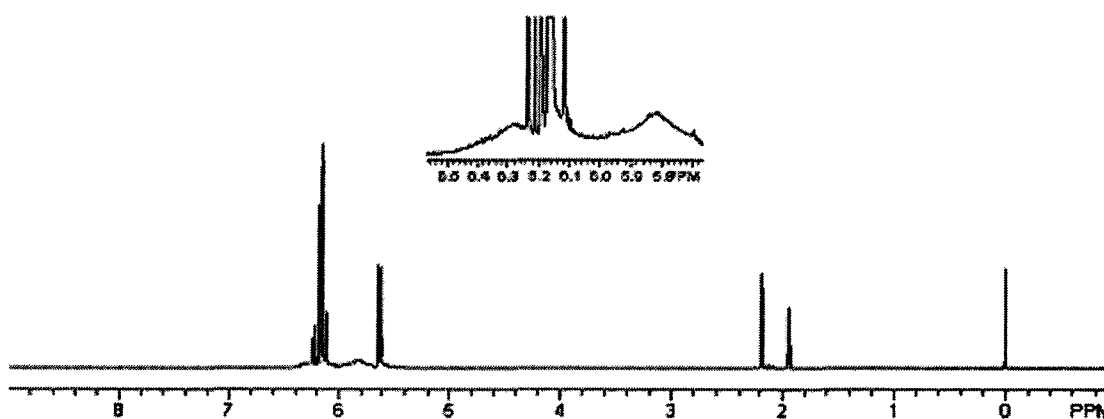


**Figure C.1.**  $^1\text{H-NMR}$  spectrum of AA in acetonitrile- $d_3$  and the concentration of AA is same as the one in which the concentration ratio of 4HBA : AA = 1:2.

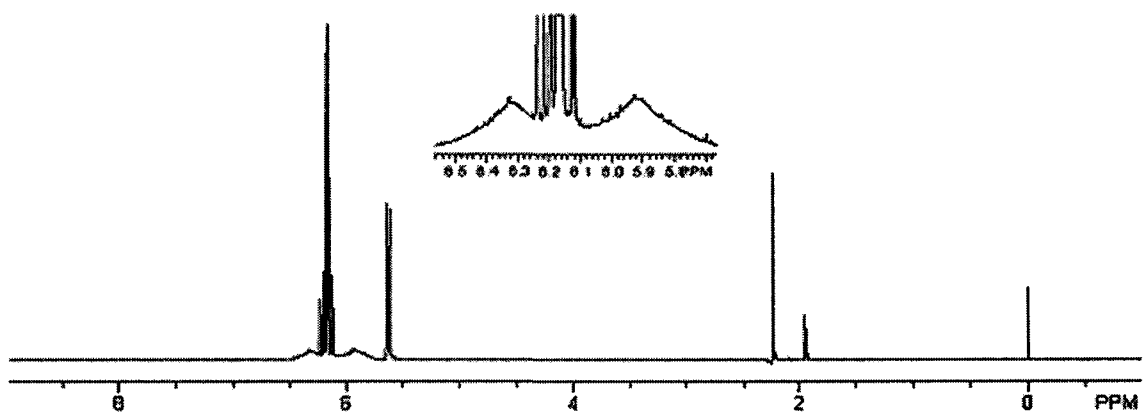


**Figure C.2.** <sup>1</sup>H-NMR spectrum of AA in acetonitrile-*d*<sub>3</sub> and the concentration of AA is same as the one in which the concentration ratio of 4HBA : AA = 1:4.

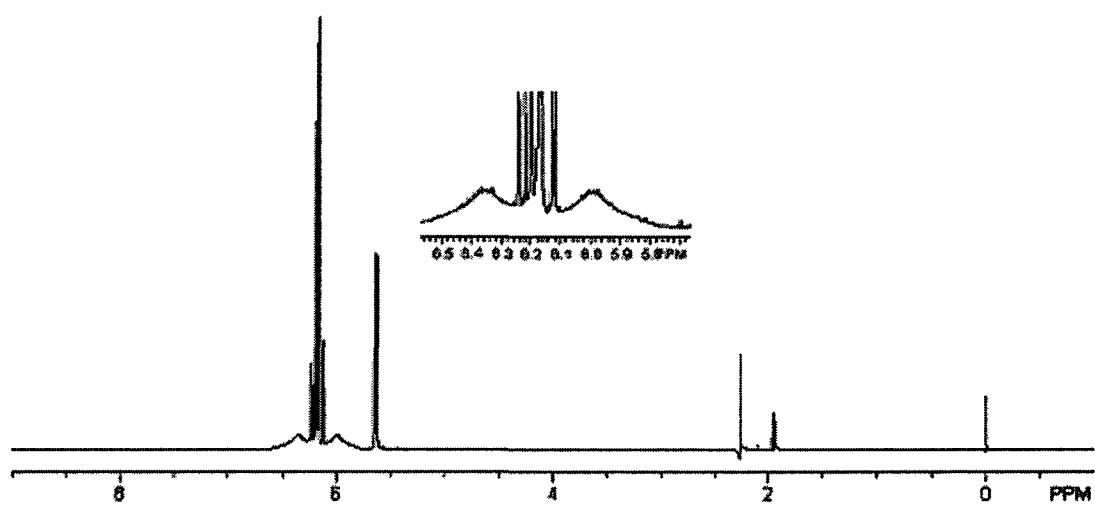


**Figure C.3.** <sup>1</sup>H-NMR spectrum of AA in acetonitrile-*d*<sub>3</sub> and the concentration of AA is same as the one in which the concentration ratio of 4HBA : AA = 1:6.

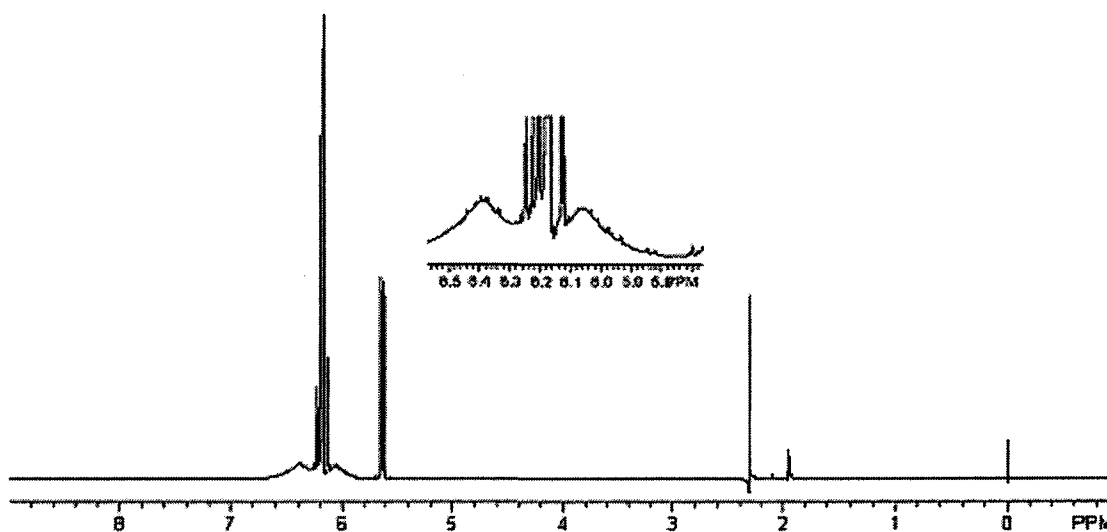


**Figure C.4.** <sup>1</sup>H-NMR spectrum of AA in acetonitrile-*d*<sub>3</sub> and the concentration of AA is same as the one in which the concentration ratio of 4HBA : AA = 1:8.

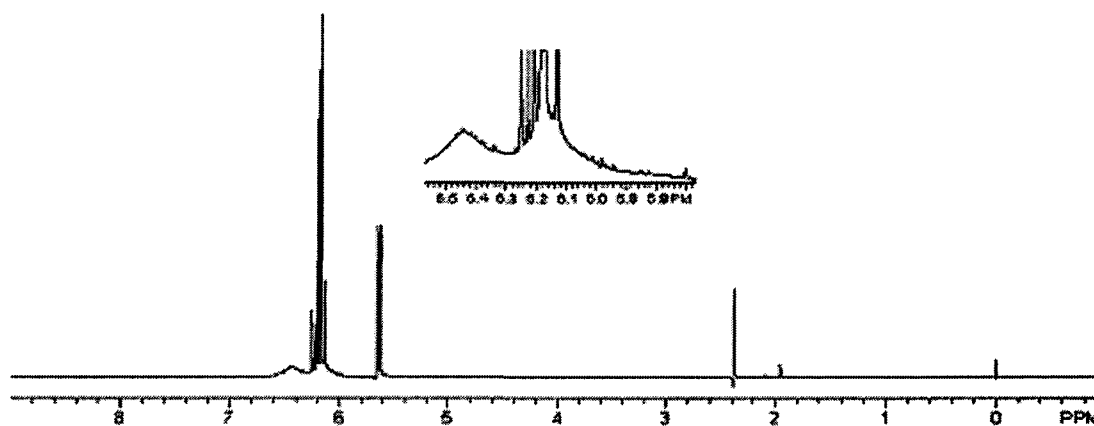


**Figure C.5.** <sup>1</sup>H-NMR spectrum of AA in acetonitrile-*d*<sub>3</sub> and the concentration of AA is same as the one in which the concentration ratio of 4HBA : AA = 1:12.

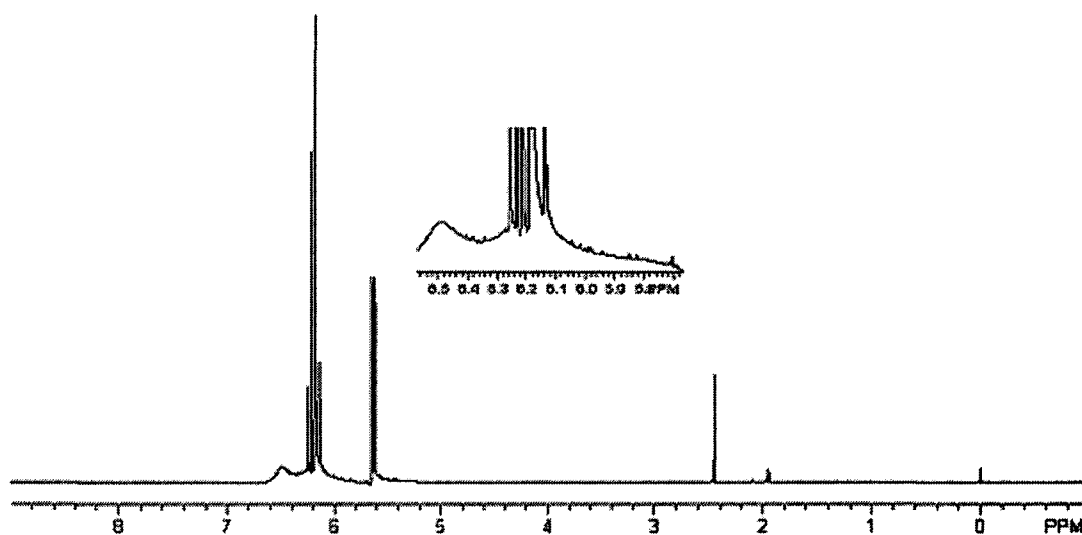


**Figure C.6.**  $^1\text{H-NMR}$  spectrum of AA in acetonitrile- $d_3$  and the concentration of AA is same as the one in which the concentration ratio of 4HBA : AA = 1:16.

**Appendix D.  $^1\text{H-NMR}$  spectra of 4HBA and AA in acetonitrile- $d_3$ .**

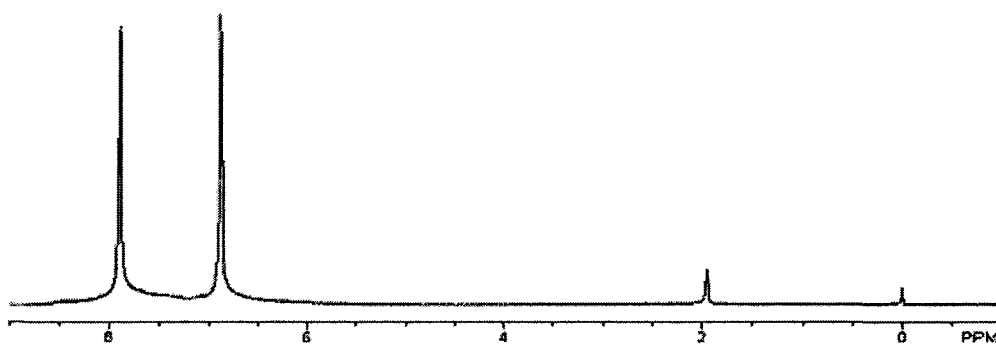


**Figure D.1.**  $^1\text{H-NMR}$  spectrum of 4HBA in acetonitrile- $d_3$ .

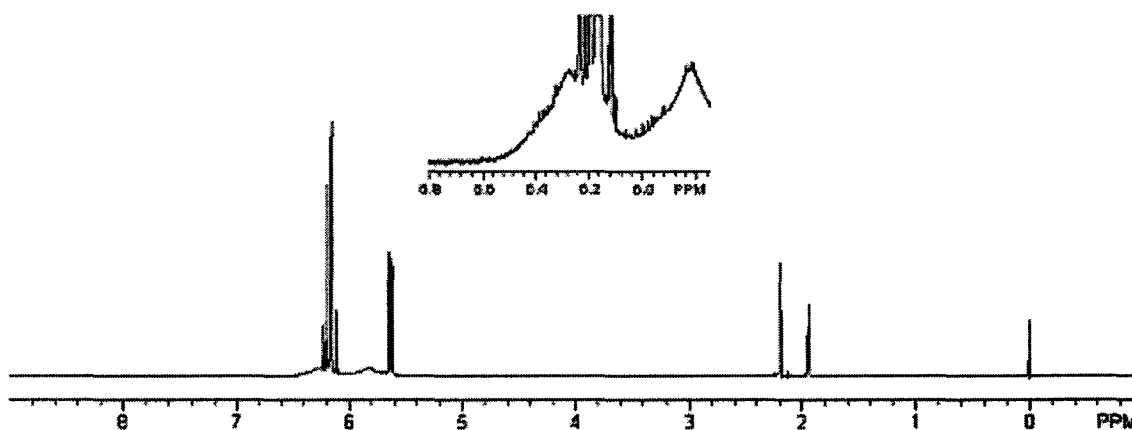


**Figure D.2.**  $^1\text{H}$ -NMR spectrum of AA in acetonitrile- $d_3$ .

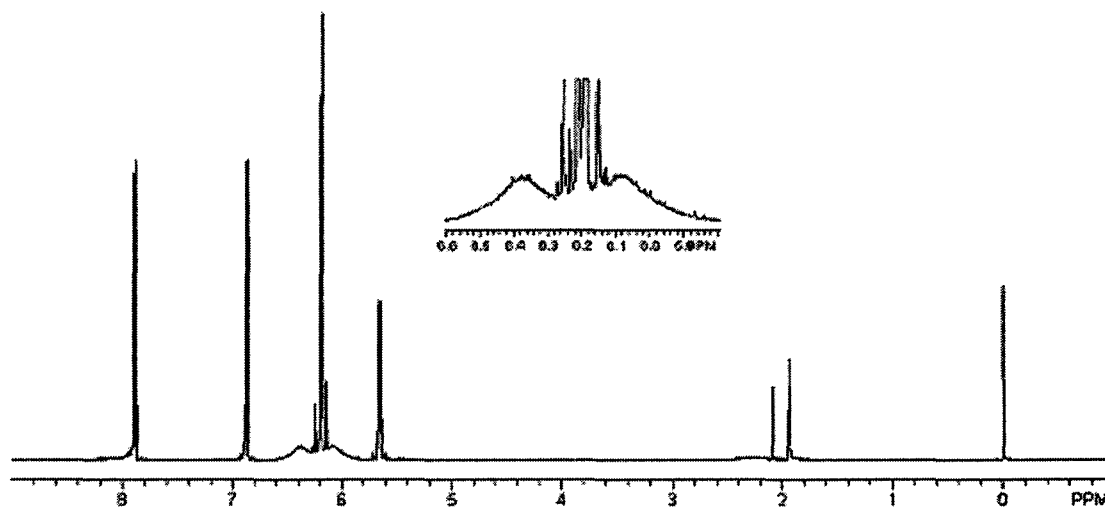


**Figure D.3.**  $^1\text{H}$ -NMR spectrum of 4HBA and AA in acetonitrile- $d_3$  in which the concentration ratio of 4HBA : AA = 1:2.

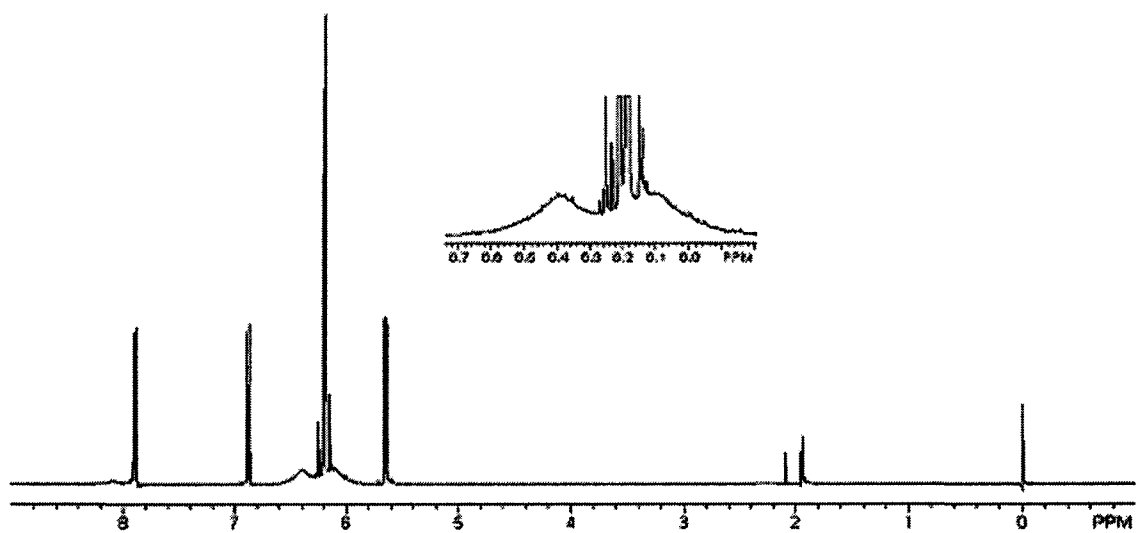


**Figure D.4.** <sup>1</sup>H-NMR spectrum of 4HBA and AA in acetonitrile-*d*<sub>3</sub> in which the concentration ratio of 4HBA : AA = 1:4.

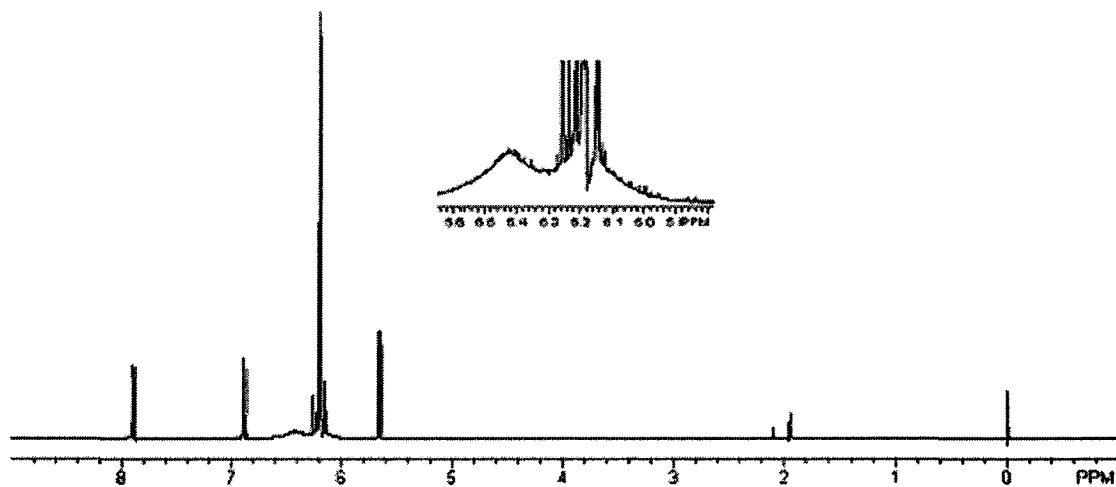


**Figure D.5.** <sup>1</sup>H-NMR spectrum of 4HBA and AA in acetonitrile-*d*<sub>3</sub> in which the concentration ratio of 4HBA : AA = 1:6.

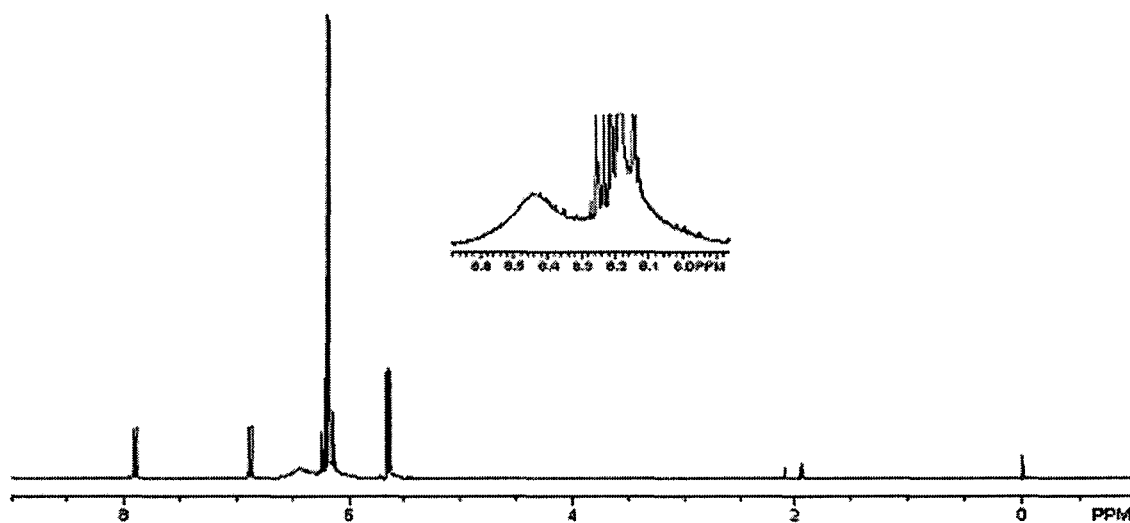


**Figure D.6.** <sup>1</sup>H-NMR spectrum of 4HBA and AA in acetonitrile-*d*<sub>3</sub> in which the concentration ratio of 4HBA : AA = 1:8.

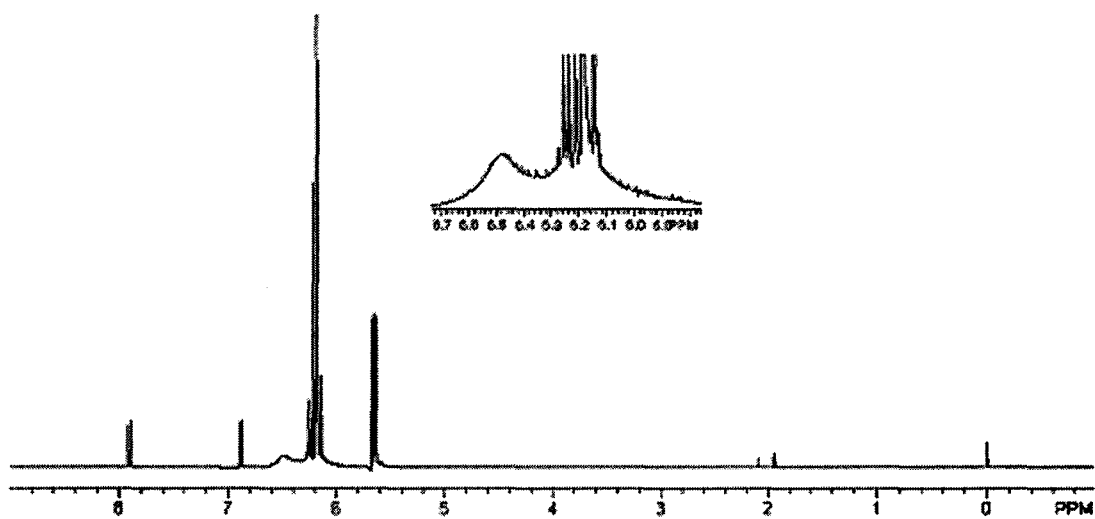


**Figure D.7.** <sup>1</sup>H-NMR spectrum of 4HBA and AA in acetonitrile-*d*<sub>3</sub> in which the concentration ratio of 4HBA : AA = 1:12.

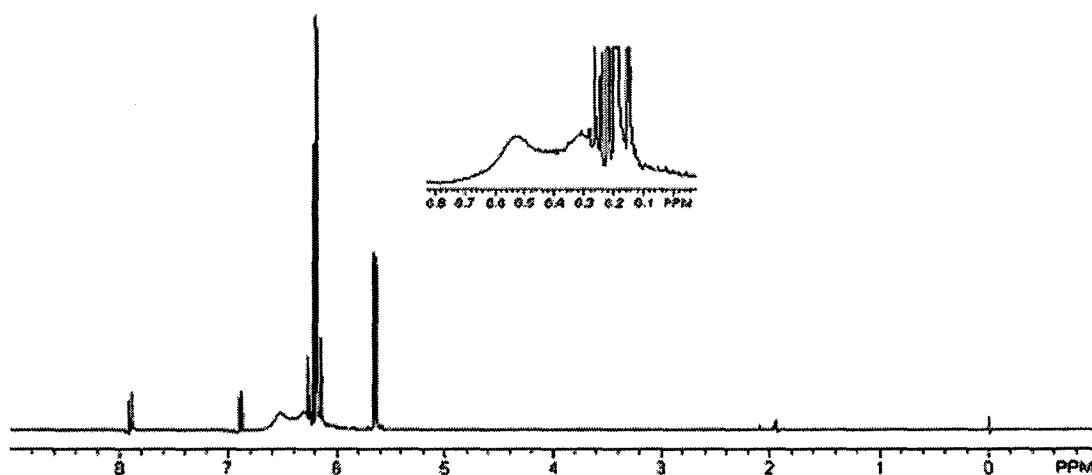


**Figure D.8.**  $^1\text{H}$ -NMR spectrum of 4HBA and AA in acetonitrile- $d_3$  in which the concentration ratio of 4HBA : AA = 1:16.

**Appendix E.  $^1\text{H}$ -NMR spectra of 3HBA and AA in acetonitrile- $d_3$**

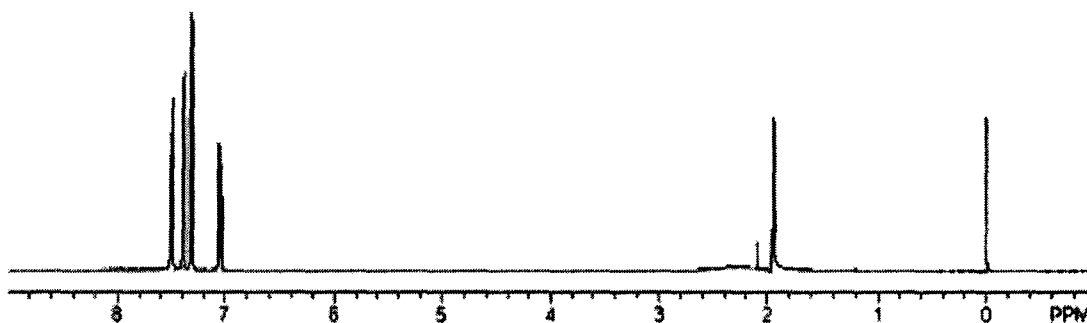


**Figure E.1.**  $^1\text{H}$ -NMR spectrum of 3HBA in acetonitrile- $d_3$

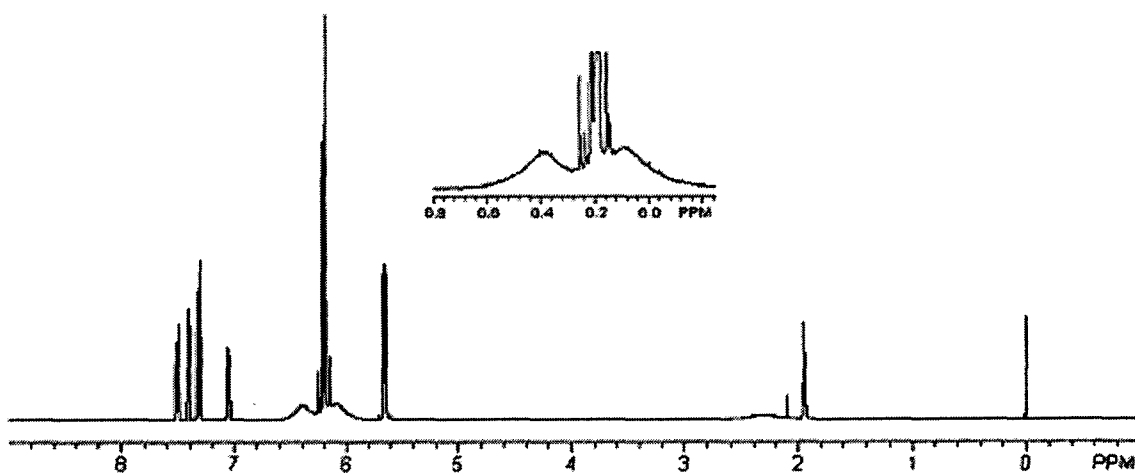


**Figure E.2.**  $^1\text{H-NMR}$  spectrum of 3HBA and AA in acetonitrile- $d_3$  in which the concentration ratio of 3HBA : AA = 1:2.

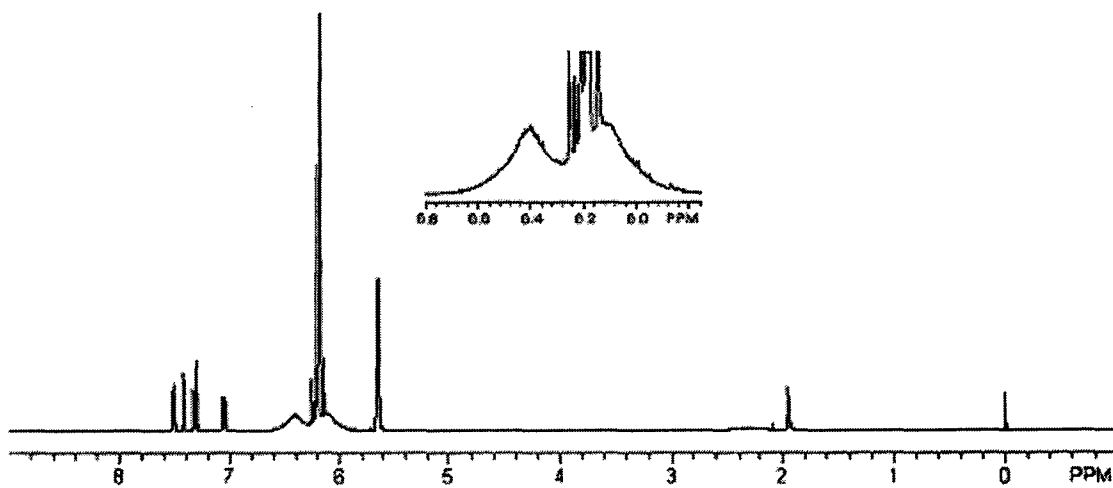


**Figure E.3.**  $^1\text{H-NMR}$  spectrum of 3HBA and AA in acetonitrile- $d_3$  in which the concentration ratio of 3HBA : AA = 1:4.

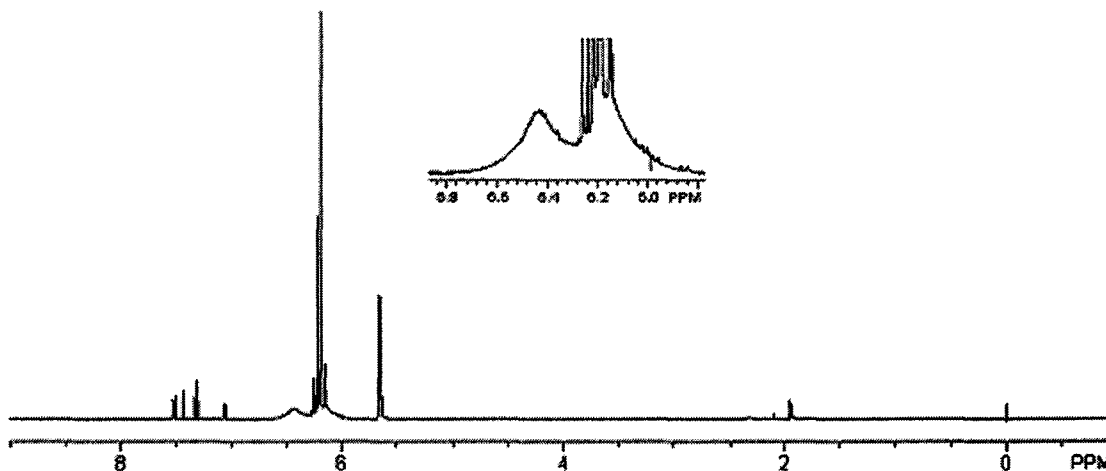


**Figure E.4.** <sup>1</sup>H-NMR spectrum of 3HBA and AA in acetonitrile-*d*<sub>3</sub> in which the concentration ratio of 3HBA : AA = 1:8.

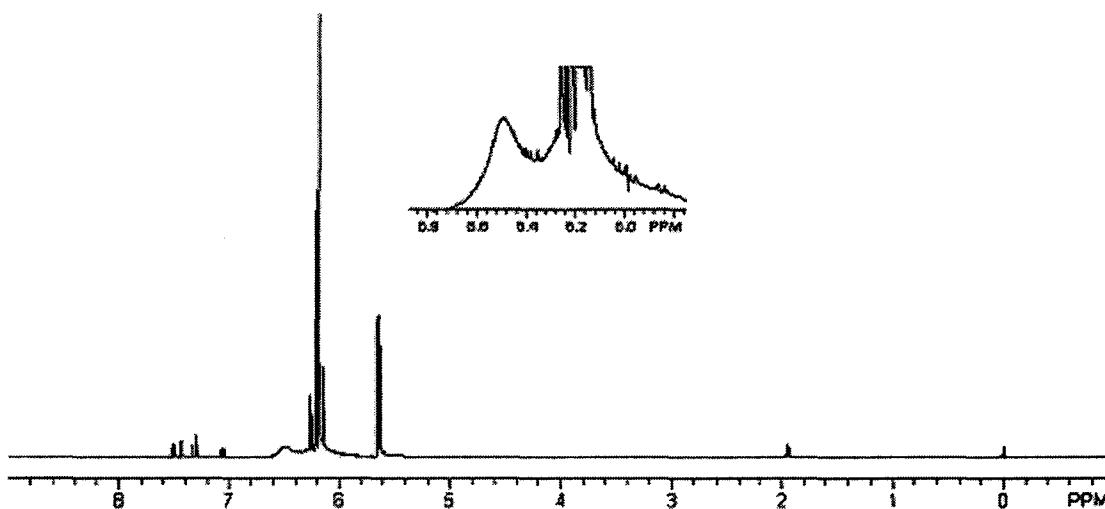


**Figure E.5.** <sup>1</sup>H-NMR spectrum of 3HBA and AA in acetonitrile-*d*<sub>3</sub> in which the concentration ratio of 3HBA : AA = 1:12.

### Appendix F. Uncertainty analysis by least-squares fitting procedure.

1. Estimate the uncertainty of the calculated concentrations from the UV absorbance measurements of the standard solutions. In this standard solutions' calibration experiment, we suppose that there were no experimental errors in the preparation of solutions and in their UV absorbance measurements.
  - 1) The UV absorbance of a series of concentrations of the standard solutions was measured in 5 different days. There were 63 sample data in total.
  - 2) Use "Linear Best Fit" function in Excel to get the best linear equation which can describe the relationship between the concentration and its UV absorbance:

$$[c] = a * UV + b .$$

The result is shown in Figure F.1 and for each UV measurement, its concentration can be calculated by the estimated slope  $\hat{a}$  and intercept  $\hat{b}$  following the equation

$$[c]_{calcd} = \hat{a} * UV + \hat{b} = (7.9057 \times 10^{-3}) \cdot UV + 5.6684 \times 10^{-6} . \text{ (F-1)}$$

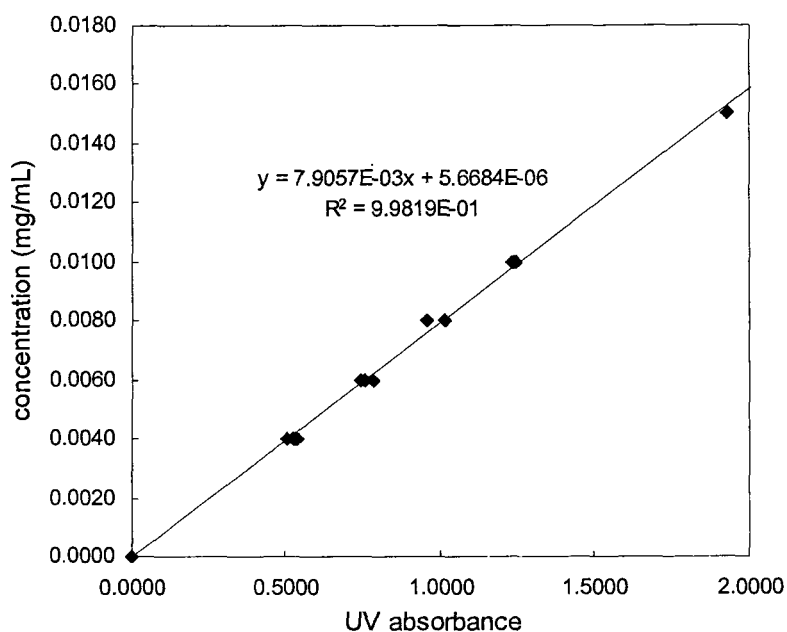


**Figure F.1.** Calibration graph for the standard solutions.

- 3) For each measurement, the error  $e$  is

$$e = [c]_{obsd} - [c]_{calcd} = [c]_{obsd} - (\hat{a} * UV + \hat{b}) \quad (F-2)$$

and the standard deviation  $\delta$  for the calculated concentration is

$$\delta = \sqrt{\frac{\sum e^2}{n-2}},$$

in which  $(n-2)$  is the degrees of freedom.

- 4) The uncertainty for the calculated concentration used in the later procedures is defined as twice that of the standard deviation in the measurements, i.e., 0.000375 mg/mL.

2. The Scatchard equation  $\frac{[MT]}{[T]} = -K_a[MT] + K_a[MT]_{\max}$  describes the relationship between the concentration of substrate in solution [T] (mmol/L) and the concentration of substrate bound in the resin at equilibrium [MT] ( $\mu\text{mol/g}$  of resin). So from 4HBA batch analysis results of NIP, its association constant  $K_a$  and the maximum number of binding sites per unit mass of the resin  $[MT]_{\max}$  and their uncertainties can be calculated respectively.

1) Based on the uncertainty of the concentration from step 1, the uncertainty of  $([MT]/[T])$  for each measurement can be calculated. During this procedure, two kinds calculations for uncertainty and relative uncertainty are used. Define  $\delta_x$ ,  $\delta_y$  and  $\delta_z$  as the uncertainty for  $x$ ,  $y$  and  $z$  respectively, the basic rules to calculate  $\delta_z$  are:

$$\text{a) If } x \pm y = z, \text{ then } \delta_z = \sqrt{(\delta_x)^2 + (\delta_y)^2}; \quad (\text{F-3})$$

$$\text{b) If } x \times y = z \text{ or } x \div y = z, \text{ then } \delta_z = z \cdot \sqrt{\left(\frac{\delta_x}{x}\right)^2 + \left(\frac{\delta_y}{y}\right)^2}. \quad (\text{F-4})$$

In addition, the relative uncertainty can be calculated as, for example,  $x$  divided by  $\delta_x$ .

2) A weight ( $w_i$ ) for each measurement<sup>1</sup> can be calculated by

$$w_i = \frac{1000}{\delta^2} \quad (\text{F-5})$$

and its relative weight ( $w_i^R$ ) is

$$w_i^R = \frac{w_i}{w_{i,\min}}. \quad (\text{F-6})$$

The calculation results are shown in Table F.1.

- 3) The Scatchard equation  $\frac{[MT]}{[T]} = -K_a[MT] + K_a[MT]_{\max}$  can be simplified as  $y = cx + d$ . From the slope and the intercept,  $K_a$  and  $[MT]_{\max}$  can be calculated. By using the least squares method, i.e., minimizing the sum of the squares of the errors, we want to find the estimates of the slope  $c$  and the intercept  $d$  (i.e.,  $\hat{c}$  and  $\hat{d}$ ) so that  $y = \hat{c}x + \hat{d}$  can best describe the data.

In the batch analyses,  $e_i = y_i - (cx_i + d)$  is the difference between the observed value  $y_i$  at  $x_i$  and the value as calculated from the linear fit.

According to the least squares method,

$$G(c, d) = \sum_{i=1}^N e_i^2 = \sum_{i=1}^N (y_i - cx_i - d)^2$$

should be minimized. The minimum of a function is specified by the vanishing of its derivative, leading to two conditions

$$\left(\frac{\partial G}{\partial d}\right)_c = 0, \quad \left(\frac{\partial G}{\partial c}\right)_d = 0.$$

Then

$$\left(\frac{\partial G}{\partial d}\right)_c = -\sum_{i=1}^N 2(y_i - cx_i - d) = 0;$$

$$\left(\frac{\partial G}{\partial c}\right)_d = -\sum_{i=1}^N 2(y_i - cx_i - d)x_i = 0.$$

Define

$$S_x = \sum_{i=1}^N x_i, \quad S_{xx} = \sum_{i=1}^N x_i^2, \quad S_y = \sum_{i=1}^N y_i, \quad \text{and} \quad S_{xy} = \sum_{i=1}^N x_i y_i,$$

the above two equations can be written as

$$dN + cS_x = S_y$$

$$dS_x + cS_{xx} = S_{xy}.$$

So  $c$  and  $d$  can be solved as

$$\hat{c} = \frac{NS_{xy} - S_x S_y}{NS_{xx} - S_x^2}$$

$$\hat{d} = \frac{S_{xx} S_y - S_x S_{xy}}{NS_{xx} - S_x^2}.$$

Taking the weight of each point into account,

$$\begin{aligned}
\hat{c} &= \frac{-\sum_i w_i x_i \sum_i w_i y_i + \sum_i w_i \sum_i w_i x_i y_i}{\sum_i w_i \sum_i w_i x_i^2 - (\sum_i w_i x_i)^2} \\
&= \frac{-(\sum_i w_i^R) \cdot (\sum_i (w_i^R x_i) / \sum_i w_i^R) \cdot (\sum_i (w_i^R y_i) / \sum_i w_i^R) + \sum_i w_i^R (x_i y_i)}{\sum_i w_i^R x_i^2 - \sum_i w_i^R \cdot (\sum_i (w_i^R x_i) / \sum_i w_i^R)^2}
\end{aligned}
\tag{F-7}$$

$$\hat{d} = y_i - \hat{c}x_i = \frac{\sum_i w_i^R y_i}{\sum_i w_i^R} - \hat{c} \cdot \frac{\sum_i w_i^R x_i}{\sum_i w_i^R}.
\tag{F-8}$$

The standard deviations in the intercept and slope can be estimated from

$$\hat{\sigma}(\hat{c}) = \left( \frac{\sum_i w_i^R}{\sum_i w_i^R \sum_i w_i^R x_i^2 - (\sum_i w_i^R x_i)^2} \right)^{\frac{1}{2}} \left( \frac{\sum_i e_i^2}{\sum_i w_i^R - 2} \right)^{\frac{1}{2}}
\tag{F-9}$$

$$\hat{\sigma}(\hat{d}) = \left( \frac{\sum_i w_i^R x_i}{\sum_i w_i^R \sum_i w_i^R x_i^2 - (\sum_i w_i^R x_i)^2} \right)^{\frac{1}{2}} \left( \frac{\sum_i e_i^2}{\sum_i w_i^R - 2} \right)^{\frac{1}{2}}.
\tag{F-10}$$

The uncertainties of  $\hat{c}$  and  $\hat{d}$  are defined as their standard deviations. Thereafter, NIP's  $K_a$  and  $[MT]_{\max}$  and their standard deviations are calculated (Table F.2).

$$K_{a,NIP} = 4.4 \pm 0.2 \text{ mM}^{-1}$$

$$[MT]_{\max,NIP} = 6.7 \pm 0.3 \text{ } \mu\text{mol/g}$$

These values are also used to describe the properties of the general binding sites in MIP, i.e.,  $K_{a,g} = K_{a,NIP}$  and  $[MT]_{\max,g} = [MT]_{\max,NIP}$ .

3. In this study, MIP4HBA resin is regarded as having two kinds of binding sites: “general” and “special”. So, we will use the same method in the calculation of general binding sites to calculate the constants for the special binding sites.

1) The concentration of substrate bound in the general binding sites in MIP resin  $[MT]_g$  is calculated by taking the concentration of the substrate in solution  $[T]$  into the equation

$$[MT]_g = \frac{K_{a,g} [MT]_{\max,g} [T]}{1 + K_{a,g} [T]}$$

Its uncertainty and relative uncertainty can be calculated following Equation (F-3) and Equation (F-4).

2) The concentration of substrate in the special binding sites  $[MT]_s$  is calculated by subtracting the amount attributed to the general sites  $[MT]_g$  from the total amount bound  $[MT]_{total}$ , i.e.,  $[MT]_{exp}$ , (Since the volume is the same, the amount difference is same as the concentration difference.)

$$[MT]_s = [MT]_{total} - [MT]_g = [MT]_{exp} - \frac{K_{a,g} [MT]_{\max,g} [T]}{1 + K_{a,g} [T]}$$

Following the method in STEP 2,  $K_a$  and  $[MT]_{\max}$  for the special binding sites and their uncertainties are calculated:

$$K_{a,s} = 0.15 \pm 0.01 \text{ mM}^{-1};$$

$$[MT]_{\max,s} = 72 \pm 2 \text{ } \mu\text{mol/g}.$$

**Table F.1.** Binding analysis of NIP.

	No. 1	No. 2	$\delta^{12}$	$\delta_r^{13}$	No. 3	$\delta$	$\delta_r$	No. 4	$\delta$	$\delta_r$	No. 5	$\delta$	$\delta_r$
$UV_0^1$	0.000	0.740			1.543			1.789			0.326		
Dilution factor	1	1			1			1			11		
$[T]_0^2$ (mg/mL)	0.0000	0.0059	0.0004	0.064	0.0122	0.0004	0.0307	0.0141	0.0004	0.0265	0.0284	0.0004	0.0132
$m_0^3$ (mg)	0.0000	0.059	0.004		0.122	0.004		0.141	0.004		0.284	0.004	
$UV^4$	0.207	0.798			1.502			1.714			0.289		
Dilution factor	1	1			1			1			11		
$[T]^5$ (mg/mL)	0.0016	0.0063			0.0119			0.0136			0.0252		
$[T]^6$ (mg/mL)	0.0000	0.0047	0.0004	0.0802	0.0102	0.0004	0.0366	0.0119	0.0004	0.0314	0.0236	0.0004	0.0159
$[T]$ (mM)	0.0000	0.0339			0.0742			0.0863			0.1707		
$m^7$ (mg)	0.0000	0.0467	0.0037		0.1024	0.0037		0.1191	0.0037		0.2355	0.0037	
$m_b^8$ (mg)	0.0000	0.0118	0.0053	0.4476	0.0197	0.0053	0.2694	0.0224	0.0053	0.2370	0.0486	0.0053	0.1090
$[MT]^9$ ( $\mu$ mol/g)	0.0000	0.8577		0.4476	1.4248		0.2694	1.6132		0.2370	3.5181		0.1090
$[MT]/[T]$ (mL/g)	0.0000	25.3288	13.5186	0.4547	19.2059	7.2219	0.2719	18.6855	6.4675	0.2391	20.6132	4.2708	0.1102
$w_i^{10}$			5.472			19.173			23.907			54.826	
$w_i^R^{11}$			1			4			4			10	

<sup>1</sup>  $UV_0$ : UV absorbance of the binding solution.

<sup>2</sup>  $[T]_0$ : Calculated concentration of the binding solution (mg/mL) according to Equation (F-1).

<sup>3</sup>  $m_0$ : Mass of analyte in 10 mL binding solution (mg).

<sup>4</sup>  $UV$ : UV absorbance of the solution after binding.

<sup>5</sup>  $[T]^5$ : Calculated concentration of the solution after binding (mg/mL).

<sup>6</sup>  $[T]^6$ : Adjusted concentration of the solution after binding (mg/mL).

<sup>7</sup>  $m$ : After binding, mass of analyte left in the binding solution (mg).

<sup>8</sup>  $m_b$ : After binding, mass of analyte bound in the resin (mg).

<sup>9</sup>  $[MT]$ : Concentration of the analyte bound in the resin ( $\mu$ mol/g).

<sup>10</sup>  $w_i$ : Weight of  $[MT]/[T]$  according to Equation (F-5).

<sup>11</sup>  $w_i^R$ : Relative weight of  $[MT]/[T]$  according to Equation (F-6).

<sup>12</sup>  $\delta$ : Uncertainty. <sup>13</sup>  $\delta_r$ : Relative uncertainty according to Equation (F-3) and Equation (F-4).

**Table F.1.** Binding analysis of NIP. (Continued)

	No. 6	$\delta^{12}$	$\delta_r^{13}$	No. 7	$\delta$	$\delta_r$	No. 8	$\delta$	$\delta_r$	No. 9	$\delta$	$\delta_r$	No. 10	$\delta$	$\delta_r$
$UV_0^1$	1.420			0.845			1.022			1.415			1.469		
Dilution factor	5			16			16			16			21		
$[T]_0^2$ (mg/mL)	0.0562	0.0004	0.0067	0.1070	0.0004	0.0035	0.1294	0.0004	0.0029	0.1791	0.0004	0.0021	0.2444	0.0004	0.0015
$m_0^3$ (mg)	0.562	0.004		1.070	0.004		1.294	0.004		1.791	0.004		2.440	0.0037	
$UV^4$	1.309			0.806			0.994			1.394			1.431		
Dilution factor	5			16			16			16			21		
$[T]^5$ (mg/mL)	0.0518			0.1020			0.1258			0.1764			0.2377		
$[T]^6$ (mg/mL)	0.0501	0.0004	0.0075	0.1004	0.0004	0.0037	0.1242	0.0004	0.0030	0.1748	0.0004	0.0021	0.2361	0.0004	0.0016
$[T]$ (mM)	0.3633			0.7275			0.8999			1.2665			1.7105		
$m^7$ (mg)	0.5013	0.0037		1.0040	0.0037		1.2170	0.0037		1.7128	0.0037		2.3605	0.0037	
$m_b^8$ (mg)	0.0603	0.0053	0.0879	0.0658	0.0053	0.0806	0.0767	0.0052	0.0684	0.0779	0.0052	0.0673	0.0795	0.0053	0.0666
$[MT]^9$ ( $\mu$ mol/g)	4.3520		0.0879	4.7600		0.0806	5.5396		0.0684	5.6478		0.0673	5.7558		0.0666
$[MT]/[T]$ (mL/g)	11.9807	3.0564	0.0882	6.5425	2.5277	0.0807	6.1560	2.4215	0.0685	4.4594	2.3002	0.0673	3.3649	2.2243	0.0666
$w_i^{10}$		107.051			156.516			170.543			188.99			188.997	
$w_i^{R 11}$		20			29			31			73			3	
											35			35	

**Table F.2.** Calculation of  $\hat{c}$ ,  $\hat{d}$  and their standard deviations  $\sigma(\hat{c})$  and  $\sigma(\hat{d})$  based on Table F.1.

$x_i$	$y_i$	$w_i^R$	$x_i^2$	$x_i \times y_i$	$w_i^R \times (x_i^2)$	$w_i^R \times (x_i \times y_i)$	$w_i^R \times x_i$	$w_i^R \times y_i$	$e^2$	$w_i^R \times (e^2)$
0.8577	25.3328	1	0.7356	21.7278	0.7356	21.7278	0.8577	25.3328	0.2765	0.2765
1.4248	19.2059	4	2.0302	27.3654	8.1207	109.4617	5.6994	76.8238	17.1592	68.6369
1.6132	18.6855	4	2.6023	30.1428	10.4092	120.5714	6.4527	74.7420	14.6631	58.6523
3.5181	20.6132	10	12.3767	72.5184	123.7670	725.1841	35.1805	206.1322	42.6393	426.3929
4.3520	11.9807	20	18.9401	52.1401	378.8016	1042.8021	87.0404	239.6133	2.5237	50.4746
4.7600	6.5425	29	22.6572	31.1422	657.0576	903.1229	138.0387	189.7336	4.1776	121.1497
5.5396	6.1560	31	30.6867	34.1016	951.2862	1057.1481	171.7262	190.8363	1.0409	32.2666
5.6478	4.4594	35	31.8980	25.1859	1116.4303	881.5070	197.6741	156.0788	0.0389	1.3601
5.7558	3.3649	37	33.1288	19.3677	1225.7661	716.6064	212.9632	124.5024	0.6624	24.5081
Sum		171			4472.3744	5578.1316	855.6329	1283.7953		4.6374
Mean							5.0037	7.5076		

According to Equation (F-7) and (F-8),  $\hat{c}$  and  $\hat{d}$  can be calculated as  $\hat{c} = -4.426$  and  $\hat{d} = 29.655$ .

According to Equation (F-9) and (F-10),  $\sigma(\hat{c})$  and  $\sigma(\hat{d})$  can be calculated as  $\sigma(\hat{c}) = 0.156$  and  $\sigma(\hat{d}) = 0.797$ .

From the Scatchard equation,  $\frac{[MT]}{[T]} = -K_a[MT] + K_a[MT]_{\max}$ , NIP's  $K_a$  and  $[MT]_{\max}$  and their standard deviations are calculated.

They are  $K_{a,NIP} = 4.4 \pm 0.2 \text{ mM}^{-1}$  and  $[MT]_{\max,NIP} = 6.7 \pm 0.3 \text{ } \mu\text{mol/g}$ .

**REFERENCES**

1. Garland, C. W.; Niber, J. W.; Shoemaker, D. P. *Experiments in Physical Chemistry*; 7th ed.; The McGraw-Hill Companies, Inc., 2003.

## VITA

Lucy Yue Hu

The author was born in Beijing, P. R. China, on April 16, 1973. Upon earning a Bachelor of Science degree with a concentration in Polymer Science and Engineering from Zhejiang University, Hangzhou, July 1996, the author worked as an engineer in the product development department of the Tongfang Technology Company at Tsinghua University. She was formerly a senior research associate for laundry technology in R& D for the Procter & Gamble Technology Company (U. S. A.) in Beijing and worked as an assistant manager and chemist for laundry research and technology in R&D for the Novo Nordisk Company (Denmark) also in Beijing.

Upon finishing the defense for the Master of Arts degree in the Department of Chemistry at the College of William and Mary in July 2001, she continued her studies working toward a doctorate in the Department of Applied Science at the same institution. The course requirements and dissertation have been completed.